DIRECTIONAL RESPONSE OF WIND WAVES TO TURNING WINDS

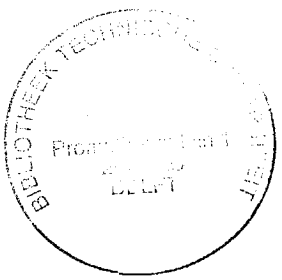

PROEFSCHRIFT

ter verkrijging van de graad van doctor aan
de Technische Universiteit Delft,
op gezag van de Rector Magnificus, prof. drs. P.A. Schenck,
in het openbaar te verdedigen ten overstaan van een
Commissie aangewezen door het College van Dekanen
op dinsdag 20 februari 1990 te 16.00 uur

door

Gerbrant Philippus van Vledder
geboren 28 juli 1957 te Hengelo (O)
civiel ingenieur

1990

Dit proefschrift is goedgekeurd door de promotor
prof. dr. ir. J.A. Battjes

dr.ir. L.H. Holthuijsen heeft als toegevoegd promotor in hoge mate bijgedragen aan het totstandkomen van dit proefschrift

STELLINGEN

behorende bij het proefschrift:

'The directional response of wind waves to turning winds'

Gerbrant Philippus van Vledder
Januari 1990

1 De door Dungey and Hui [1] ontwikkelde parametrische methode voor de berekening van de niet-lineaire wisselwerkingen in een windgolfveld is niet geschikt voor toepassing in een derde-generatie golfvoorspellingsmodel.

[1] Dungey, J.C. and W.H. Hui, 1979: Nonlinear energy transfer in a narrow gravity-wave spectrum. *Proc. Roy. Soc. London*, A 368, 239-265.

2 De empirisch bepaalde tijdschaal van de golfrichtingsresponsie is gevoelig voor de wijze van selecteren van golfrichtingsmetingen. Bijzondere zorgvuldigheid hierin is daarom onontbeerlijk.

3 De door Young et al. [1] gebruikte methode om de tijdschaal van de golfrichtingsresponsie te bepalen is daarvoor niet geschikt. Zij houdt nl. geen rekening met de variatie van deze tijdschaal met de groeifase van de golven.

[1] Young, I.R., S. Hasselmann and K. Hasselmann, 1987: Computations of the response of a wave spectrum to a sudden change in wind direction. *J. Phys. Oceanogr.*, 17, No. 9, 1317-1338.

4 In aanvulling op eerdere suggesties van bijv. Young et al. [1], heeft de huidige studie aangetoond dat de rol van dissipatie bij de richtingsresponsie van windgolven niet beperkt is tot de afbraak van het oude golfveld, doch dat zij ook de groei van het nieuwe golfveld tegenwerkt, en wel in zodanige mate dat de draaiing van de gemiddelde golfrichting wordt tegengewerkt.

[1] Young, I.R., S. Hasselmann and K. Hasselmann, 1987: Computations of the response of a wave spectrum to a sudden change in wind direction. *J. Phys. Oceanogr.*, 17, No. 9, 1317-1338.

5 Nog steeds bestaat de misvatting als zou een steekproef van extreme golfhoogten, gebaseerd op een periode van n jaar, ten hoogste de zgn. n-jaar golf uit een populatie bevatten.

6 De door Goda [1] geïntroduceerde spectrale gepiektheids-parameter (Q_p) heeft geen mathematisch- fysische relatie tot gegroeptheid van windgolven; de door Rice [2] afgeleide twee-dimensionale Rayleigh verdeling bevat een spectrale correlatieparameter (κ) die deze relatie wel heeft. Gebruik van de parameter Q_p in relatie tot golfgroepen dient derhalve vermeden te worden ten gunste van de parameter κ.

[1] Goda, Y., 1970: Numerical experiments on wave statistics with spectral simulation. *Report Port and Harbour Res. Institute*, No. 9.

[2] Rice, S.O., 1943: Mathematical analysis of random noise; Herdruk in *Selected Papers on Noise and Stochastic Processes*, Dover Pub. Inc., 1954, 133-294.

7 Vooruitgang in de mathematisch-fysische onderbouwing van spectrale golfvoorspellingsmodellen is het meest gebaat met een verbeterde beschrijving van energiedissipatie tengevolge van brekende golven, zowel op diep als op ondiep water.

8 Bij het - overigens vaak overbodige - inpakken van artikelen wordt in het algemeen meer aandacht besteed aan de economie van het inpakken dan aan de ergonomie van het uitpakken.

9 Het gebruik van een uitgebreid computerprogramma geeft vaak meer inzicht in het gebruikte computersysteem dan in het desbetreffende programma.

10 Steeds vaker misbruikt de commercie de kreet "groen" door deze te koppelen aan de milieuvriendelijke aspecten van een product met voorbijgaan aan de schadelijke kanten ervan.

11 Atonale muziek is niet toonloos.

CONTENTS PAGE

Contents of chapters 1 through 6

SAMENVATTING

In de voorliggende studie is de richtingsresponsie van windgolven op draaiende winden theoretisch bestudeerd door gebruik te maken van numerieke golfvoorspellingsmodellen, en empirisch door analyse van golfrichtingsmetingen op zee.

De studie is gericht op twee aspecten van de richtingsresponsie. Het eerste heeft betrekking op de fysische processen die plaatsvinden tijdens de responsie van de golven. Het tweede aspect is de relatie tussen de tijdschaal van richtingsresponsie en lokale wind- en golfparameters. Daartoe wordt gebruik gemaakt van een relaxatiemodel dat de lokaal geïnduceerde mate van verandering van de gemiddelde golfrichting relateert aan het verschil tussen de wind- en golfrichting.

De richtingsresponsie is theoretisch onderzocht met het derde-generatie EXACT-NL golfvoorspellingsmodel. Dit model beschrijft de fysica van de golven redelijk goed; dit geldt met name voor de niet-lineaire wisselwerkingen tussen onderling resonerende golven. Het model is toegepast voor homogenene situaties. Er zijn twee soorten windvelden gebruikt, een plotselinge verandering van de windrichting en een constant draaiende wind. In alle berekeningen is een constante windsnelheid gebruikt.

De modelresultaten laten zien dat het draaien van de golfrichting tot op zekere hoogte wordt tegengewerkt door het effect van dissipatie en niet-lineare wisselwerkingen. Zij laten ook zien dat de tijdschaal van de golfrichtingsresponsie toeneemt met toenemende groeifase van de golven. Voor bijna-volgroeide golven nemen de tijdschalen sterk toe.

Een gedeelte van de berekeningen is uitgevoerd met het operationele derde generatie WAM golfvoorspellingsmodel, om te controleren in hoeverre dit model in staat is de EXACT-NL resultaten te reprodu-

ceren. Dit is van belang omdat het WAM model de niet-lineaire wisselwerkingen op een soortgelijke, doch beperktere, manier berekent.

In het empirische deel van deze studie zijn WAVEC golfrichtingsboeien op twee lokaties in de centrale Noordzee gebruikt om tijdreeksen van integrale golfparameters, zoals de gemiddelde golfrichting, te verzamelen. Tegelijkertijd zijn op nabij gelegen boorplatforms metingen van windsnelheid en windrichting uitgevoerd. Om het effect te bepalen van lokaal geïnduceerde veranderingen van de gemiddelde golfrichting, zijn de metingen bewerkt met resultaten van het operationele WINCH golfvoorspellingsmodel om het effect van inhomogeniteiten in het golfveld te verdisconteren.

Er is voor gezorgd om alleen die metingen te analyseren die behoren bij windzee situaties op diep water. Voor elke schatting van de tijdschaal is een foutenanalyse uitgevoerd om het mogelijk te maken slechts die schattingen te presenteren waarvoor de relatieve fout beneden een vooraf bepaalde grenswaarde ligt.

De resultaten van de metingen tonen een trend van stijgende tijdschaal met toenemende groeifase van de golven, hoewel er een aanzienlijke spreiding overblijft.

Vergelijking van de huidige resultaten van de berekeningen met die van de waarnemingen geeft aan dat de trend van tijdschaal met groeifase sterker is voor de modelresultaten dan die voor de waarnemingen. Bovendien zijn de modeltijdschalen i.h.a. veel groter dan die van de waarnemingen, behalve voor jonge zeegang.

Een aantal gepubliceerde datasets is opnieuw geanalyseerd teneinde het verschil in grootte tussen twee verzamelingen van tijdschalen te verklaren. De resultaten van deze heranalyse tonen aan dat dit verschil mogelijk te wijten is aan de methode van analyse van de golfrichtingswaarnemingen.

ABSTRACT

In the present study the directional response of wind generated waves to turning winds is studied theoretically by using numerical wave prediction models, and empirically by using the results of directional wave measurements in the open ocean.

This study concentrates on two aspects of the directional response. The first aspect pertains to the physical processes active during the response of the waves. The second is the relation between the time scale of the directional response and local wind- and wave parameters. To that end a relaxation model is used which relates the locally induced rate of change of the mean wave direction to the angle between the direction of the wind and the mean wave direction.

The directional response has been studied theoretically with a third-generation wave prediction model, viz. the EXACT-NL model. This model has the ability to represent the physics of wind waves rather well, which holds especially for the nonlinear transfer between resonantly interacting waves. This model has been applied to homogeneous situations. Two types of wind fields have been used. These are a sudden shift of the wind direction and a constantly turning wind. In all computations a constant wind speed was used.

The model results indicate that the turning of the wave direction is counteracted to some degree by the effects of dissipation and nonlinear transfer. They also indicate that that the time scale of the directional response of the mean wave direction increases with increasing growth stage of the waves. For nearly fully developed waves the results show a rapid increase in time scale.

Part of the computations has also been performed with an operational third-generation wave prediction model, viz. the WAM model, to verify the capabilities of this model with respect to those of the EXACT-NL

model. This is of interest since the WAM model calculates the non-linear transfer in a similar, but more limited, way than the EXACT-NL model.

In the empirical part of this study WAVEC pitch-and-roll buoys have been used at two locations in the central North Sea, to collect time series of integral wave parameters, such as the mean wave direction, together with measurements of wind speed and direction at nearby offshore platforms. To isolate local effects on the change of mean wave direction, the measurements have been treated with results of an operational numerical wave hindcast model, viz. the WINCH model, to account for the effect of inhomogeneities in the wave field.

Care has been taken to analyse only those measurements corresponding to actively wind driven seas in deep water. In addition an error analysis has been performed on each time scale estimate to facilitate selection of those estimates for which the relative error is lower than some preset threshold value.

The results of the measurements show a trend of increasing time scale with increasing growth stage of the waves, although a considerable scatter remains.

Comparison of the present results from the computations with those from the observations shows that the trend of time scale with growth stage is stronger for the model results than for the observational results. In addition the model time scales are generally at a much higher level than the empirical ones, except for young sea states.

A number of published data sets have been reanalyzed in an attempt to reveal the reason for the existence of reported differences between published sets of time scales. The results of this re-analysis indicate that these differences are probably due to the method of analysis of the directional wave measurements.

CHAPTER 1

INTRODUCTION

1.1 Background

Knowledge of wind generated wave conditions is of great importance for many marine activities, such as operational ship routing and the design of offshore structures. An important source for this information are wave prediction models. In the determination of these wave conditions by such models, directional aspects have become increasingly important. One of these aspects, the mean direction of the waves and its relation to changing wind directions, is the subject of this thesis.

Usually the surface of the sea has a chaotic appearance. All kinds of waves are coming from different directions, each with its own wave period and wave length. The underlying structure of these waves can be fairly well described by means of the energy spectrum, which gives the distribution of wave energy as a function of frequency, wave number and direction. For many applications this spectrum is readily reduced to a two-dimensional or one-dimensional spectrum.

For a number of applications the sea surface is described in terms of a relatively few characteristic parameters, such as the total energy per unit area, the peak frequency and mean wave direction. These characteristics are easily deduced from the energy spectrum.

Simultaneous wave and wind measurements indicate that the mean wave direction is strongly related to the direction of the wind. For a wind field that is homogeneous in space and stationary in time, the mean wave direction is found to be equal to the direction of the wind. However, this coincidence is lost when the direction of the wind changes. The mean wave direction follows the wind direction with a

certain time lag. When the direction of the wind remains constant thereafter, the mean wave direction becomes equal to the wind direction again. This behaviour of wind waves is called the directional response.

Detailed measurements show that the two-dimensional spectrum of wind waves tends to have some standard shape. It is now understood that the mechanism, which is responsible for this shape, is the nonlinear transfer of energy between different spectral components. It is also assumed that this nonlinear transfer plays an important role in the directional response of wind waves.

Changing wind directions can only be observed in non-stationary wind fields. These fields are either homogeneous or inhomogeneous and generate wave fields that are also homogeneous or inhomogeneous, respectively. In inhomogeneous wave fields an observed change of the mean wave direction at a fixed location is in general due to two effects:

1) local processes (generation of wave energy by the local wind, nonlinear wave-wave interactions and dissipation), and
2) transport of wave energy from the surrounding area.

The local processes will cause the mean wave direction to turn towards the direction of the wind, whereas the transport of wave energy may turn it towards an arbitrary direction. Which of these two effects is dominant is difficult to determine on the basis of the measurements only. From a research point of view only the study of the effect of the local processes is of interest; the transport of wave energy is well known.

The directional response of wind waves has been studied by various authors using results of observations obtained from pitch-and-roll buoys (cf. Hasselmann et al., 1980, Günther et al., 1981, Allender et al., 1983 and Holthuijsen et al., 1987). However, such observations do not provide sufficient information about the separate physical processes active during the response. Therefore, the basic understanding of

the directional response is not well developed. For lack of that, in the above studies, the change of the mean wave direction is modelled as a relaxation process with an associated unknown time scale. In such a model the mean wave direction turns towards the wind direction.

Quantitative knowledge of the time scale of the response of the mean wave direction is useful for the so-called parametric wave models. Such models describe the local wave field in terms of a relatively small number of characteristic parameters. In these models the slow evolution of these parameters in time and space is calculated on the basis of conservation laws. One of the relations used in such models concerns the change of the mean wave direction with respect to the wind direction.

The collection of data that can be used for the determination of the time scale of the directional response due to local effects is hampered by the fact that for single point measurements it is impossible to estimate the effect of the transport of wave energy on the change of the mean wave direction. In the past wave measurements have been selected in such a way that the effects of the local processes can reasonably be assumed to dominate over the effects of the transport of wave energy (e.g. Hasselmann et al., 1980). To that end, in the above studies, more or less subjective criteria were applied to select the data. However, the requirements imposed on the data were often too strict to obtain a sufficiently large number of observations for a reliable, quantitative estimation of these time scales. These problems can be remedied by estimating the effect of transport on the rate of change of the mean wave direction to isolate the local effects.

From the theoretical point of view the directional response can be studied using numerical wave prediction models that should have the ability to model each relevant physical process. A class of such models are discrete spectral models that describe the wave field as the sum of a finite number of spectral components. Models of this kind

use the balance of wave energy for each spectral component as it propagates over the ocean surface, and they use source functions to model each physical process affecting the energy content of each component. Of these source terms, relatively simple formulations are available for the computation of the generation of wave energy and dissipation. For the nonlinear transfer the theory is well established, but the computation of this transfer is too time consuming for routine use in wave prediction models. However, since the nonlinear transfer has been found to be essential for the evolution of the wave field, it cannot be omitted (SWAMP, 1985).

The directional response has been studied by Young et al. (1987) using an advanced wave prediction model that has the capability to compute this nonlinear transfer rather accurately, viz. the EXACT-NL model (Hasselmann and Hasselmann, 1985a). The results of their computations provide interesting results concerning qualitative and quantitative aspects of the directional response, which can be useful for this study. However, there quantitative results provide insufficient information about the separate physical effects on the rate of change of the mean wave direction. In addition their quantitative results refer only to young sea states.

1.2 Aims and scope

The purpose of this study is to investigate the directional response of wind generated waves with respect to the different physical processes active during the response and to determine the rate of change of the frequency integrated mean wave direction as a function of local wind and wave parameters. To that end theoretical models are used to study this response. The results obtained with them are compared with careful measurements in the open ocean of locally induced changes of the mean wave direction.

1.3 Method of analysis

This study consists of three parts; a summary and synthesis of the present knowledge about the directional response of wind waves, numerical computations with advanced wave prediction models and directional observations in the open ocean.

In the first part of this study the existing literature with respect to the directional response is analysed to reveal discrepancies and shortcomings in the existing results.

In the second part the directional response is studied theoretically using the numerical wave prediction model EXACT-NL. This model has the capability to represent the physics rather well, which holds especially for the nonlinear transfer.

The model is applied to homogeneous situations for which the computations are relatively simple since the transport of wave energy can be omitted from the energy balance equation. In this study computations are carried out for two kinds of idealized situations: a sudden wind shift and a wind direction that is turning with a constant angular velocity. In all situations a constant wind speed is used. Based on these computations estimates are made of the time scale of the directional response and presented as a function of the growth stage of the waves. In addition the contributions of the different physical processes to the rate of change of the mean wave direction are studied. Finally, the sensitivity of the time scale to variations in the modelling of the dissipation source function is studied.

Part of the computations have also been carried out by an operational wave prediction model, viz. the WAM model (WAMDI group, 1988), to verify its capabilities in turning wind situations in comparison with the EXACT-NL model. This is of interest since the WAM model uses a recently developed parameterization of the nonlinear transfer, which

computes this transfer in a similar, but more limited, way than the EXACT-NL model.

In the empirical part of the study directional wave measurements are made in turning wind fields using pitch-and-roll buoys deployed in the central North Sea. To isolate the effect of the local wind on the change of the mean wave direction, the effect of the transport of energy is estimated using the results of a numerical wave prediction model, viz. the WINCH model (Eide et al., 1986). Based on the wave measurements time scale estimates are obtained of the rate of change of the directional response. In the determination of these estimates an error analysis is performed to obtain a quantified measure of the reliability of the results.

The results of this study indicate that the directional response which is primarily due to the effect of the generation of wave energy is counteracted to some degree by the effect of nonlinear transfer and wave dissipation. The results also indicate that both the model and the empirical time scales of the directional response increase with the growth stage of the waves. It is also found that the observed time scales are much lower than could be expected on the basis of existing measurements and theoretical models.

The content of this thesis is as follows. The state of the art with respect to wave modelling and the directional response is reviewed in chapter 2. Basic wind- and wave parameters needed in the subsequent analysis are defined in this chapter; it ends with a (re)-analysis of available results concerning the time scales of the directional response in an attempt to investigate and possibly remove discrepancies between them. The models used for the calculation of the theoretical directional response and the results obtained with them are described in chapter 3. Chapter 4 contains a description of the wave and wind measurements, the method of isolating local effects from the measurements, the error analysis and the results obtained with them. In chapter 5 the results of the computations and the observa-

tions are compared with each other, and with results from the literature. In addition this chapter gives some comments about the applicability of the results. Finally, a summary and conclusions are given in chapter 6.

CHAPTER 2

STATE OF THE ART

2.1 Introduction

The purpose of this chapter is to give a brief review of the present understanding of the directional response of wind waves to changing wind directions. As part of that a number of concepts and definitions are summarized, which are commonly used in the description of wind generated waves. This chapter is divided in two parts. In the first part (section 2.2) the spectral description of wind waves is presented. It is noted that state of the art formulations presented here are also used in this study, unless stated otherwise. The material in this part is rather standard and can be skipped by readers who are knowledgeable in this subject. The second part (section 2.3) presents the state of the art of the understanding and the modelling of the directional response of wind waves to changes in the wind direction; this part contains some new elements in the discussion of previous publications, which are highly relevant to the remaining chapters.

2.2 Description of wind generated waves

2.2.1 Spectral description of wind waves

In the description of wind generated waves it is customary to distinguish a number of scales in time and space. In this review three scales are considered. These scales vary from the order of a number of seconds and meters to a scale of the order of days and hundreds of kilometers. The first scale is of the order of one wave period or one wave length. Details thus revealed are random in nature. A systematic investigation of wave features requires an averaging of these details.

Such an averaging is made in the second scale which is of the order of hundreds of wave periods and wave lengths. Within this second scale characteristic statistical properties of the sea surface are considered to be stationary and homogeneous. The third and largest scale covers entire seas or oceans and has a time scale in the range of a few hours to some days. Within this third scale the statistical properties of the sea surface, as defined in the second scale, vary slowly. For the study of the directional response of wind waves, the second and third scale are used. The second scale is used to define integral wave parameters such as a mean wave direction whereas the third scale is used to study the variation of a mean wave direction in time.

In the first scale, the sea surface elevation is described as a function of time t and horizontal coordinate $\underline{x}$ and is denoted by $\eta(\underline{x},t)$. In linear wave theory the sea surface elevation is considered as the sum of an infinite number of sinusoidal wave components, where each wave component has its own period, wave length and direction of propagation. It is often represented by the random phase model:

$$\eta(\underline{x},t) = \sum_{n=1}^{\infty} a_n \cos(\omega_n t - \underline{k}_n \cdot \underline{x} + \varphi_n) \qquad (2.1)$$

in which a_n is the amplitude, $\underline{k}_n$ is the wavenumber vector and ω_n is the angular frequency. The phases φ_n of different wave components are assumed to be stochastically independent, each distributed uniformly over the interval $(0,2\pi)$. In this approximation the instantaneous surface elevation at a fixed point has a Gaussian distribution, which follows from the application of the central limit theorem.

The random phase model represents a Gaussian process which is stationary in time and homogeneous in space and which is completely determined by its auto-covariance function:

$$C(\underline{r},\tau) = \overline{\eta(\underline{x},t)\ \eta(\underline{x}+\underline{r},t+\tau)}. \qquad (2.2)$$

In Eq. (2.2) C is the auto-covariance function which is a function of a displacement vector $\underline{r}$ and a time lag τ. The overbar denotes averaging with respect to time and space in the second scale. The variance C(0,0) is equal to the mean square surface elevation $\overline{\eta^2}$.

The auto-covariance function is not as convenient for the representation of wind waves as the variance density spectrum. This spectrum is defined as the Fourier transform of the auto-covariance function:

$$E(\underline{k},f) = (2\pi)^{-2} \int_{-\infty}^{\infty} \int_{-\infty}^{\infty} C(\underline{r},\tau)\ e^{-i(\underline{k}\cdot\underline{r} + 2\pi f\tau)}\ d\underline{r}\ d\tau \qquad (2.3)$$

where $E(\underline{k},f)$ is the three-dimensional variance density spectrum.

The variance of the sea surface elevation is equal to the following integral of the spectrum:

$$\overline{\eta^2} = \int_{-\infty}^{\infty} \int_{-\infty}^{\infty} E(\underline{k},f)\ d\underline{k}\ df. \qquad (2.4)$$

Multiplication of the variance of the sea surface elevation by a factor $\rho_w g$ gives the energy per unit area of the waves. Here ρ_w is the mass density of water and g is the gravitational acceleration. Because of the close relationship between variance and energy, variance spectra are often loosely referred to as energy spectra.

The three-dimensional spectrum (2.3) is not always a convenient representation of wind waves. In this study reduced versions of this three-dimensional spectrum are used. These are obtained by projecting the three-dimensional spectrum (2.3) on a sub-space of the wavenumber-frequency space, such as the frequency axis, the frequency-direction space or the wavenumber space (e.g. Phillips, 1977).

The three-dimensional spectrum $E(\underline{k},f)$ is readily reduced to two dimensions by integrating it with respect to frequency. Since $E(\underline{k},f)$ is an even function of frequency, the two-dimensional wavenumber spectrum can be expressed as:

$$E(\underline{k}) = 2 \int_0^\infty E(\underline{k},f)\, df. \tag{2.5}$$

The wavenumber vector $\underline{k}$ in Eq. (2.5) has a magnitude k and direction θ. According to linear wave theory the wavenumber k and the frequency f are related through the linear dispersion relation. In general this relation depends on the water depth d and the mean current velocity $\underline{v}$. For deep water and without the presence of currents the linear dispersion relation is given by:

$$(2\pi f)^2 = g\, k. \tag{2.6}$$

Using the dispersion relation (2.6) the two-dimensional wavenumber spectrum $E(\underline{k})$ can be written as a function of frequency f and direction θ. This two-dimensional spectrum $E(f,\theta)$ is obtained from the two-dimensional wavenumber spectrum by:

$$E(f,\theta) = E(\underline{k})\, J \tag{2.7}$$

in which J is the Jacobian of this transformation, given by:

$$J = \frac{\partial \underline{k}}{\partial (f,\theta)} = \frac{4\pi}{g^{1/2}}\, k^{3/2}. \tag{2.8}$$

Like the wavenumber spectrum $E(\underline{k})$, the two-dimensional spectrum $E(f,\theta)$ is frequently used in this study.

The frequency spectrum is obtained from the two-dimensional spectrum $E(f,\theta)$ by integration with respect to direction:

$$E(f) = \int_0^{2\pi} E(f,\theta)\, d\theta. \qquad (2.9)$$

The frequency spectrum E(f) gives the distribution of wave energy as a function of frequency.

The two-dimensional spectrum $E(f,\theta)$ is often written as the product of the frequency spectrum E(f) and a directional distribution function $D_f(\theta)$:

$$E(f,\theta) = E(f)\, D_f(\theta). \qquad (2.10)$$

The subscript f indicates that in general the directional distribution function is frequency dependent.

The directional distribution $D_f(\theta)$ is considered as a density function with the following properties:

$$D_f(\theta) \geq 0 \qquad \text{with} \quad 0 \leq \theta \leq 2\pi \qquad (2.11)$$

and

$$\int_0^{2\pi} D_f(\theta)\, d\theta = 1. \qquad (2.12)$$

2.2.2 Frequency spectra

In this study two types of idealized frequency spectra are used. These are the Pierson-Moskowitz spectrum and the JONSWAP spectrum.

Pierson and Moskowitz (1964) proposed a spectral form which describes

the frequency spectrum of fully developed seas:

$$E_{PM}(f) = \alpha g^2 (2\pi)^{-4} f^{-5} \exp\left(-\frac{5}{4} \left(\frac{f}{f_{PM}} \right)^{-4} \right) \qquad (2.13)$$

where α is Phillips' constant, equal to 0.0081, and f_{PM} is the peak frequency of the spectrum which is related to the wind speed at 19.5 m height by:

$$f_{PM} = 0.14\ g/U_{19.5} \qquad (2.14)$$

or in terms of the wind speed at 10 m height U_{10}:

$$f_{PM} = 0.13\ g/U_{10}. \qquad (2.15)$$

The spectral form (2.13) is commonly referred to as the Pierson-Moskowitz spectrum.

During the JONSWAP project (Hasselmann et al., 1973) it was found that the spectral form (2.13) did not adequately describe the spectral form of observed young developing seas which were much more peaked than the Pierson-Moskowitz spectral form. On the basis of extensive measurements during the JONSWAP project Hasselmann et al. (1973) proposed the following spectral form:

$$E_J(f) = \alpha g^2 (2\pi)^{-4}\ f^{-5} \exp\left[-\frac{5}{4} \left(\frac{f}{f_p} \right)^{-4} \right]\ \gamma^{\exp\left[-\frac{1}{2} \left(\frac{f-f_p}{\sigma f_p} \right)^2 \right]} \qquad (2.16)$$

in which γ is the peak enhancement parameter, σ is a factor determining the width of the peak enhancement, and f_p is the frequency at which this spectrum has its maximum. The factor σ has different values at each side of the peak:

$$\sigma = \begin{cases} \sigma_a & \text{for } f \leq f_p \\ \sigma_b & \text{for } f > f_p. \end{cases} \qquad (2.17)$$

The scale parameters α and f_p were found to be fetch dependent. However, no dependence on fetch was found for the shape parameters γ, σ_a and σ_b; their mean values, given by $\gamma = 3.3$, $\sigma_a = 0.07$, $\sigma_b = 0.09$, together with the parameterized variations of α and f_p with growth stage, define a mean JONSWAP spectrum.

Essentially the JONSWAP spectrum represents a generalization of the Pierson-Moskowitz spectrum, through the inclusion of fetch as an additional parameter to wind speed. Since the JONSWAP project, spectral forms similar to Eq. (2.16), with $\gamma > 1$, have been measured by various authors (e.g. Rye et al., 1974; Bouws and Komen, 1983).

The high frequency tail

An important aspect of the shape of frequency spectra is the parameterization of the high frequency tail. At the present time two parameterizations are the subject of many studies. These studies deal with the question whether the energy density in the high frequency tail of the spectrum is proportional to f^{-4} or to f^{-5}. Some comments about this matter are made since in this study both parameterizations are used in numerical models for the calculation of the theoretical directional response of wind waves.

Phillips (1958) argued that there should be a range of frequencies where the spectral density E(f) is governed by wave breaking and saturated at a level determined exclusively by the local frequency (f) and the gravitational acceleration (g). On dimensional grounds this saturation range should be proportional to $g^2 f^{-5}$. It can be written as:

$$E(f) = (2\pi)^{-4}\alpha g^2 f^{-5} \qquad (2.18)$$

where α is a universal constant. This formulation was used by Pierson and Moskowitz (1964) for the spectrum of a fully developed sea and by Hasselmann et al. (1973) for the spectrum of growing seas (the JONSWAP spectrum). However, Hasselmann et al. (1973) found that the value of α varied with the growth stage of the waves, hence α cannot be considered as a universal constant.

Another approach to the formulation of the saturation range is given by Toba (1972 and 1973). His result is:

$$E(f) = (2\pi)^{-3}\beta g u_* f^{-4} \qquad (2.19)$$

where β is supposed to be a universal constant, and u_* is the friction velocity which is defined as the square root of the ratio of the surface stress caused by the wind and the density of air (see section 2.2.7.2). Empirical support for the Toba-parameterization is provided by e.g. Mitsuyasu et al. (1980), Kahma (1981), Forristall (1981), Donelan et al. (1985) and Battjes et al. (1987), while theoretical support for an f^{-4} parameterization is given by e.g. Kitaigorodskii (1983) and Phillips (1985).

Although both parameterizations are implemented in the numerical models used in study, a discussion about the correct parameterization of the high frequency tail is beyond the scope of this study. A recent discussion about this matter can be found in Battjes et al. (1987).

2.2.3 Directional characteristics of wind waves

2.2.3.1 Parameters of $D(\theta)$

For many applications involving wave directionality, knowledge of a few characteristic directional parameters is sufficient, such as the mean wave direction and a directional width. Various definitions exist for parameters of the directional distribution (e.g. Kuik et al., 1988). Since in this study pitch-and-roll buoys are used, directional parameters should be based on the Fourier coefficients of the directional distribution (see appendix A).

The directional distribution function $D_f(\theta)$ can be written as an infinite Fourier series (Longuet-Higgins et al., 1963):

$$D_f(\theta) = \frac{1}{\pi}\left[\frac{1}{2} + \sum_{n=1}^{\infty}\left(a_n(f)\cos(n\theta) + b_n(f)\sin(n\theta)\right)\right]. \qquad (2.20)$$

The coefficients $a_n(f)$ and $b_n(f)$ can be computed from the directional distribution $D_f(\theta)$ as:

$$\begin{pmatrix} a_n(f) \\ b_n(f) \end{pmatrix} = \int_0^{2\pi} \begin{pmatrix} \cos(n\theta) \\ \sin(n\theta) \end{pmatrix} D_f(\theta)\, d\theta. \qquad (2.21)$$

These Fourier coefficients can be used to define parameters of the directional distribution $D_f(\theta)$, such as the mean wave direction $\theta_{0,f}$ or the directional width σ_f. In this study the mean wave direction $\theta_{0,f}$ is defined as the vectorial mean of the directional distribution function:

$$\theta_{0,f} = \arctan\left(b_1(f)/a_1(f)\right). \qquad (2.22)$$

This expression has originally been suggested by Gumbel et al. (1953) and adopted by Borgman (1969) and Mardia (1972). For the directional

width σ_f the definition given by Borgman (1969, his Eq. 77) is used:

$$\sigma_f = \left(2 - 2\, m_{1,f} \right)^{1/2} \tag{2.23}$$

in which

$$m_{1,f} = \left(a_1^2(f) + b_1^2(f) \right)^{1/2}. \tag{2.24}$$

The theoretical maximum value of σ_f in this model is $\sqrt{2}$ radians $\cong 81^\circ$. It occurs for an isotropic wave field. The mean wave direction $\theta_{0,f}$ and directional width σ_f are descriptive and easy to compute.

The above defined directional parameters are defined for each frequency of the spectrum $E(f,\theta)$. For many purposes, as in this study, this is too comprehensive. In these cases the frequency averaged mean wave direction θ_0 and directional width σ are used. They are defined as:

$$\theta_0 = \arctan\,(b_E/a_E) \tag{2.25}$$

and

$$\sigma = \left(2 - 2\, m_E \right)^{1/2} \tag{2.26}$$

with

$$m_E = \left(a_E^2 + b_E^2 \right)^{1/2} \tag{2.27}$$

in which

$$a_E = \int_0^{2\pi} \int_0^{\infty} \cos(\theta)\, E(f,\theta)\, df\, d\theta \tag{2.28}$$

and

$$b_E = \int_0^{2\pi} \int_0^{\infty} \sin(\theta)\, E(f,\theta)\, df\, d\theta. \qquad (2.29)$$

2.2.3.2 Models for $D(\theta)$

In the literature a number of models for the directional distribution have been suggested. These models were proposed for wave fields that are homogeneous in space and stationary in time. Such wave fields have a directional distribution function that is symmetric with a maximum at the wind direction θ_w. A frequently used model is given by:

$$\begin{aligned} D_f(\theta) &= \frac{2}{\pi} \cos^2(\theta-\theta_{0,f}) && |\theta - \theta_{0,f}| \le \pi/2 \\ &= 0 && |\theta - \theta_{0,f}| > \pi/2 \end{aligned} \qquad (2.30)$$

where $\theta_{0,f} = \theta_0 = \theta_w$, the mean wave direction. The formulation (2.30) states that there is no wave energy propagating in upwind directions.

Another frequently used directional distribution function is the cos-2s model which is given by Longuet-Higgins et al. (1963) as:

$$D_f(\theta) = A(s) \cos^{2s}\left(\frac{\theta - \theta_{0,f}}{2} \right) \qquad (2.31)$$

with A a normalization factor given by:

$$A(s) = \frac{1}{2\sqrt{\pi}} \frac{\Gamma(s+1)}{\Gamma(s + 1/2)} \qquad (2.32)$$

in which $\Gamma()$ is the gamma function. The exponent 2s determines the width of the directional distribution. In many applications it is assumed that s is constant and equal for all frequencies. However,

observations by e.g. Mitsuyasu et al. (1975), Hasselmann et al. (1980), Holthuijsen (1983) and Donelan et al. (1985) suggest that the width of the directional distribution is frequency dependent, with a minimum near the peak of the spectrum.

For the cos-2s-model the directional width σ as defined by Eq. (2.26) is related to the exponent 2s by:

$$\sigma = \left(\frac{2}{s + 1} \right)^{1/2} . \qquad (2.33)$$

2.2.4 Energy balance equation

In the previous section the concept of the spectrum was introduced for a locally stationary and homogeneous wave field. A convenient method to study the slow evolution of the wind wave spectrum in time and space is to keep track of the energy density of each wave component as it propagates over the ocean surface, as expressed in the energy balance equation (Gelci et al., 1956; Hasselmann, 1960). For deep water and without the presence of currents this equation is given by:

$$\frac{\partial E(f,\theta;\underline{x},t)}{\partial t} + \underline{c}_g(f)\cdot\nabla E(f,\theta;\underline{x},t) = S(f,\theta;\underline{x},t). \qquad (2.34)$$

In this method each wave component propagates independently from the others. The propagation velocity of wave energy of each wave component is given by the group velocity vector $\underline{c}_g$. For deep water this has a magnitude given by:

$$c_g(f) = g/(4\pi f). \qquad (2.35)$$

The term $S(f,\theta;\underline{x},t)$ on the right-hand side of Eq. (2.34) describes the effect of local processes of growth and decay of wind waves. For deep water the source term S is normally considered as the sum of three source terms:

$$S = S_{in} + S_{ds} + S_{nl} \qquad (2.36)$$

in which S_{in} is the energy input by the wind, S_{ds} is the dissipation of energy and S_{nl} is the transfer of energy within an energy spectrum due to nonlinear wave-wave interactions. These source terms are described in the next section. The energy balance Eq. (2.34) is the basis of many numerical wave prediction models. A brief review of such models is given in section 2.2.8.

2.2.5 Description of source terms

2.2.5.1 Atmospheric input

Introduction

The first systematic studies of the generation of waves by the action of the wind date back to the beginning of this century. After some unsuccessful theories describing the growth of wind waves (e.g. Jeffreys, 1925), considerable progress was made by Phillips (1957) and Miles (1957) in two complementary papers describing the principles of the flux of momentum and energy from the atmosphere to the wave field.

In the growth of wind waves two phases can be distinguished. In the first phase the waves have no effect on the wind profile, whilst they do affect the wind profile in the second phase. The first phase was studied by Phillips (1957), who found that the energy density of a wave component increases linearly with time.

The second phase was analysed by Miles (1957) who found that the rate of input of energy to a wave component is proportional to the energy density of that wave component so that the energy density grows exponentially with time. In general the exponential growth rate is much larger than the linear growth rate of the waves.

Modelling of the wind input

The linear and the exponential growth of a wave component with frequency f, direction θ and energy density $E(f,\theta)$ can be modelled as:

$$S_{in}(f,\theta) = A + B\,E(f,\theta) \qquad (2.37)$$

in which A and B are complicated functionals of the energy spectrum

$E(f,\theta)$ and the wind vector. The linear growth term is often omitted in wave prediction models since it is usually negligible compared to the exponential growth term.

Based on a parameterization by Snyder et al. (1981) a wave generation source term was proposed by Komen et al. (1984) who scale wave growth in terms of the friction velocity u_*:

$$S_{in}(f,\theta) = \max\left(0,\ 0.25\ \frac{\rho_a}{\rho_w}\ \omega\left(28\beta\left(\frac{u_*}{c}\right)\cos(\theta-\theta_w) - 1\right)E(f,\theta)\right) \qquad (2.38)$$

where ρ_a is the density of water, $\omega = 2\pi f$ is the radian frequency, c is the phase velocity of a wave with frequency f, θ_w is the wind direction and β is an empirical coefficient which is close to unity. The factor β was introduced by Komen et al. (1984) to account for different opinions about the relation between the wind speed at a given height and the friction velocity. In this study $\beta = 1$ is used.

2.2.5.2 Dissipation of wave energy

Introduction

Dissipation of wave energy in deep water occurs mainly by wave breaking. In the open ocean waves may become instable and break, e.g. if the water particles in the crest move faster than the mean wave profile. The breaking of waves in the open ocean is manifested by the occurrence of white patches. For that reason, deep water wave breaking is also referred to as whitecapping.

Modelling of the dissipation

The quantitative description of the dissipation of energy by wave breaking is very difficult because it is a nonlinear process with very

short time scales. The precise form of the dissipation function is not (yet) known. A first theoretical study of whitecapping and its effect on the energy spectrum was given by Hasselmann (1974). He assumed that the dissipation of wave energy is related to the wavenumber spectrum in a quasi-linear manner,

$$S_{ds}(\underline{k}) = - \psi_d \omega^2 E(\underline{k}) \tag{2.39}$$

in which ψ_d is constant for a given spectrum. It depends on integral spectral parameters, such as the average wave steepness.

The dissipation source function was studied numerically by Komen et al. (1984) in an investigation of the structure of the energy balance equation of a fully developed wave spectrum. For that purpose they generalized Eq. (2.39) to

$$S_{ds}(f,\theta) = -C \bar{\omega} \left(\frac{\omega}{\bar{\omega}} \right) \left(\frac{\hat{\alpha}}{\hat{\alpha}_{PM}} \right)^m E(f,\theta) \tag{2.40}$$

in which $\bar{\omega}$ is the mean radian frequency defined by:

$$\bar{\omega} = 2\pi \int_0^{2\pi} \int_0^{\infty} f \, E(f,\theta) \, df \, d\theta \, / \, E_{tot} \tag{2.41}$$

with E_{tot} the total wave energy:

$$E_{tot} = \int_0^{2\pi} \int_0^{\infty} E(f,\theta) \, df \, d\theta. \tag{2.42}$$

$\hat{\alpha}$ is the integral mean wave steepness defined as:

$$\hat{\alpha} = E_{tot} \bar{\omega}^4 / g^2. \tag{2.43}$$

The term $\hat{\alpha}_{PM}$ is the theoretical value of $\hat{\alpha}$ for a Pierson-Moskowitz spectrum, with the value 4.57×10^{-3}. The constant C determines the overall level of dissipation. The exponent n determines the position of the maximum dissipation relative to the peak of the spectrum and the exponent m determines the dependence of dissipation on the wave steepness. For n = 2 Eq. (2.40) is in agreement with Hasselmann (1974).

In their study Komen et al. (1984) varied the values of C and n in order to determine which values gave realistic spectra. The value of m was not varied since their interest was limited to nearly fully developed spectra for which the term $(\hat{\alpha}/\hat{\alpha}_{PM})$ is nearly equal to one, in which case the value of m is of little importance. The value of m is important only for young, developing seas.

The results of their analysis demonstrated that for the combination of m = 2, n = 2 and $C = 3.33 \times 10^{-5}$ an almost stationary solution could be obtained. This solution consists of a two-dimensional spectrum $E(f,\theta)$ with spectral parameter values close to those of a Pierson-Moskowitz spectrum. The formulation (2.40) with these parameter values is also used in this study.

2.2.5.3 Nonlinear wave-wave interactions

Introduction

For many applications the sea surface can be described as the sum of an infinite number of mutually independent wave components provided the scale of the wave field is not too large in space and time. However, the wave components do interact resulting in a low rate of nonlinear transfer of energy, which becomes significant for time scales of the order of magnitude of a few hours or a large number of wave periods.

A general perturbation theory for the nonlinear resonant interactions of free waves in a random sea was developed by Hasselmann (1962, 1963a and 1963b). He found that a set of four waves could exchange energy when the following resonance conditions are satisfied:

$$\underline{k}_1 + \underline{k}_2 = \underline{k}_3 + \underline{k}_4 \tag{2.44}$$

$$f_1 + f_2 = f_3 + f_4 \tag{2.45}$$

in which f_j is related to the wavenumber $\underline{k}_j$ ($j = 1,..,4$) by the linear dispersion relation (2.6). A group of four interacting waves is also referred to as a wavenumber quadruplet.

Hasselmann (1962) describes the nonlinear interactions between wave quadruplets in terms of their action density, defined as the ratio of the energy density E and the radian frequency ω. The rate of change of action density of a wave component is given by (Hasselmann, 1962):

$$\frac{\partial N_4}{\partial t} = \int_{-\infty}^{\infty}\int_{-\infty}^{\infty}\int_{-\infty}^{\infty} G(\underline{k}_1,\underline{k}_2,\underline{k}_3,\underline{k}_4)\ \delta(\underline{k}_1+\underline{k}_2-\underline{k}_3-\underline{k}_4)\ \delta(\omega_1+\omega_2-\omega_3-\omega_4)$$

$$\times\ (N_1N_2(N_3 + N_4) - N_3N_4(N_1 + N_2))\ d\underline{k}_1\ d\underline{k}_2\ d\underline{k}_3 \tag{2.46}$$

in which G is the coupling coefficient given by:

$$G = \frac{\pi\, g^2\, D^2}{4\, \rho_w^2 \omega_1\omega_2\omega_3\omega_4} \tag{2.47}$$

where $N_i = N(\underline{k}_i)$ is the action density at wavenumber $\underline{k}_i$, D is the interaction coefficient. The delta-functions in Eq. (2.46) reflect the resonance conditions (2.44) and (2.45). The interaction coefficient D is a complicated function of the wavenumbers $\underline{k}_1$, $\underline{k}_2$, $\underline{k}_3$ and $\underline{k}_4$; it is given in appendix B.

The integral expression (2.46) is also known as the Boltzmann integral for wind waves, in analogy to similar integrals used in theoretical physics to describe the rate of change of particle density distributions in a system of interacting particles. The concept of the Boltzmann integral in the study of wind waves was introduced by Hasselmann (1963a).

The nonlinear transfer conserves the total energy and momentum of the wave field. It has therefore no effect on the mean direction of wave momentum. The main effect of nonlinear interactions is that they redistribute momentum and energy among spectral components.

A consequence of the conservation of wave action for the interactions within one wavenumber quadruplet with wavenumbers $\underline{k}_1$, $\underline{k}_2$, $\underline{k}_3$ and $\underline{k}_4$ is that the absolute value of the rate of change of the action density is equal for all wavenumbers in such a quadruplet:

$$\frac{dN_1}{dt} = \frac{dN_2}{dt} = -\frac{dN_3}{dt} = -\frac{dN_4}{dt} \,. \qquad (2.48)$$

This is useful in methods for the computation of the nonlinear transfer, e.g. the method of Hasselmann and Hasselmann (1981).

Properties of the nonlinear interactions

The nonlinear interactions near the peak of the spectrum have been studied extensively by numerous authors. Results of numerical computations of the nonlinear transfer for broad spectra, such as the Pierson-Moskowitz spectrum, were presented by Hasselmann (1963b) and Webb (1978) who show that the peak of the spectrum gains energy at the expense of wave energy at high frequencies. However, results of similar computations for narrow spectra (e.g. Hasselmann et al. 1973) show that the peak tends to lose energy, especially to frequencies

below the peak. This is illustrated in Fig. 2.1 with results of exact computations for a Pierson-Moskowitz spectrum and a mean JONSWAP spectrum, both having a Phillips' constant $\alpha = 0.01$, a peak frequency $f_p = 0.3$ Hz, and a $\cos^2(\theta)$ distribution (Eq. 2.30).

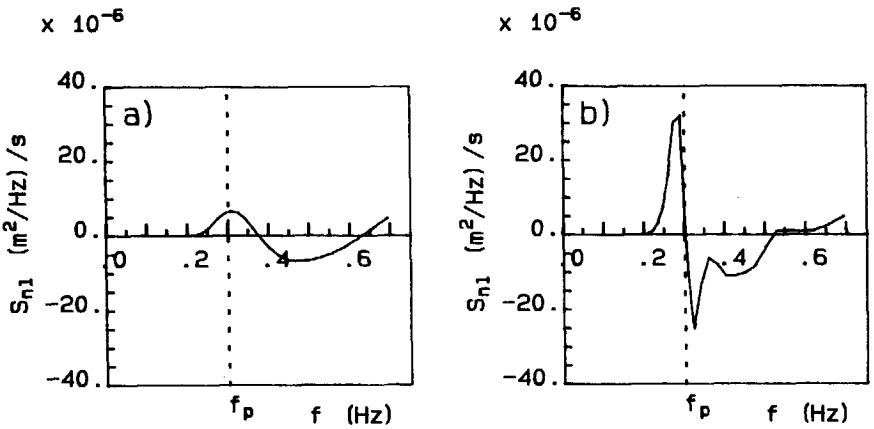

Fig 2.1: Directionally integrated nonlinear transfer for a Pierson-Moskowitz spectrum (panel a) and a mean JONSWAP spectrum (panel b). Both spectra have a Phillips' constant $\alpha = 0.01$, a peak frequency $f_p = 0.3$ Hz, and a $\cos^2(\theta)$ directional distribution. For the JONSWAP spectrum $\gamma = 3.3$, $\sigma_a = 0.07$ and $\sigma_b = 0.09$.

Fig. 2.1 shows the typical positive, negative, positive lobe shape of the nonlinear transfer source function. This figure also shows that the strongest interactions are found in a relatively small area in wavenumber space near the spectral peak, in particular for sharply peaked spectra.

The results of these computations and results obtained from measurements during the JONSWAP experiment strongly suggest that the nonlinear transfer of energy plays an important role in the evolution of the energy spectrum, particularly in the growth at low frequencies.

This can be explained as follows. During early wave growth the spectra are strongly peaked. For such spectra the low frequency positive lobe of the nonlinear transfer function is located at frequencies below the spectral peak frequency. This implies that there is a transfer of energy from wave components with frequencies just above the peak frequency to wave components with frequencies below the peak frequency. The effect is a shift of the peak to lower frequencies.

The shift of the peak frequency to lower frequencies ends by a number of effects. For decreasing frequency the magnitude of the interaction coefficient D is strongly reduced since the interaction coefficient scales with f^8 (see appendix B). This effect considerably reduces the transfer of energy to lower frequencies. Combined with the smaller effect of the wind input term for lower frequencies the result is a less peaked spectrum. Since for broad spectra, such as the Pierson-Moskowitz spectrum, the position of the low frequency positive lobe of the nonlinear transfer corresponds to the position of the peak of the spectrum, no further shift of the peak frequency towards lower frequencies occurs.

Another important property of the nonlinear interactions is their shape stabilizing effect on the energy spectrum. Small local perturbations in the spectrum are smoothed out as a result of the redistribution of wave energy by the nonlinear interactions.

2.2.6 Computation of the nonlinear transfer

2.2.6.1 Introduction

In general two categories of methods are distinguished to obtain a numerical evaluation of the Boltzmann integral (2.46). The methods of the first category are based on a straightforward numerical evaluation of the six-dimensional Boltzmann integral. Such calculations are very time consuming. The computation of the Boltzmann integral is further

complicated by the behaviour of the interaction coefficient when all the four interacting wavenumbers are almost equal. The methods of the second category are parametric methods, in which it is assumed that the energy spectrum can be approximated by a spectrum having some standard shape, for which the nonlinear transfer has been computed previously with some method of the first category, or for which the Boltzmann integral can be simplified considerably by assuming very narrow spectra.

2.2.6.2 Numerical integration methods

Explicit numerical solutions of the Boltzmann integral were found by e.g. Hasselmann (1963b), Sell and Hasselmann (1972), Webb (1978), Masuda (1980), Hasselmann and Hasselmann (1981) and Resio and Tracy (1982). A disadvantage of these methods is that they require excessive computer time. For this reason they are of no practical use for operational wave prediction methods. The only practical applications of these methods are in the study of the nonlinear transfer function for idealized spectra and for the computation of the evolution of the energy spectrum with reduced versions of the energy balance equation for idealized cases in which only one integration variable is used.

An efficient method for a sufficiently accurate computation of the nonlinear transfer has been introduced by Hasselmann and Hasselmann (1981). In this method a discretized eight-dimensional wavenumber space is constructed consisting of a large set of quadruplets of interacting wavenumbers (typically in the order of 600.000). This method is rather efficient since use is made of the fact that the rate of change of the action density of each of these wavenumber quadruplets is equal (Eq. 2.48) and of the symmetry properties of both the Boltzmann integral and the interaction coefficient. For the latter reason this method is also referred to as the symmetric method. Hasselmann and Hasselmann (1985b) claim that their method is two orders of magnitude more efficient than the other methods mentioned at

the beginning of this section.

The method of Hasselmann and Hasselmann (1981) has been incorporated in a numerical wave prediction model, called EXACT-NL. With this model detailed studies of the energy balance equation have been made for idealized cases for which only one integration variable, time or space, was used (cf. Komen et al., 1984; Young et al., 1987; Weber, 1987). The EXACT-NL model is also used in this study. Details are given in section 3.2.3 and in Van Vledder and Weber (1988).

Discrete interaction approximation

The symmetric method of Hasselmann and Hasselmann (1981) forms the basis of a simplified integration technique for the Boltzmann integral, known as the discrete interaction approximation (Hasselmann et al., 1985c). In this approximation only one type of wavenumber configuration and its mirror image are used (the total number of interacting wavenumber configurations being twice the number of spectral bins), in contrast to the symmetric method in which the nonlinear transfer is computed by considering a large number of interacting wavenumber configurations. The discrete interaction approximation has been incorporated in an advanced wave prediction model, viz. the WAM model (WAMDI group, 1988), with 300 spectral bins. Like the EXACT-NL model the WAM model is used in this study. A description of the application of these models is given in section 3.2.4.

2.2.6.3 Parametric methods

Introduction

In one type of parametric methods the nonlinear transfer of an arbitrary spectrum is simply computed by replacing it with the (scaled) precomputed exact transfer of a spectrum whose shape most

resembles the given model spectrum. The first of such methods was developed by Barnett (1968) and Ewing (1971) in which the nonlinear transfer for a given spectrum is replaced by the transfer for an equivalently scaled spectrum of prescribed (Pierson-Moskowitz) shape using the peak frequency f_p and Phillips' constant α as scaling parameters. Based on experience gained during JONSWAP (Hasselmann et al., 1973) it was understood that more general methods to compute the nonlinear transfer were needed in which more spectral shapes are taken into account. Based on such considerations Allender et al. (1985) developed a method which uses combinations of precomputed nonlinear transfers of 18 different spectra.

Another type of parametric methods is based on the narrow peak approximation, in which use is made of the fact that for some types of narrow spectra it is possible to derive analytical solutions of the Boltzmann integral (2.46). A number of methods based on this approximation are discussed next.

Narrow peak approximation

An important result was given by Longuet-Higgins (1976) who showed that the coupling coefficient G between four nearly equal wavenumbers $\underline{k}_1$, $\underline{k}_2$, $\underline{k}_3$ and $\underline{k}_4$ is finite and non-zero. According to Longuet-Higgins (1976) this implies that for narrow spectra the exchange of energy within the peak of the spectrum is of dominant importance. Longuet-Higgins (1976) also showed that the energy flow from an isolated peak in the spectrum tends to spread outward along two characteristic lines in $\underline{k}$-space making angles of $\pm \arctan(\sqrt{1/2})$ with the mean direction.

The theory of Longuet-Higgins (1976) was extended by Fox (1976) who showed that for a very narrow spectrum with a Gaussian structure, the sixfold integral in Eq. (2.46) reduces to a single one-dimensional integration. In the approximation of Fox (1976) the coupling coefficient is constant for all wavenumbers.

Further progress in parametric methods was made by Dungey and Hui (1979). They also considered narrow-peaked spectra, but they included the effect of a small but non-zero spectral width in their analysis. The coupling coefficient G is not a constant but varies with the wavenumber. Therefore the interaction coefficient D was perturbed to first order in terms of this spectral width.

In the method of Dungey and Hui (1979) the computation of the non-linear transfer for an arbitrary narrow spectrum is performed in three steps. In the first step the peak wavenumber and spectral width of an action density spectrum are determined. The second step consists of the approximation of this action density spectrum by a finite number of Gaussian shaped functions centered around the peak wavenumber. In the third step the nonlinear transfer is calculated as the sum of a finite number of one-dimensional integrals.

A comparison by Dungey and Hui (1979) of results obtained with this method and results obtained by Longuet-Higgins (1976) and Fox (1976) for a very narrow spectrum shows that the effect of spectral width cannot be neglected. Further, the results of the method of Dungey and Hui (1979) compare well with the JONSWAP results with respect to the nonlinear transfer at the forward face of the spectrum. This resemblance confirmed the notion that most of the wave growth on the forward face of the spectrum can be attributed to the nonlinear transfer of energy from the spectral peak-region to the longer waves. The method of Dungey and Hui (1979) has been extended by Van Vledder (1984) to include the effect of directional skewness of the spectrum. The method of Dungey and Hui (1979) and its extension by Van Vledder (1984) are discussed in section 3.2.5; details are given in appendix E.

Shortcomings of parametric methods

Parametric methods fail to compute the nonlinear transfer within a spectrum when the spectral shape cannot properly be approximated by the standard shape functions. Another disadvantage is that application of such methods in numerical wave prediction models is likely to give problems when the number of parameters describing a spectrum (e.g. the number of spectral components) exceeds the number of parameters describing a spectrum used in the parametric computation of the nonlinear transfer. For such situations the nonlinear transfer cannot smooth out small perturbations of the spectral shape since these are not recognized by parametric methods. For such situations instabilities are likely to occur during the integration of the energy balance equation.

2.2.7 Wind in wave modelling

2.2.7.1 Introduction

Accurate knowledge of the wind speed and wind direction in the atmospheric boundary layer (ABL) above the ocean surface is important for the prediction of wind generated waves and for the analysis of wave and wind measurements. When wind data from measurements are used, one has to be careful with the processing and interpretation because many disturbing effects should be accounted for, such as the variation of wind speed and wind direction with height, measurement errors due to flow distortions near the wind anemometer, and rapid fluctuations of the wind vector.

Since wind speed and wind direction vary with height, it is essential to state these data in combination with the height at which they are measured or to transform them to some standard height. If this is not done, interpretation errors are easily made when comparing wind data obtained at different stations having different anemometer heights. A standard height of 10 m is recommended by the World Meteorological Organization (Dobson, 1983). This, however, does not mean that all anemometers should be placed at the standard height of 10 m; good exposure to the wind to avoid flow distortions prevails.

In recent years most wind measurements at sea are made at the top of offshore structures with typical anemometer heights of 100 m. Near such structures the effect of flow distortions on the wind measurements cannot always be neglected. Normally, in the direct vicinity of the basic platform structure, undisturbed wind measurements are not possible. At the top of the tower, however, the platform structure may cause only minor deviations. Before such wind measurements are used it is desirable that the magnitude of the flow distortions is determined by model investigation (e.g. Vermeulen et al., 1985).

Since the air flow in the boundary layer is turbulent, smoothing out

the effect of short term statistical variability of the wind vector is required. Therefore, averaging techniques have to be used in the processing of the wind data. An averaging time of 10 minutes is recommended by the World Meteorological Organization (Dobson, 1983). The use of an averaging time of less than 10 minutes produces scattered results whereas averaging times of more than 20 minutes destroy information on intermediate scale motions.

For the conversion of the measured wind speed and direction to some standard height it is necessary to know which parameters play a role in the description of the atmospheric boundary layer. A related problem is the choice between the wind speed at a certain height and the friction velocity, as a parameter to scale wave growth.

In order to clarify the above mentioned points, a short description is given of the ABL as far as it is relevant for wave modelling. Attention is given to the variation of wind speed and wind direction with height. In the present study these are important for the analysis of wind and wave measurements.

2.2.7.2 The atmospheric boundary layer

The atmospheric boundary layer can be defined as that part of the atmosphere that is influenced by frictional effects due to the underlying land or sea surface. The ABL is normally divided in two parts. The lowest part of the ABL, called the surface layer, is characterized by a constant shear stress and strong variations of wind speed. Typically the surface layer has a height of about 100 m. The upper part of the ABL has a typical height of 1000 m and is characterized by slow variations of wind speed and wind direction. Most of the wind veering with height occurs in the upper layer, whereas most of the reduction of the wind speed occurs in the surface layer.

A measure for the turbulent momentum transport in the surface layer is

the friction velocity u_*, which is defined as the square root of the ratio of the surface stress (τ) caused by the wind and the density of air (ρ_a):

$$u_* = \sqrt{\tau/\rho_a}. \tag{2.49}$$

Knowledge of u_* is important for wave modelling, since u_* is directly related to the downward flux of horizontal momentum from the surface layer to the ocean. Based on this consideration, preference for scaling wave growth with friction velocity rather than with the wind speed at a certain height is argued by various authors (e.g. Miles, 1959, Komen et al., 1984). Empirical support favoring the scaling with u_* is given in Forristall (1981) and in Janssen et al. (1987).

2.2.7.3 Variation of wind speed with height

The most common method to compute the variation of wind speed with height is based on a logarithmic velocity profile in the surface layer, given by:

$$U_z = (u_*/\kappa)\ \ln(z/z_0) \tag{2.50}$$

in which κ is the Von Karman constant ($\kappa \approx 0.41$), and z_0 is a roughness length. According to Charnock (1955) the roughness length z_0 is given by:

$$z_0 = a u_*^2/g \tag{2.51}$$

in which the constant a was measured by Garratt (1977) who found a value of 0.0144. In relating wind speeds at different height, often use is made of the drag coefficient C_d, defined as:

$$C_d(z) = (u_*/U_z)^2. \tag{2.52}$$

The drag coefficient is not constant but varies with height z and the wind speed U_z. For z = 10 m the drag coefficient $C_d(10)$ can be well approximated by the formula (Wu, 1982):

$$C_d(10) = (0.8 + 0.065(s/m)\ U_{10}) \times 10^{-3}. \qquad (2.53)$$

Combining Eqs. (2.50), (2.52) and (2.53) gives an implicit relation from which the wind speed at 10 m height can be computed:

$$U_{10} = U_z \left(1 + \frac{C_d(10)^{1/2}}{\kappa} \ln(z/10\ m) \right)^{-1}. \qquad (2.54)$$

After the wind speed at 10 m height has been computed, the friction velocity u_* is computed using Eq. (2.52).

In this study it is assumed that the drag coefficient C_d only depends on the height z and the wind speed U_z. However, recent studies by Janssen (1989) and Maat et al. (1989) indicate a dependence of the drag coefficient with wave age. The consequences of such a dependence could not be taken into account in this study.

2.2.7.4 Variation of wind direction with height

The variation of wind direction with height in the upper part of the ABL is easily explained in a qualitative way by means of a simple model. Above the ABL the air flow is geostrophic and determined by the pressure gradient force and the Coriolis force only. In the ABL the surface drag causes a reduction of the wind speed with decreasing height. With decreasing wind speed there is also a decrease of the Coriolis force. The combined effect of these reductions is a counter-clockwise rotation of the direction to which the wind is blowing with decreasing height (Northern Hemisphere). This effect is often called the Ekman effect. Above open sea the magnitude of this effect in the

ABL can be as much as 15° (Brown and Liu, 1982). Typical values for the wind veering at sea over a height interval between 100 m and 10 m can be found in Riissanen (1975) to be 5°. This value is supported by Wieringa (1987, personal communication).

2.2.8 Wave prediction methods

2.2.8.1 Introduction

In this study a number of recently developed wave prediction models is used. To provide an idea of the capabilities of these models in comparison with older models, a brief description is given of both types. Emphasis is put on discrete spectral models. A recent review of wave prediction techniques is given by Sobey (1986).

2.2.8.2 Review of wave prediction models

One of the first wave prediction models was developed by Sverdrup and Munk (1946). It is a parametric model in terms of a small number of characteristic parameters describing the wave field, viz. the significant wave height and the mean wave period. The input for this model consists of simple meteorological variables, such as wind speed, fetch and duration of the wind. This model was rather limited in its capability to predict wind generated waves.

Important progress in wave prediction was made by the introduction of the wave spectrum concept by Pierson et al. (1955) and by the introduction of the energy balance equation concept by Gelci et al. (1956) and Hasselmann (1960). These developments opened the way to the development of spectral models. Most spectral models are of the discrete type, which means that the spectrum is represented by a finite number of wave components.

The basis of spectral wave prediction models is the energy balance Eq. (2.34) in which the evolution in time and space of each wave component is calculated using the balance of energy density. A major problem in spectral wave prediction models is the computation of the nonlinear transfer. Following the terminology of the SWAMP group (1985), discrete spectral models can generally be grouped into three classes or

generations according to their treatment of the nonlinear transfer and to their limitations with respect to the spectral shape.

In the first-generation models the wave components are decoupled, which means that each wave component grows, decays and propagates independently from the other wave components. In these models the input term is generally represented as:

$$S(f,\theta) = A + B\,E(f,\theta). \qquad (2.55)$$

The growth of the spectrum is limited explicitly to an equilibrium spectrum, usually the Pierson-Moskowitz spectrum, thereby avoiding the need for a dissipation source term. The nonlinear transfer is not included in Eq. (2.55) explicitly, but its absence is compensated for indirectly through tuning of A and B of Eq. (2.55).

In the second-generation models the wave components are coupled by the nonlinear transfer. Since the full representation of the nonlinear transfer is still too complicated, the nonlinear source term is described in terms of a few spectral parameters. Therefore, the second-generation models have constraints on the spectral shape, just as first-generation models.

Third-generation models try to reflect the physics of wind waves as well as possible and cover each physical process for the generation or dissipation of wave energy by a source term. For the nonlinear transfer source function, this has only become feasible by the development of the discrete interaction approximation (Hasselmann et al., 1985c). An important characteristic of third-generation models is their lack of constraints on the spectral shape.

The first operational third-generation wave prediction model is the so-called WAM model (WAMDI group, 1988). It has been shown by Hasselmann et al. (1985c) that application of the discrete interaction approximation in a preliminary version of the WAM model produces the

same wave growth characteristics in terms of total energy and peak frequency as the EXACT-NL model.

Another type of second-generation wave prediction models are parametric windsea models. They are based on the assumption that the evolution of the windsea spectrum is strongly controlled by the nonlinear transfer and that this spectrum can be described with relatively few parameters; the slow variation of these parameters in time and space is calculated starting from the energy balance equation. The growth of the windsea part of the spectrum is expressed in terms of a small set of only a few characteristic spectral parameters. A general method for projecting the energy balance equation in the complete (f,θ) space on an approximate parameters space is described in Hasselmann et al. (1976). One of such models is described by Günther et al. (1981) who use a five parameter JONSWAP spectrum and the integral mean direction of wave momentum.

Parametric models that use the integral wave direction as a parameter need information on the rate of change of this direction after variations in the wind field. For such models results of this study are of interest.

2.3 The directional response of wind waves to variations in wind direction

2.3.1 Introduction

The directional response of wind waves has been the subject of some theoretical and empirical studies, e.g. Hasselmann et al. (1980), Günther et al. (1981), Kuik and Holthuijsen (1981), Allender et al. (1983), Holthuijsen et al. (1987), and Young et al. (1987). Results of the above mentioned authors are summarized in this review.

This section is divided in two parts. In the first part a qualitative description is given of the directional response of wind waves to changing wind directions. The second part contains a quantitative review of modelling attempts and a discussion of their results.

2.3.2 Qualitative description of directional response

In the qualitative description of the directional response, two types of wind fields are distinguished: homogeneous and non-homogeneous wind fields. For both types some theoretically and empirically determined effects of the wind field on the underlying wave field are given with emphasis on the directional response.

Homogeneous wind fields

The most simple wind field considered is homogeneous and stationary. For such a wind field the following directional characteristics of wind waves are known (c.f. Hasselmann et al., 1980):

- The directional distribution is symmetric with respect to the wind direction and has its maximum in the direction of the wind.
- Both the frequency spectrum and the directional distribution tend

to a standard form due to the shape stabilizing effect of the nonlinear interactions.

This situation changes when the wind shifts. From directional wave observations in an almost homogeneous wind field the following characteristics were inferred after a change of the wind direction (cf. Hasselmann et al., 1980, and Kuik and Holthuijsen, 1981):

- The mean wave direction follows the wind direction, but not immediately; it lags behind the wind direction.
- The rate of change of the mean wave direction is frequency dependent with higher frequencies responding faster than lower frequencies. Very low frequencies do not respond to a change in the wind direction; these frequencies can be considered as swell.
- During the transition the directional distribution is skewed towards the new wind direction.
- The directional width of the initial two-dimensional spectrum increases during the turning of the mean wave direction and subsequently decreases to a value corresponding with the new equilibrium situation for the new wind direction and speed.
- A second peak may develop in the direction of the wind when the direction of the wind changes sufficiently rapid.

These characteristics have also been found by Young et al. (1987) who performed numerical computations to study the response of the two-dimensional energy density spectrum after a sudden shift of wind direction. These computations, performed with the EXACT-NL model and the WAM model, have increased the qualitative understanding of the physical processes occurring during the transition of the mean wave direction.

Presently only three local physical processes are identified which can contribute to the change of the mean wave direction:

1. Growth of waves in the direction of the new wind direction.
2. Gradual decay of the old wave system due to dissipation.
3. Nonlinear interactions exchanging energy between waves of

different frequency and direction.

These three processes correspond to the three source functions described in section 2.2.5.

The net effect of these mechanisms is the observed change of the mean wave direction towards the wind direction. However, the precise role of each of these physical effects has not yet been inferred from the observations.

Nonhomogeneous and instationary wave and wind fields

In case of a nonhomogeneous wind field where both the wind speed and the wind direction vary with time and space, the change of the mean wave direction in a fixed point is caused by two effects. These are the local effects, described above, and the net effect of radiation of wave energy into the point of measurement. In order to study the response of the mean wave direction to the local wind, the radiation effect has to be eliminated from the observations. A method to achieve this is described in chapter 4.

Another process which may be of importance in a nonhomogeneous wave field is the interaction with swell (if present). It is suggested by Hasselmann et al. (1980) that swell has a tendency, although normally rather weak, to align the entire wave field to the swell direction. The strength of these interactions depends on the separation between the peaks of the wind sea spectrum and the swell spectrum in the f-θ space. A theoretical study of the interaction between two wave systems has been carried out by Young et al. (1985). In that study computations were made of the nonlinear transfer of a spectrum consisting of the sum of two JONSWAP spectra with different peak frequencies and mean wave directions. In general the results of Young et al. (1985) indicate that the coupling between the two wave systems is negligible when the directions of the respective spectral peaks are separated by more than 60^0.

2.3.3 Modelling of the directional response

Hasselmann et al. (1980) were among the first to study the directional response. They analysed a series of directional wave measurements that were made within the framework of the JONSWAP project (Hasselmann et al., 1973). They proposed a relaxation model in an attempt to describe the response of the mean wave direction to veering winds. This model is formulated as:

$$\frac{\partial \theta_{0,f}}{\partial t} = \frac{1}{\tau_1(f)} \sin\left(\theta_w - \theta_{0,f} \right) \qquad (2.56)$$

in which τ_1 is the time scale of the directional response and θ_w is the wind direction. In this model the time scale τ_1 is frequency dependent according to:

$$\tau_1 = (2\pi\ b\ f)^{-1}. \qquad (2.57)$$

In Eq. (2.57) b is the relaxation coefficient which is supposed to be a function of the dimensionless wave age (U_{10}/c). Values of b were estimated from measurements by Hasselmann et al. (1980) and by Allender et al. (1983) using a regression technique (model fitting to the data). The results are tabulated as a function of the wave age (U_{10}/c) and averaged over each band of U_{10}/c. They are given in Table 2.1. In all cases the correlation between the estimates of b and U_{10}/c is rather low. Allender et al. (1983) report a mean correlation of 0.25, whereas Hasselmann et al. (1980) report a correlation of about 0.3.

	Hasselmann et al. (1980)	Allender et al. (1983)
Range of U_{10}/c	$b \times 10^5$	$b \times 10^5$
(1.0, 1.2)	1.6 ± 0.4	1.3
(1.2, 1.6)	2.4 ± 0.5	1.7
(1.6, 2.0)	2.0 ± 0.5	2.2

Table 2.1: Average values of the relaxation coefficient b of the time scale model (2.56) as a function of wave age U_{10}/c, after Hasselmann et al. (1980) and Allender et al. (1983).

Young et al. (1987) have also calculated b-values based on computations with the EXACT-NL model and the WAM model for the cases of a sudden wind shift of 30° and 60°. Their results computed with the EXACT-NL model are given in Table 2.2 (the corresponding WAM model results are practically the same):

f (Hz)	U_{10}/c	b ($\Delta\theta = 30°$)	b ($\Delta\theta = 60°$)
0.25	1.60	4.3×10^{-5}	4.2×10^{-5}
0.34	2.18	1.1×10^{-4}	1.0×10^{-4}
0.40	2.56	1.6×10^{-4}	1.5×10^{-4}
average		1.0×10^{-4}	1.0×10^{-4}

Table 2.2 Values of the relaxation coefficient b of the relaxation model (2.56) as a function of wave age U_{10}/c, determined with the EXACT-NL model, from Young et al. (1987).

Young et al. (1987) compare their computed b-value for $U_{10}/c = 1.60$ ($b \approx 4 \times 10^{-5}$) with the measured b-value of Hasselmann et al. (1980)

and Allender et al. (1983) corresponding to U_{10}/c values lying in the range 1.0 - 1.8. They erroneously quote the latter value as 3×10^{-5}, and they state that their value ($b \cong 4.2 \times 10^{-5}$) is in reasonable agreement with this. Actually, the average b-value of Hasselmann et al. (1980) is about 2×10^{-5} (see Table 2.1), so that the result of Young et al. (1987) exceeds this with more than a factor two. The reason for this discrepancy is not clear.

The above analysis was performed per frequency. A similar analysis in terms of the integral mean wave direction was performed by Günther et al. (1981) and Holthuijsen et al. (1987).

Günther et al. (1981) parameterized the energy balance equation to obtain a relation for the rate of change of the integral mean wave direction as a function of parameters of the wave field and wind field, for use in their parametric wave prediction model. They argue that the source function for the mean wave direction should include the wind velocity component perpendicular to the mean wave direction. The result of their parameterization is given by the following relaxation model:

$$\frac{\partial \theta_0}{\partial t} = \frac{1}{\tau_2} \sin(\theta_w - \theta_0). \tag{2.58}$$

The time scale τ_2 is related to the dimensionless peak frequency ν as follows:

$$\tilde{\tau}_2 = \chi^{-1} \nu^{-2} \tag{2.59}$$

in which $\tilde{\tau}_2 = \tau_2 g/U_{10}$ is the dimensionless time scale and ν is the dimensionless peak frequency defined by $\nu = f_p U_{10}/g$. Although the exponent -2 in Eq. (2.59) is based on theoretical grounds, Günther et al. (1981) determined the proportionality constant χ empirically. From four observations of the time scale $\tilde{\tau}_2$ they found an average value of $\chi = 0.21 \times 10^{-2}$.

Another formula for the change of the mean wave direction θ_0, similar to Eq. (2.58), is given by Holthuijsen et al. (1987). Their formula is also based on a parameterization of the energy balance equation (2.34) for the case of a homogeneous wave field, with zero divergence of transport of energy. An intermediate result presented by them is:

$$\frac{\partial \theta_0}{\partial t} = \frac{\cos(\theta_0) \int_0^{2\pi} \int_0^{\infty} \cos(\theta)\, S(f,\theta)\, df\, d\theta}{\cos(\theta_s) \int_0^{2\pi} \int_0^{\infty} \cos(\theta)\, E(f,\theta)\, df\, d\theta} \sin(\theta_s - \theta_0) \qquad (2.60)$$

in which θ_s is the mean direction of the source function $S(f,\theta)$ which is defined similar to the mean wave direction, i.e. replace $E(f,\theta)$ by $S(f,\theta)$ in Eqs. (2.28) and (2.29). The derivation of Eq. (2.60) is given in appendix C.

In order to arrive at a simpler model than (2.60) Holthuijsen et al. (1987) make two rather crude assumptions. Firstly they assume that the shapes of the directional distributions of $E(f,\theta)$ and $S(f,\theta)$ are frequency independent, equal to one another and symmetric around θ_0 and θ_s respectively. The second assumption is that the source function is centered around the wind direction θ_w so that $\theta_s = \theta_w$. Expression (2.60) then reduces to the following relaxation model:

$$\frac{\partial \theta_0}{\partial t} = \frac{1}{\tau_3} \sin(\theta_w - \theta_0) \qquad (2.61)$$

in which τ_3 is given by:

$$\tau_3 = \left(\frac{1}{E_{tot}} \frac{\partial E_{tot}}{\partial t} \right)^{-1} \qquad (2.62)$$

with E_{tot} the total wave energy defined according to Eq. (2.42). In dimensionless form the time scale of this relaxation model is as follows:

$$\tilde{\tau}_3 = \left(\frac{1}{\varepsilon} \frac{\partial \varepsilon}{\partial \tilde{t}} \right)^{-1} \tag{2.63}$$

in which $\varepsilon = E_{tot} g^2 / U_{10}^4$, $\tilde{\tau}_3 = \tau_3 g / U_{10}$ and $\tilde{t} = tg/U_{10}$. In this model the time scale $\tilde{\tau}_3$ can be computed from empirical parameterized growth curves, but also from observed wave growth.

Holthuijsen et al. (1987) have used the growth curve from the BMO (British Meteorological Office), given by:

$$\varepsilon = a^b \tanh (b\tilde{t}^c) \tag{2.64}$$

in which $a = 3.6 \times 10^{-3}$, $b = 2.1 \times 10^{-22}$, $c = 4.7$ and $d = 0.3$. This growth curve is for an ideal situation in which a homogeneous wind field starts to blow over an infinite ocean at time $t = 0$. Substitution of Eq. (2.64) in Eq. (2.63) allows the determination of $\tilde{\tau}_3$ as a function of the growth stage as represented by the dimensionless energy ε. For purposes of later comparison, the result is presented in Fig. 2.2 in a slightly different form, viz. scaled with u_* instead of U_{10} using $U_{10} = 24.0\ u_*$ (as explained in section 2.3.4) and using the dimensionless peak frequency (ν_*) to represent the growth stage. The conversion from ε to ν was done by the following universal relationship between ε and ν as presented by Hasselmann et al. (1976, their Table 1):

$$\varepsilon = 7.4 \times 10^{-6} \nu^{-3.05} \tag{2.65}$$

or in terms of ε_* and ν_*:

$$\varepsilon_* = 1.52 \times 10^{-4}\ \nu_*^{-3.05}. \tag{2.66}$$

The model of Holthuijsen et al. (1987) predicts an increasing time scale with increasing growth stage of the waves; the model predicts that $\tilde{\tau}_3 \longrightarrow \infty$ when the waves approach the fully developed stage.

Holthuijsen et al. (1987) have determined time scales of the directional response based on directional wave measurements of young sea states with as little influence of swell as possible using a finite difference scheme. After accounting for measurement errors, they obtained 8 time scale estimates. Seven of these estimates are plotted as a function of growth stage in Fig. 2.2 (the eighth estimate is not plotted since in the present study it is regarded as swell due to another nondimensionalization). Holthuijsen et al. (1987) show that the average observed time scale of their model is in reasonable agreement with the theoretical one although a considerable scatter exists. However, the expected dependence of their time scale on dimensionless wave energy could not be identified in their measurements.

In their analysis of directional wave observations Holthuijsen et al. (1987) use a number of selection criteria which influence the range of time scales that can be observed. Among others, they require that in an interval of two hours the wave energy growth should be at least 20%:

$$\frac{\Delta E_{tot}}{E_{tot}} > 0.2. \qquad (2.67)$$

This implies that the estimated time scale τ according to Eq. (2.62) is always less than 10 hours. This follows by approximating Eq. (2.62) with $\tau_3 \approx E_{tot}/(\Delta E_{tot}/\Delta t)$ and by substituting the inequality (2.67) and Δt = 2 hours in this approximation.

Similarly, their requirement that in a time interval of two hours the change of the mean wave direction should be at least 10 degrees yields a maximum to the observed time scales estimated with the central

difference scheme applied by Holthuijsen et al. (1987) (their Eq. 20). Rewriting their Eq. (20) in dimensional form and using $\Delta t = 2$ hours and the inequality $\Delta\theta_0 \geq 10^\circ$ it follows:

$$\tau_{max} \leq \sin(\theta_w - \theta_0)\ 11.46 \text{ hours.} \qquad (2.68)$$

These results indicate that relatively high time scales cannot be detected due to the requirements imposed on the data. This may have biased the value of the average time scale to a lower value.

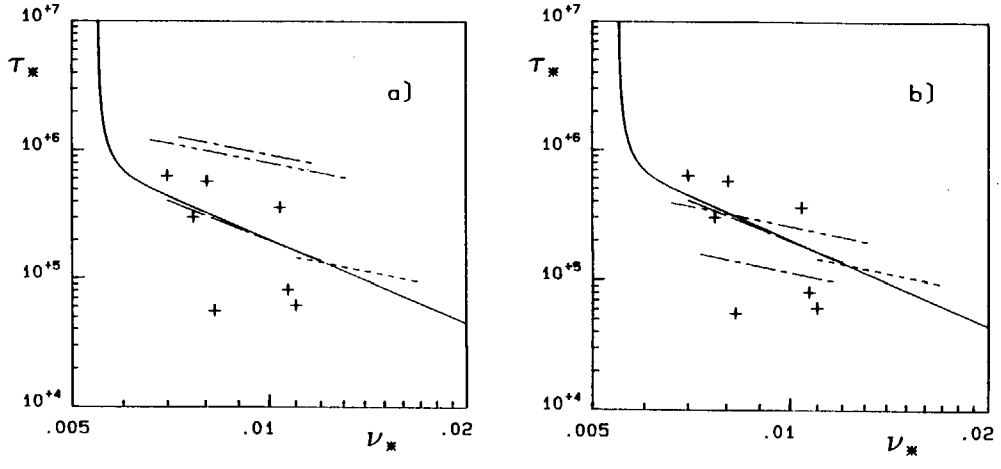

Fig. 2.2: Dimensionless time scale τ_* as a function of dimensionless peak frequency ν_*; parameterized data of Hasselmann et al., 1980 (—— – – ——), parameterized data of Günther et al., 1981 (—— ——), parameterized data of Allender et al., 1983 (—— – ——), model of Holthuijsen et al., 1987 (————), observational results of Holthuijsen et al., 1987 (+), computational results of Young et al., 1987 (– – – –). Results are shown as obtained from the literature (panel a), and after re-analysis of data from Hasselmann et al., 1980 and Allender et al., 1983 (panel b).

2.3.4 Comparison of time scales

For the comparison of the three time scale models and the data points mentioned above, all dimensionless time scale models and observational results are expressed in terms of a relation between the dimensionless time scale and dimensionless peak frequency, both normalized with the friction velocity u_*. To that end, some transformations have to be made for the time scales given as a function of wave age frequency-dependent U_{10}/c (Hasselmann et al., 1980, Allender et al., 1983, and Young et al., 1987), or as a function of dimensionless peak frequency ν (Günther et al., 1981). The results of these transformations are presented in Fig. 2.2a.

Since in the present study computations are made with two wind speeds (U_{10} = 10 m/s and U_{10} = 20 m/s) and since the friction velocity u_* does not depend linearly on the wind speed U_{10}, a mean ratio between u_* and U_{10} is used. This ratio is 26.3 for U_{10} = 10 m/s, and 21.8 for U_{10} = 20 m/s. By taking the average of these two values, the mean ratio of U_{10}/u_* = 24.0 is obtained, and used in the following.

In these transformations the model of Günther et al. (1981) (Eq. 2.59) is rewritten as:

$$\tau_{*,2} = 19.8\ \nu_*^{-2}. \tag{2.69}$$

To estimate the time scales of the variation of the frequency-averaged mean wave direction from the frequency dependent results of Hasselmann et al. (1980), Allender et al. (1983) and Young et al. (1987) it is assumed that the directional response near the peak frequency is representative for the response of the integral mean wave direction. On this basis it follows that the model of Hasselmann et al. (1980) can be written as (in dimensionless form):

$$\frac{\partial \theta_0}{\partial t_*} = \frac{1}{\tau_{*,1}} \sin(\theta_w - \theta_0) \qquad (2.70)$$

with

$$\tau_{*,1} = \nu_{*,1}^{-1} (2\pi b)^{-1} \qquad (2.71)$$

in which $\nu_{*,1} = f_p u_*/g$ and $t_* = tg/u_*$.

In Fig. 2.2a the curves corresponding to the results of Hasselmann et al. (1980), Allender et al. (1983) and Young et al. (1987) are based on the mean values for the coefficient b of 2.0×10^{-5}, 1.7×10^{-5} and 1.0×10^{-4} respectively (see Tables 2.1 and 2.2). These curves are only plotted for the ν_*-ranges corresponding to the U_{10}/c-ranges given by the above authors.

Fig. 2.2a shows that there is a good agreement between the parameterized results of Günther et al. (1981) and the model of Holthuijsen et al. (1987). These results also agree with the results of Young et al., (1987) for ν_*-values of about 0.015, but the trend in the results of Young et al. (1987) is lower than the trend in the other two models. However, the time scales of Günther et al. (1981) and Holthuijsen et al. (1987) are considerably lower than those based on the results obtained by Hasselmann et al. (1980) and Allender et al. (1983).

From Fig. 2.2a it is obvious that there are two families of proposed time scale models, those of Hasselmann et al. (1980) and Allender et al. (1983) on the one hand and those found by Günther et al. (1981), Holthuijsen et al. (1987) and Young et al. (1987) on the other hand. The time scales of these families differ by a factor varying from three to six. A possible reason for this difference is investigated below.

A reason for the discrepancy could be the different methods to estimate time scales from the data. Hasselmann et al. (1980) and

Allender et al. (1983) mention the use of regression analysis to estimate the relaxation coefficient b in their frequency dependent model (Eqs. 2.56 and 2.57). However, both publications provide insufficient information to allow definite conclusions about their method of analysis or what selection if any was applied to the data. Therefore part of the results (specified below) published by Hasselmann et al. (1980) and Allender et al. (1983) has been reanalysed in an attempt to reveal the possible reason for the discrepancy mentioned above.

Allender et al. (1983) have published their full data set, whereas in the publication of Hasselmann et al. (1980) only 37% is presented. Therefore only a re-analysis of the data by Allender et al. (1983) can be used to draw firm conclusions.

For that purpose time series of mean wave directions for various frequencies were read from the Figs. 3, 4 and 5 of Allender et al. (1983). This was done by measuring the position of each observation result in the time- and direction- coordinate system.

From these time series of mean wave direction per frequency band the relaxation coefficient b was estimated with a central difference scheme:

$$b_j = \frac{\theta_{0,j+1} - \theta_{0,j-1}}{t_{j+1} - t_{j-1}} \frac{1}{2\pi f \sin\left(\theta_{w,j} - \theta_{0,j}\right)} \qquad (2.72)$$

in which f is the frequency of the band considered. The index j refers to the sequence number in the wave record.

The finite difference scheme (2.72) was applied to the time series constructed from the figures mentioned above. Following Hasselmann et al. (1980) the estimated b_j-values are presented as a function of wave age U_{10}/c, see Fig. 2.3a. To avoid analysis of swell frequencies, only

U_{10}/c values corresponding to frequencies larger than the Pierson-Moskowitz frequency are taken into account, viz. $U_{10}/c > 0.82 = 0.13\ (2\pi)$. The b_j-values show no correlations with U_{10}/c and have a scatter in a large range in excess of two orders of magnitude.

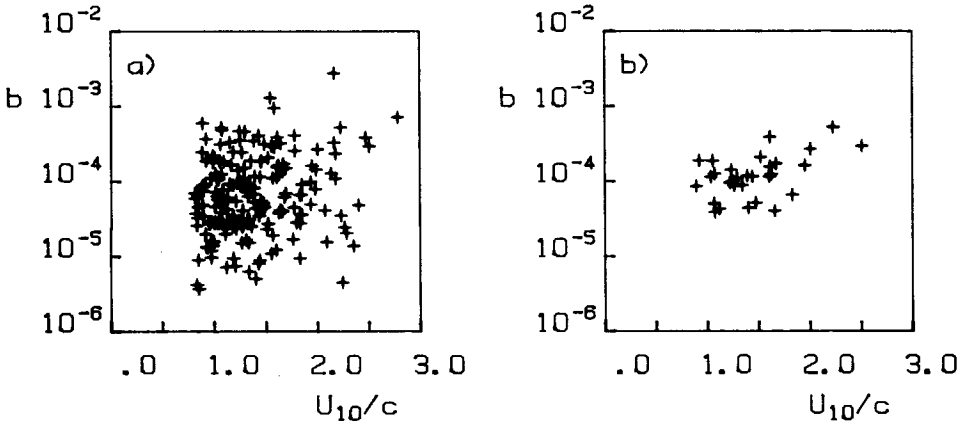

Fig. 2.3: Observed b-values as a function of wave age U_{10}/c based on time series of mean wave direction inferred from Allender et al. (1983). Results are shown without any selection (panel a) and with the selection (panel b) according to the criteria described in section 2.3.4.

This set of estimates was further analysed by imposing the following set of constraints on the parameters in the time intervals for which the coefficient b was estimated (cf. Holthuijsen et al., 1987):

1) the wave direction turns towards the wind direction,
2) the maximum difference between the mean wave direction and wind direction is 90°,

and, to account for measurement errors in the wind and wave directions:

3) the minimum difference between the mean wave direction and wind direction is 10°,
4) the mean wave direction changes at least 10°.

Since information on the observed peak frequencies is not sufficiently available, criteria using the peak frequency are not used. The results of the re-analysis are shown in Fig. 2.3b and summarized in Table 2.3.

	No selection		selection	
range of U_{10}/c	nr. of estimates	mean value b	nr. of estimates	mean value b
0.8-1.2	74	9.7×10^{-5}	8	1.0×10^{-4}
1.2-1.6	61	1.4×10^{-4}	11	1.1×10^{-4}
1.6-2.0	32	1.1×10^{-4}	8	1.5×10^{-4}
2.0-2.4	14	3.2×10^{-4}	2	4.0×10^{-4}
2.4-2.8	4	3.6×10^{-4}	1	3.0×10^{-4}
weighted average	185	1.4×10^{-4}	30	1.4×10^{-4}

Table 2.3: Summary of estimates of the relaxation coefficient b, based on published results of Allender et al. (1983).

The results shown in Table 2.3 indicate that application of the selection criteria imposed on the data has no effect on the mean value of the coefficient b. However, as can be seen in Fig. 2.3, the scatter in the results decreases significantly although a considerable scatter remains. These results also show that there is no clear dependence of the coefficient b on the frequency f. This means that the time scale of the response of the mean wave direction per frequency is inversely proportional to the frequency f.

The re-analysis shows that the mean value of the relaxation coefficient b is about a factor 8 larger than the average value of 1.7×10^{-5} reported by Allender et al. (1983). The re-analysed results

of Allender et al. (1983) have been plotted in Fig. 2.2b (among other results) on the basis of Eq. (2.71).

The same analysis was also performed on the published data of Hasselmann et al. (1980) (their Figs. 7, 8 and 9, containing about 37% of the data used for the results in Table 2.1). The results of this analysis also show that application of selection criteria has no effect on the mean b-value, and that the scatter in the results reduces considerably. Without selection a mean b-value of 6.1×10^{-5} (195 estimates) is obtained and with application of the above selection criteria a mean b-value of 6.2×10^{-5} (43 estimates) is found. These mean values are about a factor 3 larger than the mean value of 2×10^{-5} reported by Hasselmann et al. (1980). The re-analysed results of Hasselmann et al. (1980) have also been plotted in Fig. 2.2b, again on the basis of Eq. (2.71).

The above results indicate that the method of finite differences, applied to the data presented in the respective publications, yields substantially lower time scales than those presented by Hasselmann et al. (1980) and Allender et al. (1983), which were based on a regression analysis.

Based on the results of the re-analysis it follows that the two significantly different families of time scales can no longer be identified. Now only one family of time scales exists, though with a wide variation in magnitude. In the following the re-analysed results of Hasselmann et al. (1980) and Allender et al. (1983) will be referred to as their results.

2.4 Conclusions

Present day knowledge of the directional response of wind waves shows a number of gaps. There is a practical need to improve this knowledge because this can be used in parametric wind wave prediction models.

In all observations the number of time scale estimates is very low and there exists considerable scatter in those estimates.

Large discrepancies exist between reported estimates of the rate of change of the mean wave direction of different sources. This discrepancy in the values of the time scale has not yet received a satisfactory explanation. In this study a re-analysis has been performed of published data using a finite difference method of analysis. The results appear to remove the apparent discrepancy to a large extent.

In order to increase our understanding and practical knowledge of the directional response of wind waves, theoretical models should be developed and used to investigate this response. The results should be compared with careful measurements in the open ocean in order to clarify the remaining differences mentioned above.

CHAPTER 3

NUMERICAL SIMULATION OF DIRECTIONAL RESPONSE

3.1 Introduction

In this chapter results are presented of computations that have been performed with two advanced numerical wave prediction models for the calculation of the directional response of wind waves to variations of the wind field. The purpose of these computations is to study the different physical processes active during the response and the rate of change of the frequency integrated mean wave direction after a change of wind direction.

In the presentation of the results a distinction is made between qualitative and quantitative aspects. The qualitative aspects are:

1) the shape of the response curves of the mean wave direction and the directional width, total wave energy and peak frequency,
2) the shape of the two-dimensional spectrum, and
3) the physical processes active during the response.

The quantitative aspects are:

4) the time scale of the directional response of the mean wave direction,
5) the separate effects of generation, dissipation and nonlinear wave-wave interactions on the rate of change of the mean wave direction, and
6) the sensitivity of the directional response to variations in the modelling of the dissipation source function.

To study the above mentioned aspects a number of computations are made for homogeneous wind and wave fields. For this situation the energy balance equation (2.34) simplifies to:

$$\frac{\partial E(f,\theta;t)}{\partial t} = S_{tot}(f,\theta;t). \qquad (3.1)$$

This equation is integrated with respect to time to simulate duration limited wave growth. All computations are performed for one spatial point which is representative for the whole homogeneous wave field.

The time history within a simulation consists of two stages. In the first stage the simulation starts with an almost flat sea, represented by a spectrum with a high peak frequency and little energy. The waves grow under the influence of a constant wind until they have reached the so-called half developed stage, i.e. until the peak frequency has decreased to twice the Pierson-Moskowitz frequency. At that moment the wind direction is suddenly changed, and the second stage starts. This stage is different for each simulation run. For one type of simulation runs the new wind direction remains constant, and from that point on, the computation is continued with the same wind speed until the mean wave direction is almost equal to the wind direction. Another type of simulation runs comprises a homogeneous wind field turning with a constant angular velocity. Here, the computation is continued until the mean wave direction has a constant lag with the wind direction and the spectral shape remains constant.

For the sensitivity analysis of the directional response only variations in the modelling of the dissipation source function are considered. Sensitivity to variations in the modelling of the source functions for wind input and nonlinear transfer is not considered here. The reason for this limitation is that a correct modelling of the dissipation is still a difficult problem which is the subject of many studies (by others) whereas the physics behind the other source functions is fairly well known and satisfactory models for these are available.

The content of this chapter is as follows. In section 3.2 a description is given of the numerical models that are used. Emphasis is laid on the computation of the source function for the nonlinear transfer, and the technique to integrate the energy balance equation. In section 3.3 the conditions for the simulation runs are given: i.e. a specification of the wind fields and the initial conditions. The methods to analyse the simulation results for the estimation of the time scale of the directional response are described in section 3.4. Section 3.5 gives a presentation of the results, which are discussed in section 3.6. Conclusions are given in section 3.7.

3.2 Description of numerical models

3.2.1 Introduction

In this chapter three numerical wave prediction models are described. These are the EXACT-NL model, a modified WAM model and the so-called DH model in which the nonlinear interactions are computed with a parametric method based on work by Dungey and Hui (1979).

The three models mentioned above differ in a number of aspects. The most important of these aspects are the computation of the source function for the nonlinear transfer S_{nl} and the integration of the energy balance equation. The models have in common that they belong to the class of coupled discrete spectral wave prediction models and that they use the same formulations for the source functions for wind input S_{in} and dissipation S_{ds}.

Descriptions of each of the methods for the computation of the nonlinear transfer and the integration of the simplified energy balance equation are given in the paragraphs describing the corresponding wave models.

Only the EXACT-NL and the WAM model are used to perform the numerical simulations. The DH model could not be used for the computations since it was found to give rise to instabilities.

3.2.2 Source functions

For the wind input and dissipation source terms the Eqs. (2.38) and (2.40) are used respectively. For the dissipation source function the EXACT-NL model uses (except for the sensitivity analysis) the value 2 for both of the exponents m and n, and the value 3.33×10^{-5} for the

proportionality coefficient C. In the WAM model, however, another value of the coefficient C (= 5.43×10^{-5}) is used because of another definition of the mean radian frequency ω_m and as a result of tuning of the WAM model (WAMDI group, 1988). In the WAM model the harmonic mean frequency is used:

$$f_m = \left[\int_0^\infty \frac{1}{f} E(f)\, df \;/\; E_{tot} \right]^{-1} . \qquad (3.2)$$

Application of definition (3.2) was found to improve the stability of the computations (WAMDI group, 1988). For the computation of the nonlinear transfer Eq. (2.46) is used as a basis. The different methods to compute the nonlinear transfer are described in the next sections.

3.2.3 The EXACT-NL model

3.2.3.1 Introduction

The EXACT-NL model was developed by K. and S. Hasselmann at the Max-Planck-Institut für Meteorologie, Hamburg. The model is meant to compute duration or fetch limited growth curves with a simplified energy balance equation in which the nonlinear interactions are computed by a straightforward evaluation of the Boltzmann integral (2.46). For this evaluation the symmetric method of Hasselmann and Hasselmann (1981) is used.

The model consists of three related programs: two preprocessing programs and one main program. In the preprocessing programs a grid in wavenumber space is generated over which the numerical integration of the Boltzmann integral is performed. In the main program results of the preprocessing programs are used to compute the nonlinear transfer

for any spectrum arising during the integration of the simplified energy balance equation.

A detailed description of the use of the EXACT-NL model is given in Van Vledder and Weber (1988).

3.2.3.2 Computation of the nonlinear transfer

Basically the Boltzmann integral is evaluated by considering the interactions between a very large number of wavenumber quadruplets. For that purpose the six-fold Boltzmann integral is reduced to a three-fold integral by taking account of the delta-functions in Eq. (2.46). In this reduction process a number of transformations are used. Based on a certain discretization, a set of wavenumber quadruplets is generated and stored in memory together with the corresponding interaction coefficients and transformation Jacobians. This discretization is performed in the first preprocessing program.

To compute the nonlinear transfer of an arbitrary spectrum results of the first preprocessing program need to be used. However, since not all wavenumber quadruplets have interactions which contribute significantly to the nonlinear transfer a filtering is used to optimize the computation. For that purpose use is made of a reference spectrum which should have about the same shape as all spectra arising during integration of the energy balance equation (3.1). In the following the latter spectra are referred to as arbitrary spectra.

The filtering of the set of interacting wavenumber quadruplets is performed in the second preprocessing program. In this filtering process the rates of change of the action density for all wavenumbers in a quadruplet are used. These rates are equal for all four wavenumbers in an interacting quadruplet (see Eq. 2.48). During the numerical integration of the Boltzmann integral, the rate of change of action density of one of the wavenumbers in a quadruplet is compared

with some preset threshold value. If this rate is lower than the threshold value, the corresponding wavenumber quadruplet is rejected since it is assumed not to contribute significantly to the nonlinear transfer. Otherwise it is accepted and the wavenumber quadruplet is stored in memory together with the corresponding interaction coefficients and Jacobians.

In this way a filtered and a non-filtered nonlinear transfer of the reference spectrum are obtained which can then be compared to check upon the choice of the threshold value.

Computations by Hasselmann and Hasselmann (1981) indicate that only 5-10 % of the interacting wavenumber quadruplets make up for about 95 % of the nonlinear transfer. Thus the use of the filtered wavenumber space introduces an error of about 5 % in the computed nonlinear transfer, while it saves a considerable amount of computing time and memory space. In the present study the filtered set contains about 600.000 wavenumber quadruplets.

To compute the nonlinear transfer of an arbitrary spectrum use is made of the filtered set of wavenumber quadruplets and corresponding coefficients. This computation is performed in the main program and consists of three steps. In the first step the arbitrary spectrum is transformed in f-θ space such that it occupies almost the same region in f-θ space as the reference spectrum, such that the peak frequencies are equal and the mean directions are almost equal. This may require a linear scaling of the frequencies and a rotation of the arbitrary spectrum.

In the second step the nonlinear transfer for the transformed arbitrary spectrum is computed using the filtered wavenumber space, the precomputed interaction coefficients, and the Jacobians of the reference spectrum.

In the third and last step the computed nonlinear transfer of the

transformed arbitrary spectrum is scaled to obtain the nonlinear transfer of the original arbitrary spectrum. Apart from a possible rotation, this scaling consists of a transformation of the frequency axis and a multiplication of the nonlinear transfer with a scale factor (see appendix D):

$$S_{nl}^{(2)}(f/f_{p2},\theta) = S_{nl}^{(1)}(f/f_{p1},\theta-\Delta\theta)\ (f_{p1}/f_{p2})^{23} \qquad (3.3)$$

in which

$S_{nl}^{(1)}(f,\theta)$	:	nonlinear transfer of the transformed arbitrary spectrum, using the set of filtered wavenumber quadruplets of the reference spectrum
$S_{nl}^{(2)}(f,\theta)$	:	nonlinear transfer of the arbitrary spectrum
f_{p1}	:	peak frequency of reference and transformed arbitrary spectrum
f_{p2}	:	peak frequency of arbitrary spectrum
$\Delta\theta$	:	angle of rotation

If the arbitrary spectrum and the reference spectrum differ too much in shape, this procedure cannot be used. Then a new reference spectrum must be chosen and a new filtered set of wavenumber quadruplets must be determined.

3.2.3.3 Numerical integration of the energy balance equation

The energy balance equation is integrated with an explicit first order forward time scheme. The size of the time step is determined dynamically in each integration step to keep the integration stable. For each integration step, a rough estimate of the size of the time step is made based on the elapsed integration time (t). In this study $\Delta t = t/5$ is used. Then the size of the time step is adjusted by dividing it by two repeatedly until for each spectral bin of the energy density spectrum $E(f,\theta)$ and source function $S(f,\theta)$ the follow-

ing conditions are satisfied:

$$\Delta t\ S(f,\theta) \ < a\ E(f,\theta)$$

or

$$|\Delta t\ S(f,\theta)| < b\ \alpha\ (2\pi)^{-4} g^2\ f^{-5} \qquad (3.4)$$

and

$$E(f,\theta) + \Delta t\ S(f,\theta) > 0 \qquad (3.5)$$

with a = 1/3, b = 0.3 and α = 0.01. The values of the coefficients a and b in (3.4) are based on experience by previous users of the EXACT-NL model (S. Hasselmann, 1985, personal communication).

The spectrum is predicted explicitly in the frequency range $f \leq 2.5\ f_p$, whereas for higher frequencies the spectrum is continued with an f^{-5} tail with the same directional distribution as the highest frequency band predicted explicitly.

3.2.4 The WAM model

3.2.4.1 Introduction

The first operational version of the WAM model has been developed in a cooperation of the Max-Planck-Institut für Meteorologie, Hamburg and the Royal Netherlands Meteorological Institute (KNMI), De Bilt. An operational version of the WAM model has been implemented on the computer system of the European Centre for Medium-Range Weather Forecasts (ECMWF), Reading, England. It is used for daily global wave forecasts. A detailed description of the WAM model is given by the WAMDI group (1988). In this study a one-dimensional version of the WAM model is used to compute duration limited wave growth curves. It uses 12 directions (30° resolution) and 26 frequencies.

3.2.4.2 Computation of nonlinear transfer

Like the EXACT-NL model, the WAM model computes the nonlinear transfer of a certain spectrum by considering the interactions between a set of interacting wavenumber quadruplets. Whereas the EXACT-NL model uses a very large set of wavenumber quadruplets with many different configurations, the WAM model uses a rather small number of quadruplets which all have the same configuration.

In this configuration two wavenumbers are identical ($\underline{k}_1 = \underline{k}_2$), whereas the other two wavenumbers ($\underline{k}_3$ and $\underline{k}_4$) are of different magnitude and lie at an angle to the first two wavenumbers. The corresponding four frequencies are related by:

$$\left.\begin{aligned} f_1 &= f_2 = f \\ f_3 &= f\,(1+\lambda) = f^+ \\ f_4 &= f\,(1-\lambda) = f^- \end{aligned}\right\} . \qquad (3.6)$$

The four wavenumbers should also satisfy the resonance condition (2.44). Following the WAMDI group (1988) $\lambda = 0.25$ is used. The corresponding wavenumber configuration and its mirror image are shown in Fig. 3.1.

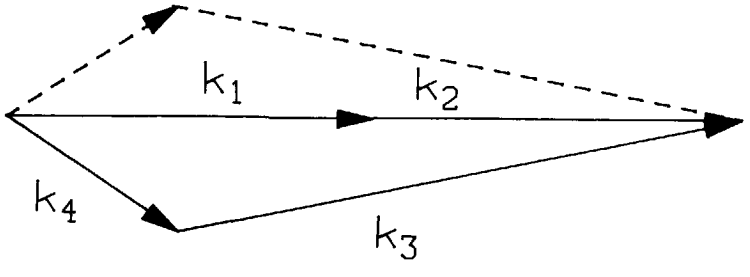

Fig. 3.1 The two wavenumber configurations used in the discrete interaction approximation.

The rates of change of the energy densities (δS_{nl}, δS_{nl}^{+} and δS_{nl}^{-}) within one such wavenumber quadruplet are given by:

$$\begin{pmatrix} \delta S_{nl} \\ \delta S_{nl}^{+} \\ \delta S_{nl}^{-} \end{pmatrix} = \begin{pmatrix} 2 \\ -1 \\ -1 \end{pmatrix} C\, g^{-4} f^{11} \left[\left(E^2 \frac{E^{+}}{(1+\lambda)^4} + \frac{E^{-}}{(1-\lambda)^4} \right) - \frac{E\, E^{+} E^{-}}{(1-\lambda^2)^4} \right] \qquad (3.7)$$

in which g is the gravitational acceleration and C is a constant equal to 3×10^7. In Eq. (3.7) E, E^{+} and E^{-} are the energy densities at the interacting wavenumbers, which are calculated by bilinear interpolation within a discretized spectrum in f-θ space (see Fig. 3.2).

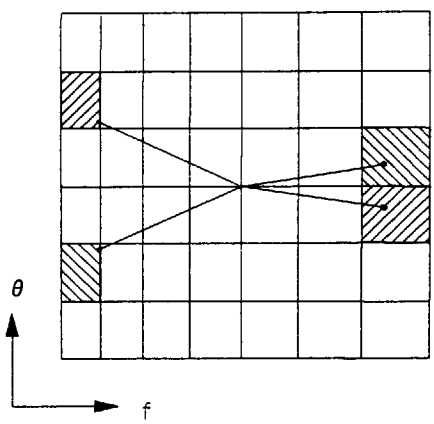

Fig. 3.2 Interpolation in (f,θ)-space of energy densities of interacting wavenumbers for each mirror-image in the discrete interaction approximation.

To compute the nonlinear transfer for a given discretized energy spectrum, all interactions between four wavenumbers satisfying the resonance conditions (2.44) and (3.6) are considered, and for which the central wavenumber $\underline{k}$ (= $\underline{k}_1$ = $\underline{k}_2$) loops over all wavenumbers of the discretized spectrum. In this way the number of wavenumber quadruplets taken into account is twice the number of spectral bins of the energy

density spectrum. So, in the present study 624 configurations are used.

Application of Eq. (3.7) to a discretized spectrum needs some modification for a few high and a few low frequencies since the energy densities E^+ and E^- cannot be computed for frequencies falling outside the range of model frequencies. For high frequencies the energy densities E^+ are computed by using an f^{-4} tail beyond the highest model frequency. For the lowest frequencies the densities E^- are set to zero. This implies that energy, momentum and action are not conserved, since wave energy may leak to or from both higher and lower frequencies.

The method described above for computing the nonlinear transfer is also referred to as the discrete interaction approximation.

3.2.4.3 Numerical integration of the energy balance equation

In the WAM model the frequency range of the discretized spectrum is divided in two parts. The first part ranges from the lowest model frequency to a certain frequency, denoted by f_{lim}, given by:

$$f_{lim} = \min \left(f_{high}, \max \left(2.5\, f_m, 4\, f_{PM} \right) \right) \qquad (3.8)$$

in which f_m is the mean frequency (computed from Eq. 3.2), f_{high} is the highest model frequency and f_{PM} is the peak frequency of a Pierson-Moskowitz spectrum. The second part ranges from f_{lim} to the highest model frequency f_{high}.

In the first part the spectrum is predicted prognostically, i.e. the rate of change of the spectral density is determined exclusively by the source functions. For the other part of the frequency range an f^{-4} tail is assumed with the same directional distribution as the frequency band with frequency f_{lim}.

A (quasi)-implicit scheme is used for the integration of the energy balance equation with respect to time. This scheme is implemented as a hybrid scheme in the sense that for some spectral bins the implicit scheme is changed to an explicit scheme. To ensure stability of integration the growth of a spectral component per time step is limited. This limitation, however, does not impose constraints on the spectral shape. In the present computations the time step is equal to 900 s. Details of this integration procedure are given in the WAM paper (WAMDI group, 1988).

3.2.5 The DH model

3.2.5.1 Introduction

The main feature of the DH model is the parametric method for the computation of the nonlinear transfer. This method is based on a narrow peak approximation of the nonlinear transfer and has been developed by Dungey and Hui (1979) and extended by Van Vledder (1984). The principle of this method and its application in a discrete spectral wave model are described below.

3.2.5.2 Computation of nonlinear transfer

Dungey and Hui (1979) derived a method to compute the nonlinear transfer in an action density spectrum with a characteristic spectral width ε and a spectral peak with wavenumber $\underline{k}_0$, defined in Fig. 3.3. In order to compute the nonlinear transfer for an arbitrary spectrum, this spectrum is written as an action density as a function of the wavenumber components k_x and k_y. In case the direction of the peak wavenumber $\underline{k}_0$ is not in the direction of the k_x-axis, the spectrum should be rotated such that $\underline{k}_0$ becomes equal to $(k_0,0)$. Next, this action density spectrum is approximated with a finite number of

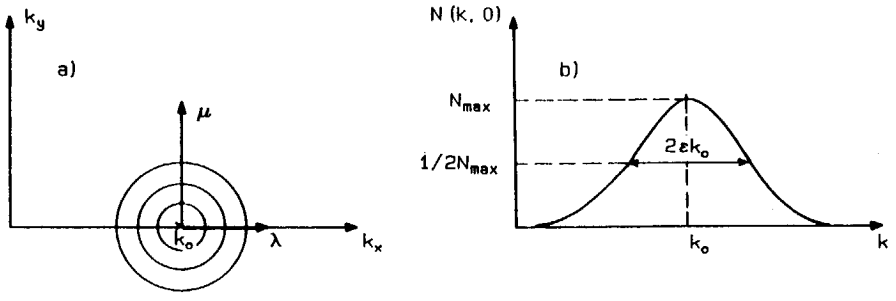

Fig. 3.3 Definition sketch of local coordinate system (panel a), and of peak wavenumber $\underline{k}_0$ and spectral width ε (panel b).

Gaussian shaped surfaces, centered near the peak wavenumber $\underline{k}_0$. For that purpose a local coordinate system, denoted by (λ,μ) is used. The relation between the global and the local coordinate system is:

$$k_x = k_0 + \varepsilon\ \lambda \tag{3.9}$$

$$k_y = \varepsilon\ \mu \tag{3.10}$$

in which λ and μ are the local coordinates and k_x and k_y are the global coordinates. In the local coordinate system around the spectral peak the action density spectrum $N(k_x,k_y)$ is approximated by the sum of n Gaussian shaped functions:

$$N(\lambda,\mu) = \sum_{j=1}^{n} R_j \exp\left[-\tfrac{1}{2} P_j(\lambda-U_j)^2 - Q_j\mu^2 \right] \tag{3.11}$$

in which the terms P_j, Q_j, R_j and U_j are coefficients determining the width, scale and location relative to $\underline{k}_0$ of the Gaussian surfaces. Eq. (3.11) is only suited for a representation of directionally symmetrical action density spectra. The extension by Van Vledder (1984) generalizes this to directionally skewed spectra. For that purpose an extra term V_j is added to Eq. (3.11) to specify the location of the

Gaussian surface with respect to the peak wavenumber $\underline{k}_0$:

$$N(\lambda,\mu) = \sum_{j=1}^{n} R_j \exp\left[-\tfrac{1}{2} P_j(\lambda-U_j)^2 - Q_j(\mu-V_j)^2 \right]. \qquad (3.12)$$

The values of the shape parameters P_j, Q_j, R_j, U_j and V_j are obtained with a fit procedure based on a least squares method that is applied to spectral points near the peak of the spectrum (Van Vledder, 1984).

When the shape factors are known the nonlinear transfer can be computed by substitution of Eqs. (3.9), (3.10) and (3.12) in the equation for the Boltzmann integral (2.46). For action density spectra of the form (3.12) the corresponding rate of change is given by (see Appendix E):

$$\frac{\partial N(\lambda_1,\mu_1)}{\partial \tau} =$$

$$\frac{16\,\pi\, k_0^{15/2}}{\sqrt{g}\;\rho_w^{\,2}} \sum_{\ell=1}^{4} \sum_{p,q,r=1}^{n} \left\{ I_1 + \frac{\varepsilon}{k_0} \left[6\lambda_1 I_1 + 3I_2 - I_3 - I_4 \right] \right\} + O(\varepsilon^2) \qquad (3.13)$$

with $\tau = \varepsilon^2 t$ and in which I_1, I_2, I_3 and I_4 are one-dimensional integrals. A detailed description of the computation of the nonlinear transfer with this method is given in Appendix E and in Van Vledder (1984).

3.2.5.3 Numerical integration of the energy balance equation

The integration of the energy balance equation is performed with an explicit first order forward time method. For each integration step the position of the peak wavenumber $\underline{k}_0$, the spectral width ε and the values of the shape factors determining the location and curvature of

the Gaussian surfaces are calculated.

Numerical experiments with the DH model have shown that the integration method in which the nonlinear transfer is computed with the DH method is unstable. Computations show that initially small perturbations of the spectrum became larger with each time step by the effect of the wind input source term. They were not smoothed out by the nonlinear transfer. The result was a very ragged spectrum which finally could not be handled by the integration scheme. It is suggested that these instabilities are due to the method of computing the nonlinear transfer. A possible reason is given below.

It is a principal property of the nonlinear interactions to force the spectrum into some standard shape, thereby smoothing out local perturbations. It is therefore necessary that a method for the computation of the nonlinear transfer recognizes these local perturbations and smoothes them. The DH method detects these local perturbations only to a certain degree, viz. in the fit procedure for the determination of the shape factors of the Gaussian surfaces, but it cannot smooth out these local perturbations. Application of smoothing procedures to the spectrum may remedy this problem. However, solution of this problem is considered to be outside the scope of this study.

3.3 Description of simulations

3.3.1 Introduction

This section describes the conditions for the computations. This includes a specification of the homogeneous wind fields, the initial conditions for the simulation runs and the variations of each of the coefficients in the dissipation source function used in the sensitivity analysis.

The strategy and the conditions for these simulations are adopted from the SWAMP study (1985) and similar computations by Young et al. (1987).

In the SWAMP study (1985) the behaviour of ten wave prediction models (including the EXACT-NL model) was investigated. A set of test cases was designed to focus separately on various critical properties of the wave models. One of the tests was to study the directional response of the spectrum after a wind direction shift of 90° (SWAMP case VII) at a constant wind speed of 10 m/s. Young et al. (1987) considered also other cases, i.e. a sudden shift of the wind direction of 30°, 60°, 120°, 150° and 180°, each at constant wind speed of 10 m/s. The computations by Young et al. (1987) were performed with the EXACT-NL model and a preliminary version of the WAM model.

Young et al. (1987) provide interesting results concerning qualitative and quantitative aspects of the directional response. It was nevertheless deemed useful to carry the analysis further. Moreover, Young et al. (1987) study the directional response per frequency, whereas the present study focuses on the frequency integrated mean wave direction.

In this study part of the calculations by Young et al. (1987) is repeated and other turning wind cases are included. Two new types of wind fields were added. In the first of these types the new direction

of the wind has a constant angular velocity. For this case it is easy to compute the time scale of the directional response once a stationary situation has been reached, in which the mean wave direction has a constant lag relative to the wind direction and the other spectral parameters remain constant. The second new type of wind field is a mixture of a sudden wind shift and a turning wind. Here, the new wind direction initially has a constant angular velocity, but the turning stops after 90°. In addition, for one of the cases of the present study a sensitivity analysis is performed of the time scale estimates with respect to variations in the modelling of the dissipation source function.

3.3.2 Wind fields

In all simulations the magnitude of the wind velocity is constant, while the direction of the wind changes. Two wind speeds are used, U_{10} = 10 m/s and U_{10} = 20 m/s. Starting from an almost flat sea the wave field grows until the peak frequency has decreased to twice the value of the Pierson-Moskowitz peak frequency for the corresponding wind speed. At that moment the wind direction is changed to a new constant value or it is made to rotate at a constant rate, denoted by Ω. From then on the computation is continued until either the mean wave direction is almost equal to the new wind direction or the mean wave direction has a constant lag relative to the turning wind.

Seven wind fields are distinguished, which are listed in Table 3.1. Each of the cases in Table 3.1 is simulated with the EXACT-NL model for both wind speeds, whereas the WAM model is only used for the cases 1 through 4, also for both wind speeds.

In all these computations the EXACT-NL model results are the most reliable, since this model has a superior modelling of the nonlinear transfer compared to the WAM model. It was nevertheless deemed useful to perform at least part of the computations also with the WAM model

to verify its capabilities in turning wind situations with respect to the EXACT-NL model.

Case	Description of wind direction
1	sudden wind shift 30°
2	sudden wind shift 45°
3	sudden wind shift 60°
4	sudden wind shift 90°
5	turning wind, $\Omega = 10^{\circ}$/hour
6	turning wind, $\Omega = 45^{\circ}$/hour, max. 90°
7	turning wind, $\Omega = 90^{\circ}$/hour, max. 90°

Table 3.1: Specification of the wind fields that are used for the numerical computation of the directional response.

3.3.3 Initial conditions for simulation runs

For all simulations the initial spectrum is a spectrum of the JONSWAP-type with a relatively high peak frequency and little energy. The values of the parameters α and f_p are taken from the two-parameter model of Hasselmann et al. (1976). These parameters depend on the wind speed. The initial conditions are listed in Table 3.2.

	Wind speed	
Parameter	10 m/s	20 m/s
α	0.018	0.024
f_p	0.4 Hz	0.3 Hz

Table 3.2: Initial conditions for simulation runs at two wind speeds.

For the EXACT-NL model runs the initial value of the peak enhancement parameter γ was equal to 3.3 whereas for the WAM model runs γ was initially equal to 1.

3.3.4 Discretization of the spectrum

EXACT-NL

In the EXACT-NL model 28 frequencies and 12 directions are used. For the runs with U_{10} = 10 m/s the range of frequencies is 0.070 Hz - 0.918 Hz with an exponential frequency spacing of $\Delta f/f = 0.1$. For the runs with U_{10} = 20 m/s the frequency range is 0.030 Hz - 0.640 Hz with an exponential spacing of $\Delta f/f = 0.12$.

WAM model

For both wind speeds the spectrum is discretized in 26 frequencies and 12 directions. The range of frequencies is 0.042 Hz - 0.453 Hz with an exponential frequency spacing of $\Delta f/f = 0.1$.

3.3.5 Conditions for sensitivity analysis

To study the sensitivity of the directional response to variations in the modelling of the dissipation source term (Eq. 2.40) the coefficients m, n and C are varied around their basic values given by Komen et al. (1984). To avoid unrealistic spectra the values of these must all be close to the basic values.

The following five combinations of parameter values are selected. For each case, the selected parameter values are given in Table 3.3.

Case	m	n	C x 10^5	code
1	2	2	3.33	basic case
2	1	2	3.33	m^{-1}
3	3	2	3.33	m^{+}
4	2	3	3.33	n^{+}
5	2	2	1.67	C-

Table 3.3: Values of the coefficients and exponents in the dissipation source function.

For each of these combinations of parameters the directional response of the spectrum after a sudden shift of the wind direction over 90° was computed.

3.4 Methods for the quantitative analysis of the directional response

3.4.1 Introduction

For the quantitative analysis of the directional response it is assumed that the response of the mean wave direction can be described by the relaxation model:

$$\frac{\partial \theta_0(t)}{\partial t} = \frac{1}{\tau} \sin \left(\theta_w(t) - \theta_0(t) \right). \qquad (3.14)$$

Three methods are considered that can be used to estimate the time scale τ from time series of the mean wave direction. The first method is based on analytical solutions of Eq. (3.14) for the cases of a sudden wind shift and a constantly rotating wind. The second method uses finite differences, whereas the third method uses a discrete convolution technique, which in a sense is also based on finite differences.

As was found by various authors (cf. Günther et al., 1981) the time scale of the directional response varies with the growth stage of the waves. It is therefore necessary that the method of analysis has the ability to detect such variations.

3.4.2 Analytical solutions

For a number of homogeneous wind fields, analytical solutions can be found for Eq. (3.14). In this study two of such wind fields are considered:

1) the wind direction suddenly shifts, remaining constant thereafter, and
2) the wind turns with a constant angular velocity.

Case 1: sudden wind shift

For this situation the initial condition for Eq. (3.14) is:

$$\theta_0 = 0 \qquad \text{for} \quad t = 0 \tag{3.15}$$

with θ_w given by:

$$\begin{cases} \theta_w = 0 & \text{for} \quad t = 0 \\ \theta_w = \theta_{w,s} & \text{for} \quad t > 0 \end{cases} \tag{3.16}$$

in which θ_w is the wind direction and $\theta_{w,s}$ is the angle of the wind shift. Assuming a constant time scale, the following solution to Eq. (3.14) has been given by Young et al. (1987):

$$-\ln \left[\frac{\tan\left(\frac{1}{2} \left(\theta_{w,s} - \theta_0(t)\right)\right)}{\tan\left(\frac{1}{2} \theta_{w,s}\right)} \right] = \frac{t}{\tau} \tag{3.17}$$

which can be written as:

$$\theta_0(t) = \theta_{w,s} - 2 \arctan \left[\tan\left(\frac{1}{2} \theta_{w,s} \right) \exp\left(-t/\tau \right) \right]. \tag{3.18}$$

A graph of Eq. (3.18) is shown in Fig. 3.4 for the cases of a wind shift of 30° with time scales of 5 and 10 hours.

To estimate the time scale τ, time series of the mean wave direction are transformed according to Eq. (3.17) and plotted against time t. Then for a constant time scale τ all data points should lie on a straight line, where the slope of this line is equal to $1/\tau$. When a number of data points is available, the slope of a best-fit straight line, and thus the time scale τ, can be estimated by a regression analysis. This method has been used by Young et al. (1987).

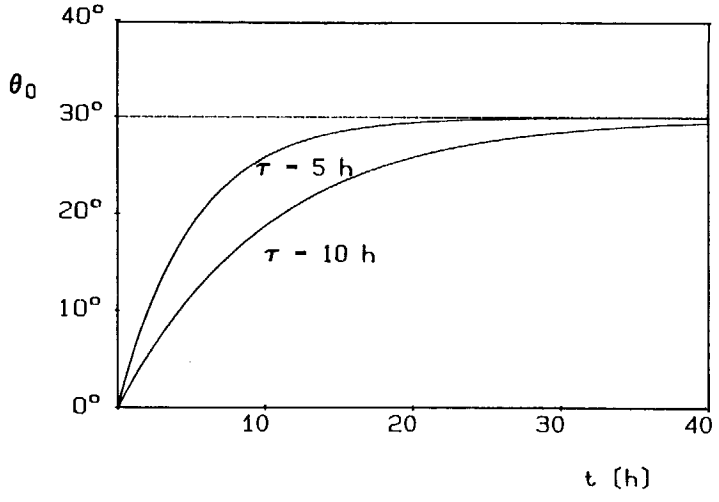

Fig. 3.4 Two analytical solutions of Eq. (3.14) for the case of a sudden wind shift over 30 degrees, with time scales of 5 and 10 hour.

This method has been tested with results of computations with the EXACT-NL model for the cases of a sudden wind shift of 30°, 45°, 60° and 90° and for a wind speed of 20 m/s. The results are given in Fig. 3.5 in which it can be seen that the transformed time series of the mean wave direction do not lie on a straight line, thus the time scale τ cannot be regarded as a constant.

A disadvantage of this method is the assumption of a constant time τ scale during the transition. Possible variations in the time scale cannot be detected.

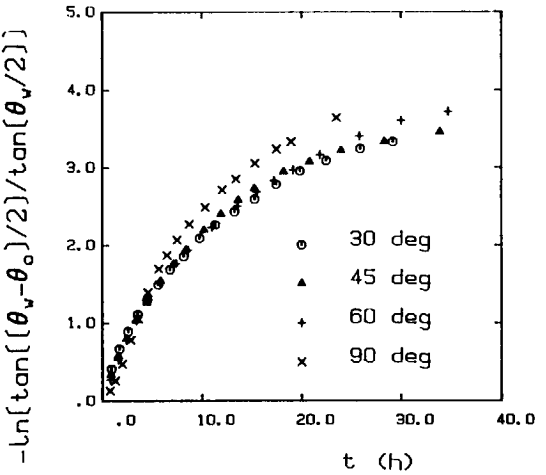

3.5 Transformed time series of mean wave direction according to Eq. (3.17) for the cases of a sudden wind shift of 30°, 45°, 60° and 90° and a wind speed of 20 m/s. Computed with the EXACT-NL model.

Case 2: Constant angular velocity

Here the wind direction is given by:

$$\theta_w(t) = \Omega\, t. \tag{3.19}$$

For this case the analytical solution of Eq. (3.14) is:

$$\frac{\partial \theta_0}{\partial t} = \Omega \tag{3.20}$$

so

$$\theta_w(t) - \theta_0(t) = \text{const.} = \Delta\theta_w. \tag{3.21}$$

Thus the mean wave direction has a constant directional lag $\Delta\theta_w$ relative to the wind direction. The time scale is easily computed by substitution of Eq. (3.19) in Eq. (3.14):

$$\tau = \frac{\sin(\Delta\theta)}{\Omega} \quad . \tag{3.22}$$

3.4.3 Finite differences

An estimate of the time scale τ can be obtained by applying the central difference scheme to the time series of the mean wave direction:

$$\tau(t_j) = \frac{t_{j+1} - t_{j-1}}{\theta_{0,j+1} - \theta_{0,j-1}} \sin\left(\theta_{w,j} - \theta_{0,j} \right) \tag{3.23}$$

in which j is a time index. An advantage of this method above the method described above is the possibility to determine variations in the magnitude of the time scale during the transition.

In the time series obtained with the EXACT-NL model, small variations of the mean wave direction occur which are regarded here as numerical noise. The effect of these small fluctuations is that estimates of the time scale with the finite difference scheme (3.23) show relatively large fluctuations. In order to avoid these fluctuations, a method has been developed to smooth the time series so that stable estimates of the time scale are obtained. This method is a discrete convolution filter and is described below.

3.4.4 Smoothing of the time series with a discrete convolution filter

3.4.4.1 Introduction

To suppress rapid variations of the mean wave direction the time series are smoothed by a low pass filter. Care must be taken with the choice of the cut-off frequency of this filter. It must be high enough

to ensure that only rapid variations are suppressed which have a time scale that is much smaller than the time scale of the directional response.

Below a discrete convolution technique is developed that can be used to smooth unequally spaced time series, such as those generated by the EXACT-NL model. This filter is based on a convolution in the time domain of the raw (i.e. obtained from the numerical computations) time series of the mean wave direction with a window function. A description of this smoothing technique and its application are given below.

3.4.4.2 Derivation of discrete convolution filter

Consider a continuous time signal F(t). This signal is smoothed by a convolution with a certain non-negative window function $W(\tau)$ to obtain a smoothed continuous time signal G(t):

$$G(t) = \int_{-\infty}^{\infty} F(\tau)\, W(\tau-t)\, d\tau \tag{3.24}$$

with:

$$\int_{-\infty}^{\infty} W(\tau)\, d\tau = 1. \tag{3.25}$$

In a similar way a smoothed estimate of the first time derivative of F(t) can be computed by:

$$G'(t) = \frac{dG(t)}{dt} = -\int_{\infty}^{\infty} F(\tau)\, W'(\tau-t)\, d\tau \tag{3.26}$$

in which $W'(\tau)$ is the first derivative with respect to τ of the window

function $W(\tau)$.

In this study the window function $W(\tau)$ consists of two linear functions of τ with a maximum at $\tau = 0$ (its shape is like a triangle). This window function $W(\tau)$ and its derivative $W'(\tau)$ are shown in Fig. 3.6.

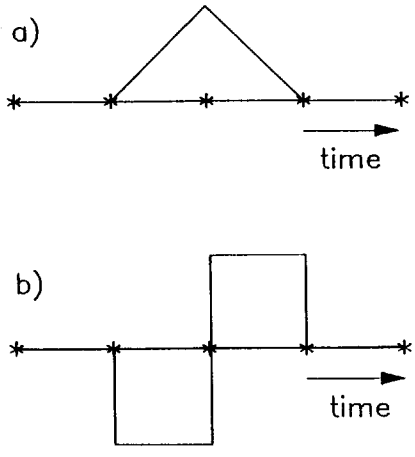

Fig. 3.6 Discrete window function (with m = 1) for the smoothing of discrete time series (panel a), and discrete window function (with m = 1) for the smoothing of the first time derivative of discrete time series (panel b).

Consider a time series with N unequally spaced data points. Now, the convolution operation is applied to m points on the left and m points on the right around each element of the time series. Thus, the filter is applied to 2m + 1 points of the time series centered around an element with index j, where j = m, (m+1), ..,(N-m). The begin and end time of the window function are given by respectively t_{j-m} and t_{j+m}. The width of the window is equal to $(t_{j+m} - t_{j-m})$.

Given a "raw" discrete time series $F(t_i)$, the smoothed discrete time series F_s can be computed as:

$$F_s(t_j) = \sum_{i=j-m}^{j+m} w_i F(t_i) \qquad j = m,\ldots,(N-m) \tag{3.27}$$

and a smoothed estimate F_d of the first time derivative of the time series is computed as:

$$F_d(t_j) = \sum_{i=j-m}^{j+m} w'_i F(t_i) \qquad j = m,\ldots,(N-m). \tag{3.28}$$

3.4.4.3 Computation of weights for filter

The weights are computed as:

$$w_i = \int_{\frac{1}{2}(t_{j-1}+t_j)}^{\frac{1}{2}(t_j+t_{j+1})} W(t)\,dt \qquad \text{for } j = i-m,\ldots,i+m \tag{3.29}$$

and

$$w'_i = \int_{\frac{1}{2}(t_{j-1}+t_j)}^{\frac{1}{2}(t_j+t_{j+1})} W'(t)dt \qquad \text{for } j = i-m,\ldots,i+m. \tag{3.30}$$

Since the time series obtained by the EXACT-NL model are unequally spaced, the weights w_i and w'_i vary with i.

The convolution technique is also used to smooth the discrete time series of other spectral parameters, such as the total wave energy. These spectral parameters are used to relate time scale estimates to the growth stage of the waves in terms of dimensionless wave energy and dimensionless peak frequency.

Estimates of the time scale τ are obtained with the scheme:

$$\tau_j = \frac{\sin(\tilde{\theta}_w - \tilde{\theta}_j)}{\tilde{\theta}'_j} \qquad \text{for } j = m,\ldots,(N-m) \qquad (3.31)$$

in which $\tilde{\theta}_j$ and $\tilde{\theta}'_j$ are the smoothed estimates of the mean wave direction and its time derivative respectively. In order to determine to what degree the data have to be smoothed, a test has been performed with a time series of the mean wave direction obtained with the EXACT-NL model. Six values of m are used, varying from 0 through 5. For each of these smoothed time series estimates are made of the dimensionless time scale as a function of the dimensionless wave energy, defined as:

$$\tau_* = \tau\, g/u_* \qquad (3.32)$$

and

$$\varepsilon_* = E_{tot}\, g^2/u_*^4. \qquad (3.33)$$

The results of the computations are shown in Fig. 3.7. In this figure it can be seen that a value of m = 3 (i.e. 7 points used in the smoothing procedure) or more gives satisfactorily smooth results. The value m = 3 is used in the following.

The time scales that are removed are of the order of the reciprocal value of the cut-off frequency of the convolution filter. Since the time step in the EXACT-NL model is dynamically adjusted, the width of the convolution filter varies per step (see section 3.2.3.3). Therefore, the time scales that are removed by the convolution filter are always lower than the time scale of the directional response. In this way local smoothing of the time series of the mean wave direction has no effect on the magnitude of the time scale estimates of the directional response.

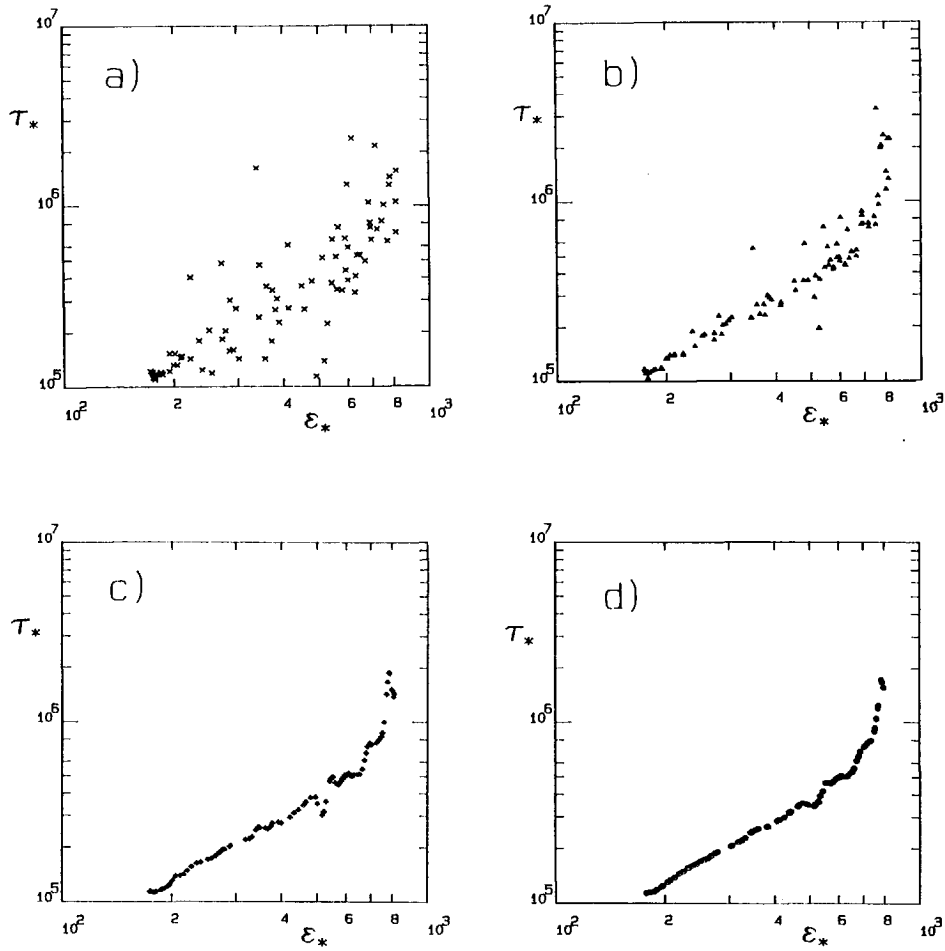

Fig. 3.7 Estimates of the dimensionless time scale τ_* as a function of dimensionless wave energy ε_* for different discrete filter widths of the discrete smoothing filter. Computed with the EXACT-NL model for the case of a sudden wind shift of 60° at a wind speed of 20 m/s. The panels (a), (b), (c) and (d) refer to discrete filter width of 0, 1, 3 and 5 respectively.

The smoothing procedure described above is also used to smooth the time series of the parameters f_p, E_{tot} and $\partial E_{tot}/\partial t$ which are used in the presentation of the results of the time scale analysis (section 3.5).

3.4.5 The effect of each separate source term on the directional response

In order to investigate the separate effects of generation, dissipation and nonlinear wave-wave interactions on the directional response of wind waves, intermediate results of a computation are used, viz. the two-dimensional energy density spectrum and the corresponding source functions at the beginning of a time step. As a rule, during integration the sum of all source functions S_{tot} is used to compute a new spectrum. Here, one step is computed in which only one of the three source functions is used to compute a new spectrum. In this way per time step three spectra are obtained which are compared with the spectrum at the beginning of the integration step. By comparing the spectrum at the beginning of a time step with each of these three spectra, the rate of change of the mean wave direction due to the effect of each source term is obtained. The new spectra are computed using an explicit method with a time step Δt= 100 s. The resulting spectra are given by (omitting the f-θ dependence):

$$E_{in}(t+\Delta t) = E(t) + \Delta t\, S_{in} \tag{3.34}$$

$$E_{ds}(t+\Delta t) = E(t) + \Delta t\, S_{ds} \tag{3.35}$$

$$E_{nl}(t+\Delta t) = E(t) + \Delta t\, S_{nl}. \tag{3.36}$$

Analysis of time scale per source term

As is shown by Holthuijsen et al. (1987) the rate of change of the mean wave direction θ_0 is given by (see also appendix C):

$$\frac{\partial \theta_0}{\partial t} = \frac{\cos(\theta_0) \int_0^{2\pi} \int_0^{\infty} \cos(\theta)\, S(f,\theta)\, df\, d\theta}{\cos(\theta_s) \int_0^{2\pi} \int_0^{\infty} \cos(\theta)\, E(f,\theta)\, df\, d\theta} \sin(\theta_s - \theta_0). \qquad (3.37)$$

Now, Eq. (3.37) is written in the form:

$$\frac{\partial \theta_0}{\partial t} = \pm \frac{1}{\tau} \sin(\theta_s - \theta_0) \qquad (3.38)$$

in which the reciprocal value of the time scale τ is given by:

$$\frac{1}{\tau} = \left| \frac{\cos(\theta_0) \int_0^{2\pi} \int_0^{\infty} \cos(\theta)\, S(f,\theta)\, df\, d\theta}{\cos(\theta_s) \int_0^{2\pi} \int_0^{\infty} \cos(\theta)\, E(f,\theta)\, df\, d\theta} \right| . \qquad (3.39)$$

The ± sign in Eq. (3.38) is equal to the sign of the fraction in the r.h.s. of Eqs. (3.37) or (3.39). This notation is used to ensure positive time scales, since the concept of a negative time scale has no meaning.

Since

$$S(f,\theta) = S_{in}(f,\theta) + S_{ds}(f,\theta) + S_{nl}(f,\theta) \qquad (3.40)$$

it follows:

$$\frac{1}{\tau} = \left| \frac{\cos(\theta_0) \int_0^{2\pi} \int_0^{\infty} \cos(\theta) \left(S_{in}(f,\theta) + S_{ds}(f,\theta) + S_{nl}(f,\theta) \right) \, df \, d\theta}{\cos(\theta_s) \int_0^{2\pi} \int_0^{\infty} \cos(\theta) \, E(f,\theta) \, df \, d\theta} \right| \tag{3.41}$$

Based on Eq. (3.41) a time scale for each source function can be defined. The time scale τ_{in} is defined as:

$$\frac{1}{\tau_{in}} = \left| \frac{\cos(\theta_0) \int_0^{2\pi} \int_0^{\infty} \cos(\theta) \, S_{in}(f,\theta) \, df \, d\theta}{\cos(\theta_s) \int_0^{2\pi} \int_0^{\infty} \cos(\theta) \, E(f,\theta) \, df \, d\theta} \right| . \tag{3.42}$$

In a similar way the time scales τ_{ds} and τ_{nl} can be defined. From Eqs. (3.40) and (3.42) it follows that the time scales of the separate source functions are related to the overall time scale as:

$$\frac{1}{\tau} = \pm \frac{1}{\tau_{in}} \pm \frac{1}{\tau_{ds}} \pm \frac{1}{\tau_{nl}} \tag{3.43}$$

where in all cases the signs are those of the functionals over the respective source functions. The times scales of the response of the mean wave direction and of the response per source term are determined with a finite difference method applied to the computed time series of the mean wave direction.

3.5 Results of simulations

3.5.1 Introduction

This section summarizes the results from the EXACT-NL model and WAM model computations without discussions; these are deferred until section 3.6. Since a presentation of all results is too comprehensive, only the most relevant results are presented. For most cases of Table 3.1 (page 79) only the EXACT-NL model results computed for a wind speed of 20 m/s are presented.

Results concerning the total wave energy E_{tot} and the peak frequency f_p are presented in dimensionless form. These parameters are normalized with the friction velocity u_* using Eqs. (3.32) and (3.33). For the transformation of the wind speed U_{10} to the friction velocity u_*, Eqs. (2.52) and (2.53) are used. For the wind speeds 10 m/s and 20 m/s, the friction velocity u_* is then equal to 0.381 m/s and 0.917 m/s respectively.

The results of the computations are presented in the Figs. 3.8 through 3.33. These figures are given at the end of this section, they are discussed in section 3.6.

The remainder of this section consists of three parts. In the first part general characteristics of the directional response are presented by means of time series of integral wave parameters and plots of the two-dimensional spectrum. The physical processes active during the response are studied by inspection of the shape of the two-dimensional source functions. In the second part the results of the time scale analysis are given. The third part contains the results of the sensitivity analysis.

3.5.2 General characteristics of the response of the spectrum

The sudden wind shift cases

For the situations of a sudden wind shift over 30°, 45°, 60° and 90° (see Table 3.1) and a wind speed of 20 m/s the response of the mean wave direction θ_0, the directional width σ, the dimensionless wave energy ε_* and the dimensionless peak frequency ν_* as computed with the EXACT-NL model are given in Figs. 3.8, 3.9, 3.10 and 3.11 respectively. It is noted that these figures are based on the raw, nonfiltered EXACT-NL data.

For the situations of a sudden wind shift of 30°, 60° and 90° polar contour plots of the spectral density are given for a number of times during the response (Figs. 3.12, 3.13 and 3.14 respectively). These results are based on EXACT-NL computations at a wind speed of 20 m/s. To illustrate the flow of energy within the spectrum extra information is given for the relatively small wind shift of 30° and for the relatively large wind shift of 90° (Figs. 3.15 through 3.17 and Figs. 3.18 through 3.20 respectively). This information consists of polar plots of the energy density spectrum and corresponding source functions at three points during the response; at the beginning, halfway (in terms of directions) and near the end of the response when the mean wave direction is almost equal to the wind direction. To illustrate the effect of the nonlinear transfer two plots are given for this transfer; one for the positive part and one for the negative part.

In all polar plots the energy density spectra and source functions are normalized with the maximum absolute value. Isolines of constant energy density and its time derivative (corresponding to each separate source function) are given at relative heights of 0.8, 0.4, 0.2, 0.1, 0.05 and 0.025.

In the last series of polar plots (Figs. 3.15 through 3.20) the frequency axis is normalized with the peak frequency to facilitate

examination of the energy flows in the energy density spectrum relative to the peak frequency.

For the sudden wind shifts of 30°, 60° and 90° the development of the two-dimensional spectrum at a wind speed of 20 m/s as computed with the WAM model is shown in the Figs. 3.21 through 3.23.

The constantly turning wind case

For the constantly turning wind case of $\Omega = 10^{\circ}/h$ and $U_{10} = 10$ m/s, polar plots of the two-dimensional energy density spectrum and corresponding source functions are given for the equilibrium situation in Fig. 3.24, as computed by the EXACT-NL model. In these polar plots the same normalizations are used as for the sudden wind shift cases. Numerical values of the main spectral parameters in the equilibrium situation are: $\Delta\theta = \theta_w - \theta_0 = 60.2^{\circ}$, $f_p = 0.188$ Hz, $E_{tot} = 0.141$ m^2 and $\sigma = 57.8^{\circ}$.

3.5.3 Time scale analysis of integral mean wave direction

3.5.3.1 The sudden wind shift cases

As described in section 3.4 time scale estimates of the rate of change of the mean wave direction are computed with the discrete convolution technique of section 3.4.4. For the EXACT-NL model a seven-point scheme was used. For the WAM model a three point scheme was sufficient to obtain satisfactorily smooth results. Since the WAM model uses a constant time step the corresponding weights are equal to 1/8, 3/4 and 1/4.

For each simulation time series are obtained of the mean wave direction θ_0, the total wave energy E_{tot} and the peak frequency f_p. Based

on these time series estimates of the time scale τ are obtained at every time step during a simulation run. In order to keep the number of time scale estimates manageable, every fifth estimate of the time scale τ is used in the presentation.

To generalize the computational results and to compare these results with information from the literature, the time scale estimates are normalized using the friction velocity u_* and the gravitational acceleration g. They are given as a function of growth stage, represented by the nondimensional peak frequency ν_* or nondimensional wave energy ε_*.

Results of the EXACT-NL model show that for the cases with a relatively large wind shift of 90° suspiciously high time scales occur for low values of ε_*, the same is true for the WAM model results for all cases of a sudden wind shift. This is illustrated in Fig. 3.25 for the EXACT-NL computations and in Fig. 3.26 for the WAM computations, both using U_{10} = 20 m/s. In these figures it can be seen that the trend of increasing τ_* with increasing ε_* is violated for low values of ε_*. For the lowest values of ε_* some relatively high time scale estimates τ_* appear, whereas for slightly higher values of ε_* much lower time scales τ_* are found. Inspection of the time series used for the analysis shows that these time scale estimates refer to the situation just after the shift of the wind direction. The spectrum needs some time to react to the new wind direction before the turning of the mean wave direction begins. (In some cases the total wave energy initially decreases before it resumes to grow, see Figs. 3.8 and 3.10.) Since such situations cannot be regarded as directional relaxation, corresponding time scale estimates will be excluded from further presentation.

Dimensionless time scale estimates τ_* based on the computations with the EXACT-NL model and the WAM model for all available cases are given in Fig. 3.27 and Fig. 3.28 respectively for both wind speeds. They are given as a function of ε_* (panel a) and ν_* (panel b).

The WAM model results show a wave-like character for the variation of the time scale with growth stage. An explanation for this phenomenon has not been found.

Results from the EXACT-NL and WAM model are compared in Fig. 3.29 in terms of the dimensionless time scale τ_* as a function of ε_* and ν_*.

3.5.3.2 The constantly turning wind cases

For the constantly turning wind case (case 5 of Table 3.1) the time scale τ is easily computed using Eq. (3.22), yielding τ = 17900 s. Dimensionless values of the time scale, total wave energy and peak frequency are: $\tau_* = 4.61 \times 10^5$, $\varepsilon_* = 644$ and $\nu_* = 7.30 \times 10^{-3}$. The EXACT-NL model result is shown in Fig. 3.27.

3.5.4 Analysis per source term

3.5.4.1 Sudden wind shift cases

To study the effect of each source term on the directional response, the mean direction of these source terms is of interest (see section 3.4.5). This is illustrated in Fig. 3.30 for the case of a sudden wind shift of 30°, with a wind speed of 20 m/s (similar results have been obtained for the case of a sudden wind shift of 60°). Results are based on EXACT-NL model computations. The corresponding values of the reciprocals of τ, $\pm\tau_{in}$, $\pm\tau_{ds}$ and $\pm\tau_{nl}$ are given in Fig. 3.31 as a function of time, using the sign convention stated in section 3.4.5.

3.5.4.2 Constantly turning wind case

For the stationary solution obtained with the EXACT-NL model it is found the that the effect of dissipation and nonlinear interactions is to counteract the turning of the mean wave direction: dimensionless time scales of the overall and separate source terms are $\tau_* = 4.61 \times 10^5$, $\tau_{*,in} = 2.76 \times 10^5$, $\tau_{*,ds} = 1.66 \times 10^6$ and $\tau_{*,nl} = 1.18 \times 10^6$.

3.5.5 Sensitivity analysis

The effect of variations in the modelling of the dissipation source function on the directional response is illustrated in terms of time series plots of integral wave parameters and scatter diagrams of time scale estimates. The five different cases are given in Table 3.3, section 3.3.5. Results are based on the EXACT-NL model computations in which $U_{10} = 20$ m/s. For the cases investigated time series plots of the mean wave direction θ_0, directional spread σ, dimensionless energy ε_* and peak frequency ν_* are given in Fig. 3.32, the panels a trough d respectively. Time scale estimates τ_* as a function of ε_* and ν_* are given in Fig. 3.33.

It is noted that the time series of ν_* for case 3 of Table 3.3 shows a sudden change, which can be attributed to the existence of an initially low, second spectral peak with a relatively high peak frequency which at some time obtains a higher energy density than the first peak frequency associated with the old wave system; as a consequence the frequency at the largest spectral density in the overall spectrum suddenly shifts.

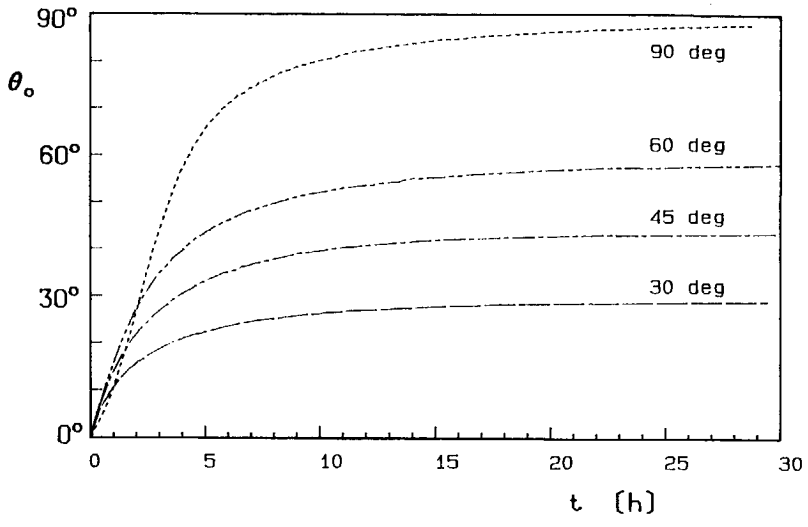

Fig. 3.8 Time series of mean wave direction θ_0 for the cases of a sudden wind shift of 30°, 45°, 60° and 90° at a wind speed of 20 m/s. Computed with the EXACT-NL model

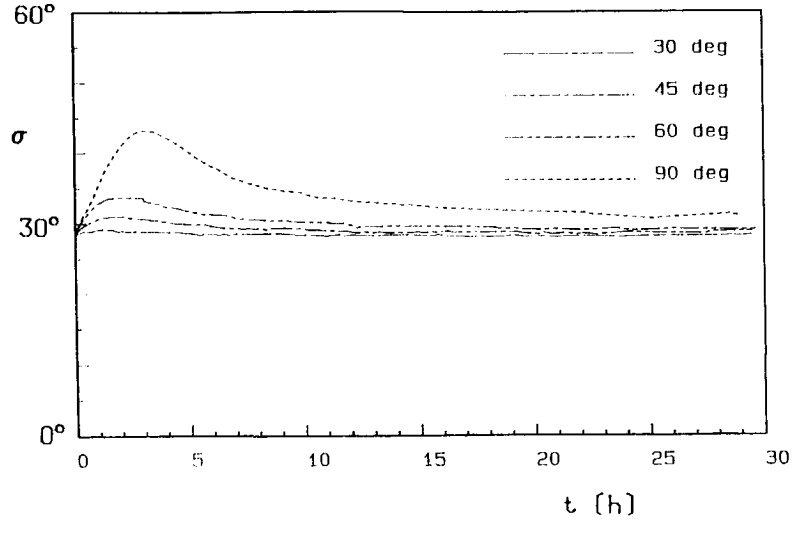

Fig. 3.9 Time series of directional width σ for the cases of a sudden wind shift of 30°, 45°, 60° and 90° at a wind speed of 20 m/s. Computed with the EXACT-NL model.

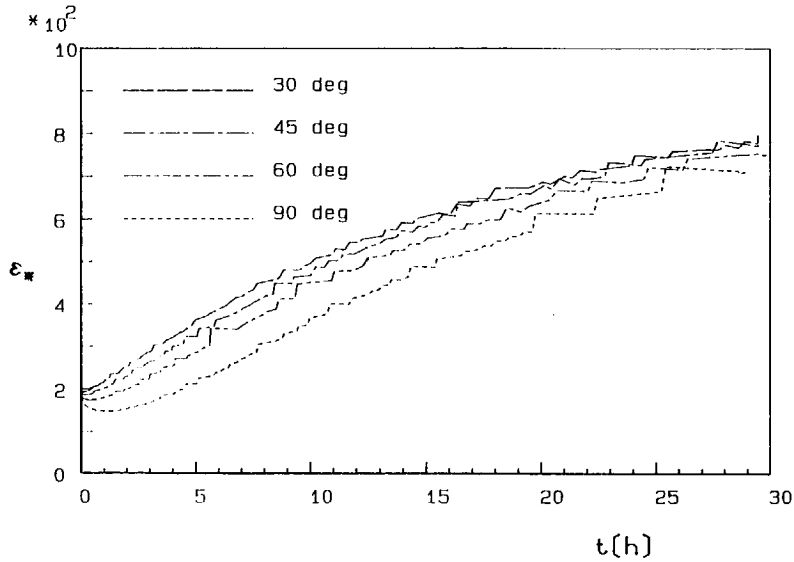

Fig. 3.10 Time series of dimensionless wave energy ε_* for the cases of a sudden wind shift of 30°, 45°, 60° and 90° at a wind speed of 20 m/s. Computed with the EXACT-NL model.

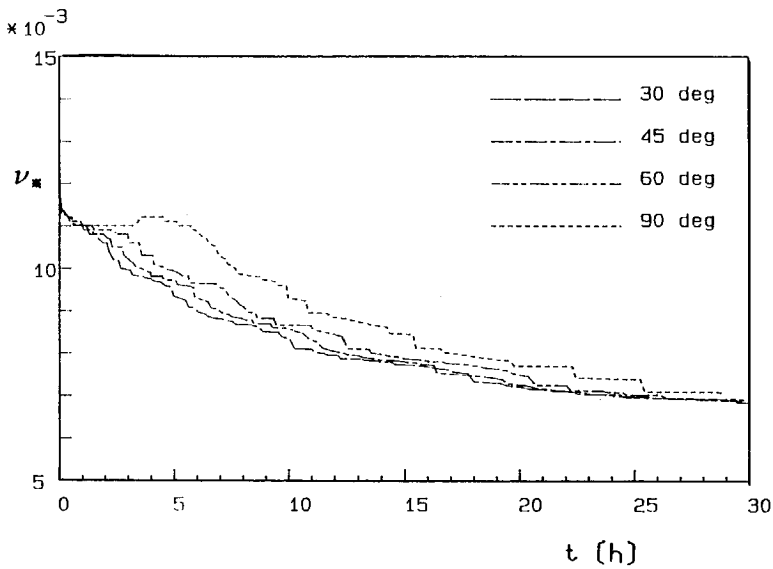

Fig. 3.11 Time series of dimensionless peak frequency ν_* for the cases of a sudden wind shift of 30°, 45°, 60° and 90° at a wind speed of 20 m/s. Computed with the EXACT-NL model.

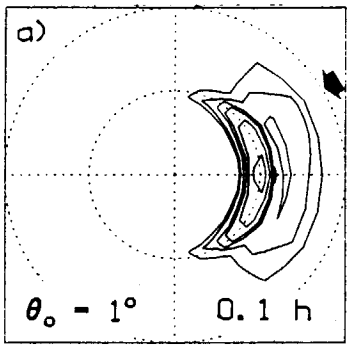
a)
θ_o = 1°
0.1 h

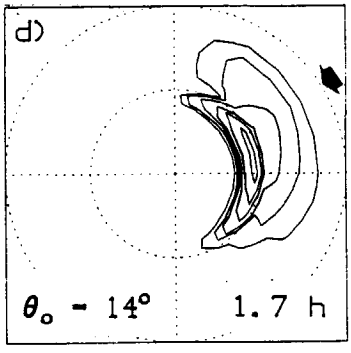
d)
θ_o = 14°
1.7 h

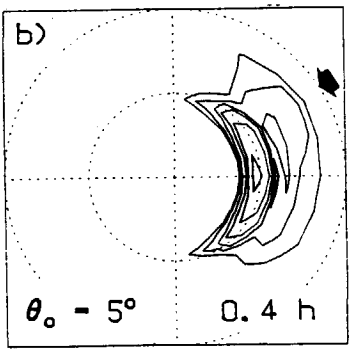
b)
θ_o = 5°
0.4 h

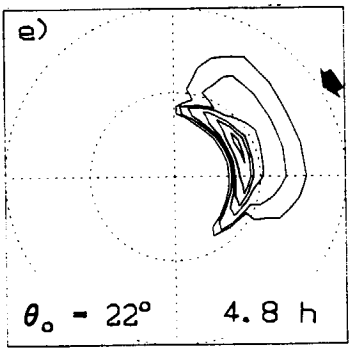
e)
θ_o = 22°
4.8 h

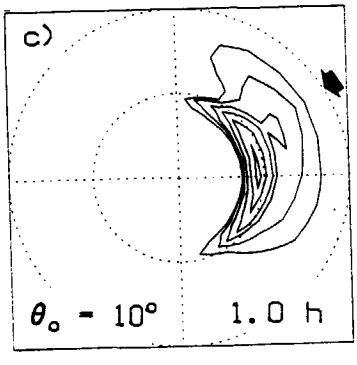
c)
θ_o = 10°
1.0 h

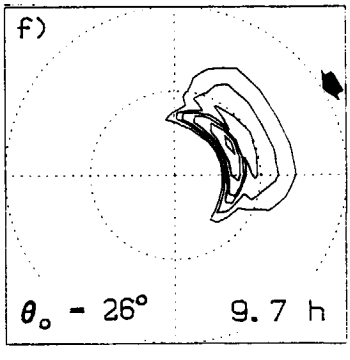
f)
θ_o = 26°
9.7 h

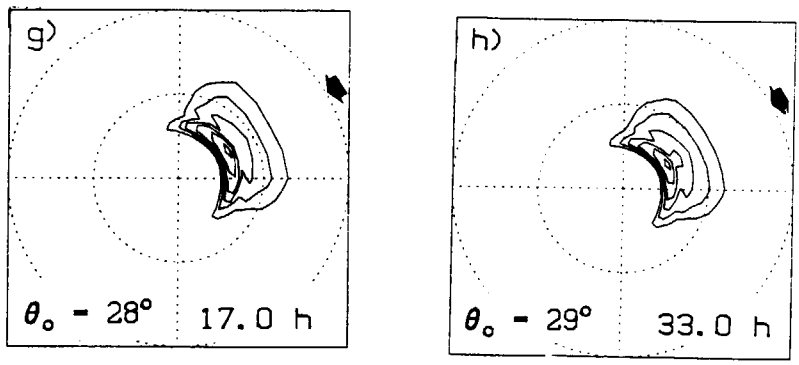

Fig. 3.12 Polar plots of normalized two-dimensional energy density spectrum after a sudden shift of 30° of the wind direction, computed with the EXACT-NL model at a wind speed of 20 m/s. Isolines at relative heights of 0.8, 0.4, 0.2, 0.1, 0.05 and 0.025. In each panel the new wind direction is shown by an arrow. Also indicated are the corresponding mean wave direction in degrees and the time in hours after the wind shift. Direction anti-clockwise from positive x-axis, dotted circles at 0.125 Hz and 0.25 Hz.

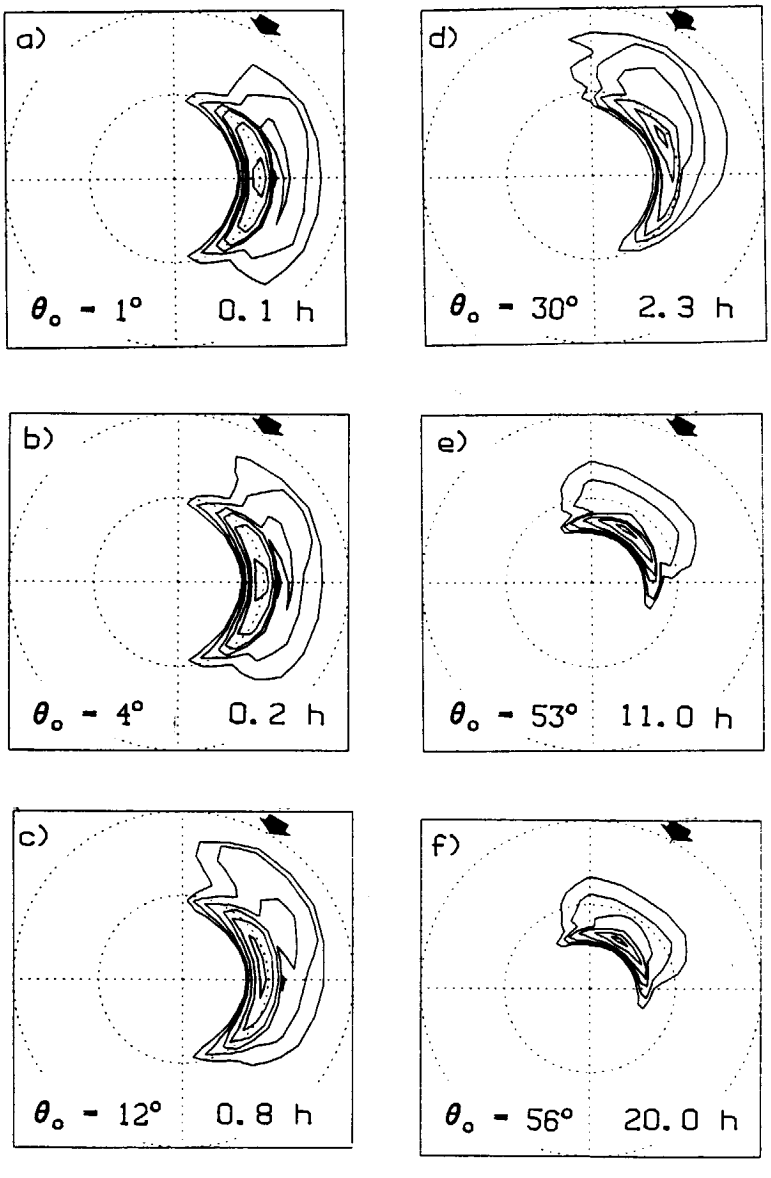
a)
θ_o = 1°
0.1 h
d)
θ_o = 30°
2.3 h
b)
θ_o = 4°
0.2 h
e)
θ_o = 53°
11.0 h
c)
θ_o = 12°
0.8 h
f)
θ_o = 56°
20.0 h

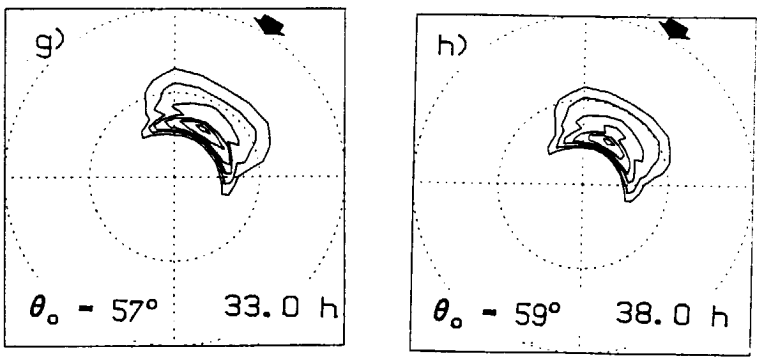

Fig. 3.13 Polar plots of normalized two-dimensional energy density spectrum after a sudden shift of 60° of the wind direction as a function of frequency and direction, computed with the EXACT-NL model at a wind speed of 20 m/s. Explanation as for Fig. 3.12.

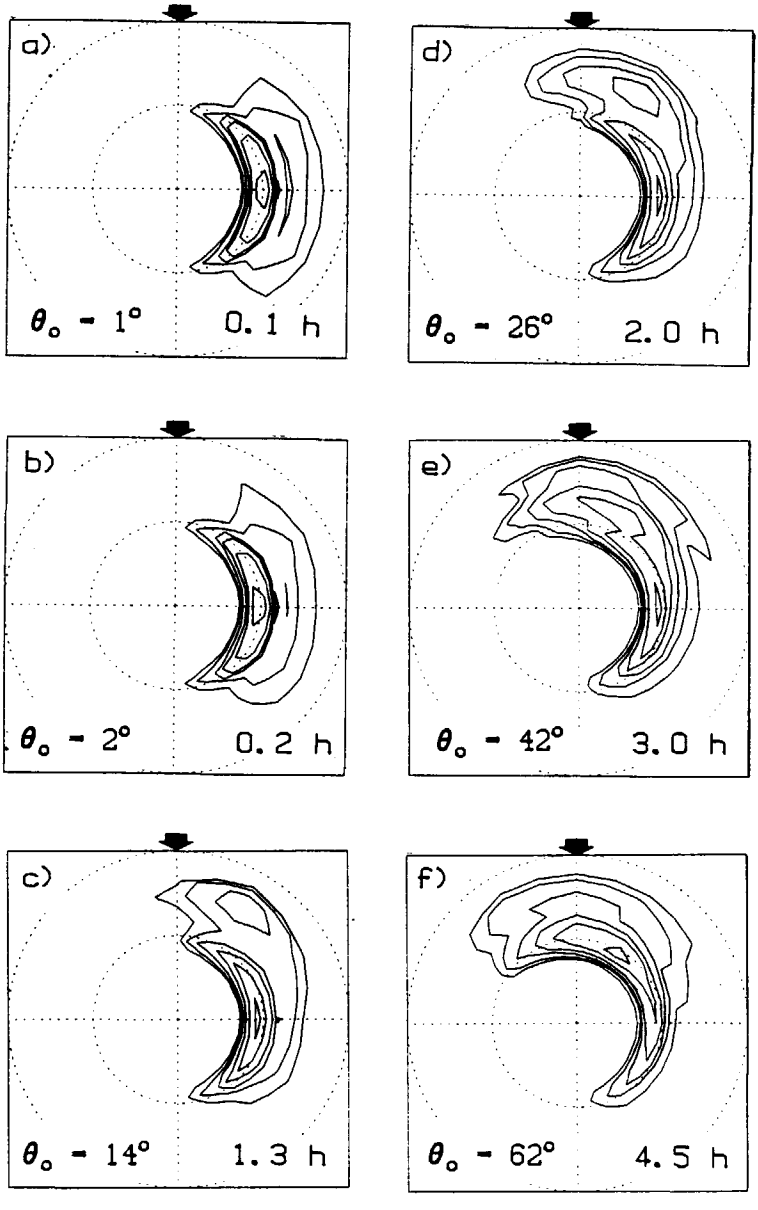
a)
θ_o = 1°
0.1 h
d)
θ_o = 26°
2.0 h
b)
θ_o = 2°
0.2 h
e)
θ_o = 42°
3.0 h
c)
θ_o = 14°
1.3 h
f)
θ_o = 62°
4.5 h

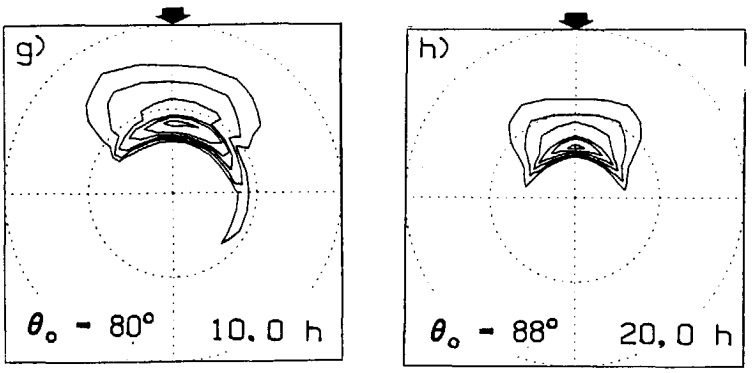

Fig. 3.14 Polar plots of normalized two-dimensional energy density spectrum after a sudden shift of 90° of the wind direction as a function of frequency and direction, computed with the EXACT-NL model at a wind speed of 20 m/s. Explanation as for Fig. 3.12.

Figure 3.15

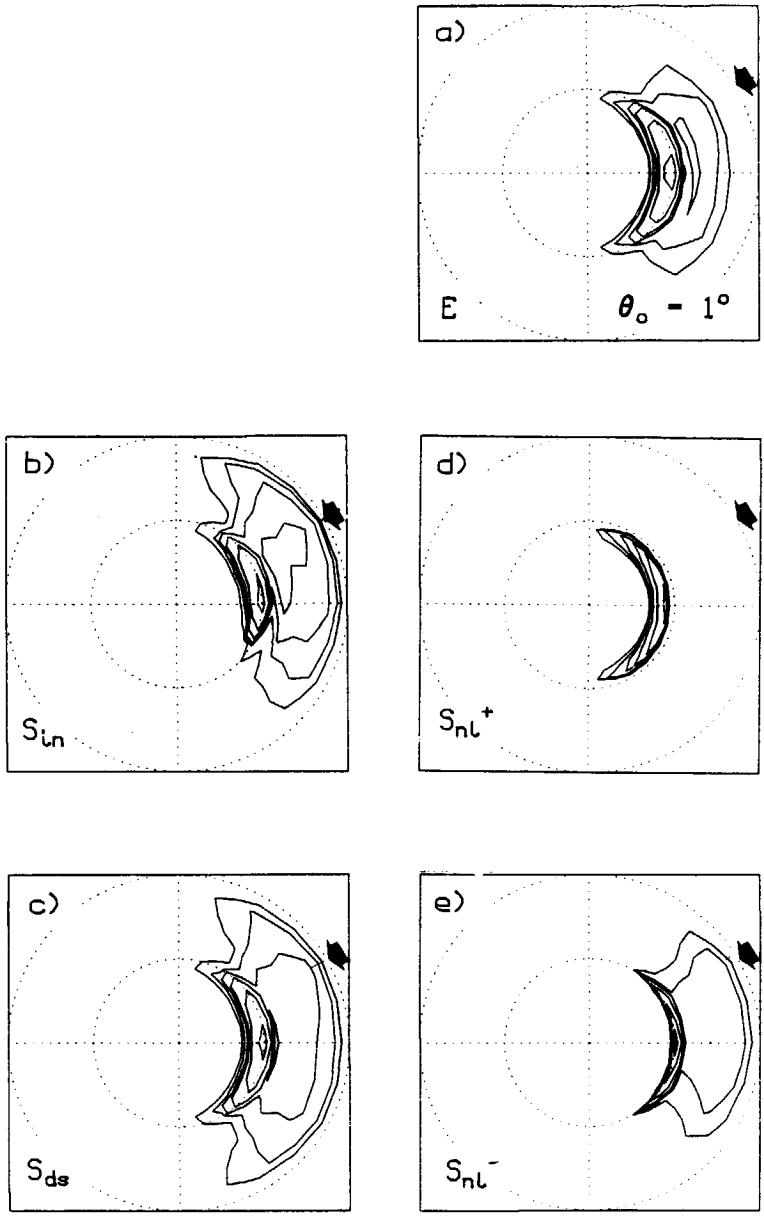

Fig. 3.15 Polar plots of normalized two-dimensional energy density spectrum and corresponding normalized source functions after a sudden shift of 30° of the wind direction for the situation $\theta_0 = 1°$, computed with the EXACT-NL model at a wind speed of 20 m/s. In each panel the new wind direction is shown by an arrow. Isolines at relative heights of 0.8, 0.4, 0.2, 0.1, 0.05 and 0.025. Direction anti-clockwise from positive x-axis. In the panels (a) through (e) the frequency axis has been normalized with the peak frequency. Dotted circles at $f/f_p = 1$ and 2. Normalized energy density spectra (panel a), wind input source function (panel b), dissipation source function (panel c), positive part of nonlinear transfer source function (panel d) and negative part of nonlinear transfer source function (panel e).

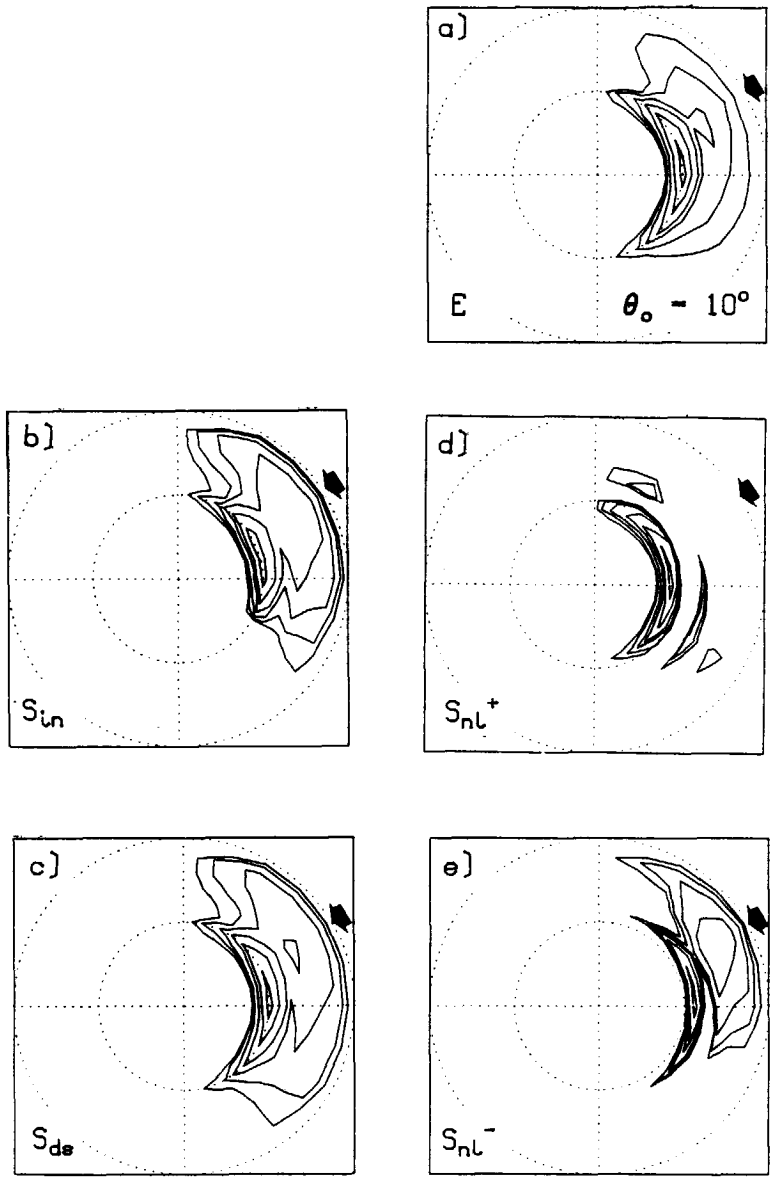

Fig. 3.16 Polar plots of normalized two-dimensional energy density spectrum and corresponding normalized source functions after a sudden shift of 30° of the wind direction for the situation θ_0 = 10°, computed with the EXACT-NL model at a wind speed of 20 m/s. Explanation as for Fig. 3.13.

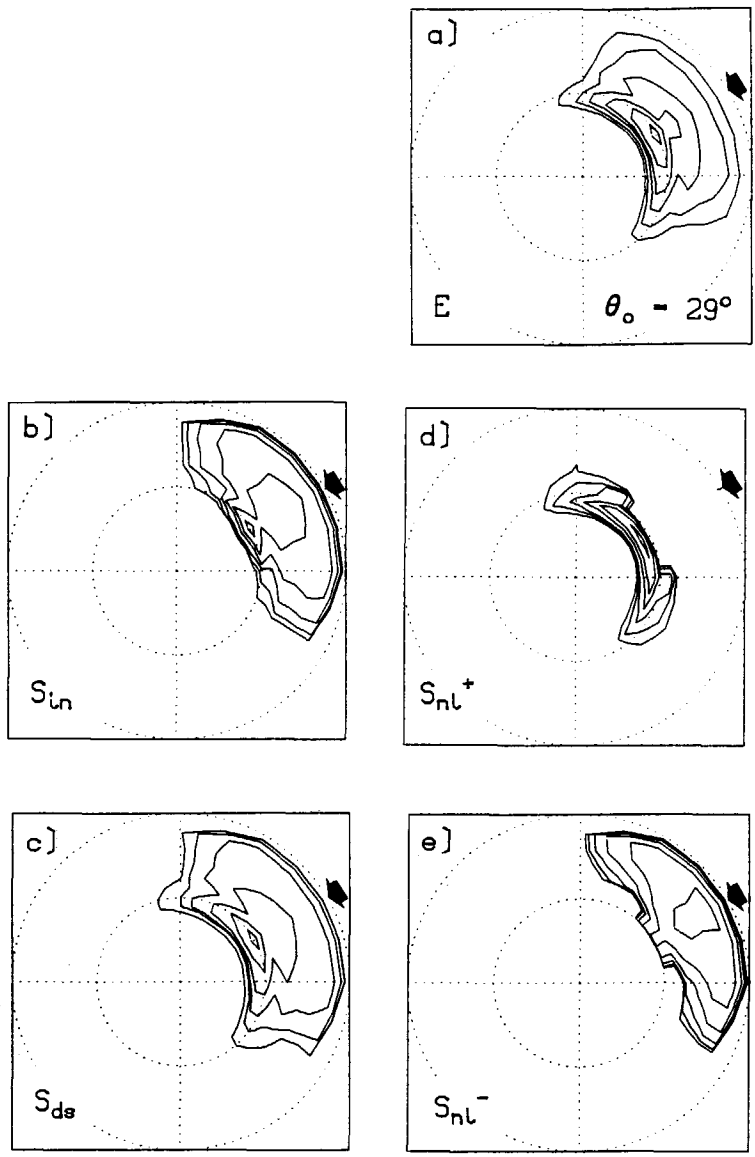

Fig. 3.17 Polar plots of normalized two-dimensional energy density spectrum and corresponding normalized source functions after a sudden shift of 30° of the wind direction for the situation θ_0 = 29°, computed with the EXACT-NL model at a wind speed of 20 m/s. Explanation as for Fig. 3.15.

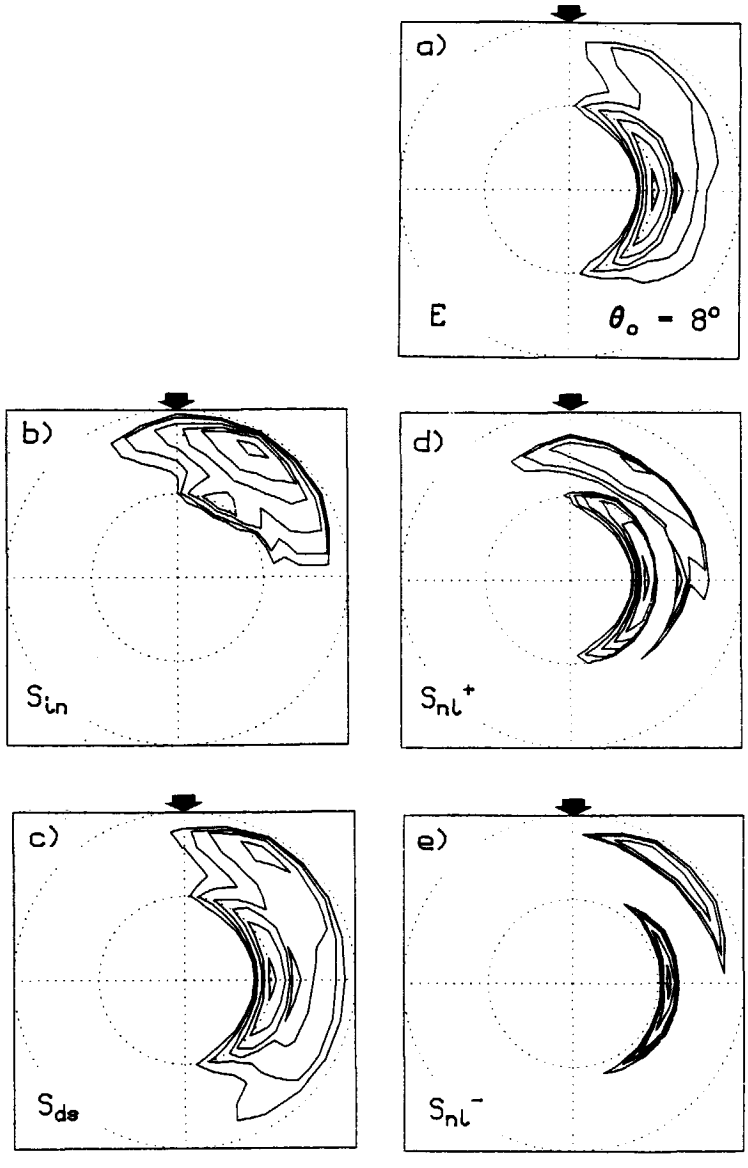

Fig. 3.18 Polar plots of normalized two-dimensional energy density spectrum and corresponding normalized source functions after a sudden shift of 90° of the wind direction for the situation θ_0 = 8°, computed with the EXACT-NL model at a wind speed of 20 m/s. Explanation as for Fig. 3.15.

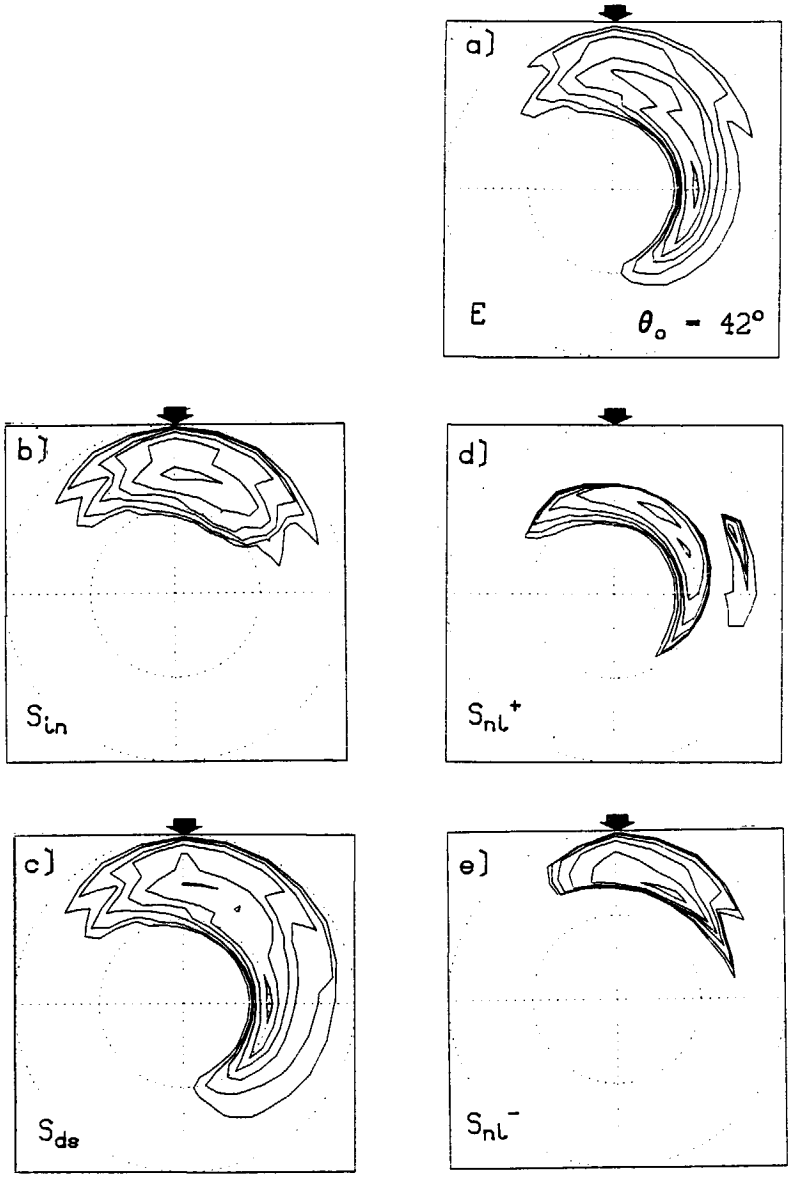

Fig. 3.19 Polar plots of normalized two-dimensional energy density spectrum and corresponding normalized source functions after a sudden shift of 90° of the wind direction for the situation θ_0 = 42°, computed with the EXACT-NL model at a wind speed of 20 m/s. Explanation as for Fig. 3.15.

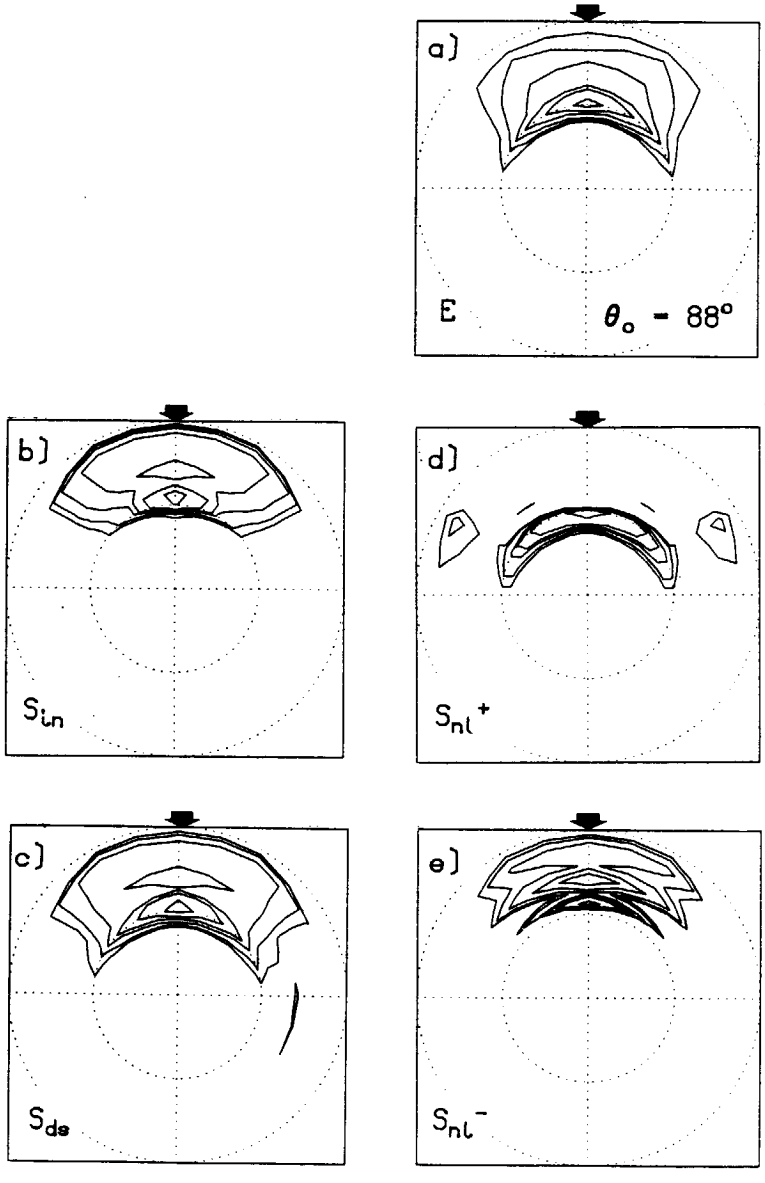

Fig. 3.20 Polar plots of normalized two-dimensional energy density spectrum and corresponding normalized source functions after a sudden shift of 90° of the wind direction for the situation θ_0 = 88°, computed with the EXACT-NL model at a wind speed of 20 m/s. Explanation as for Fig. 3.15.

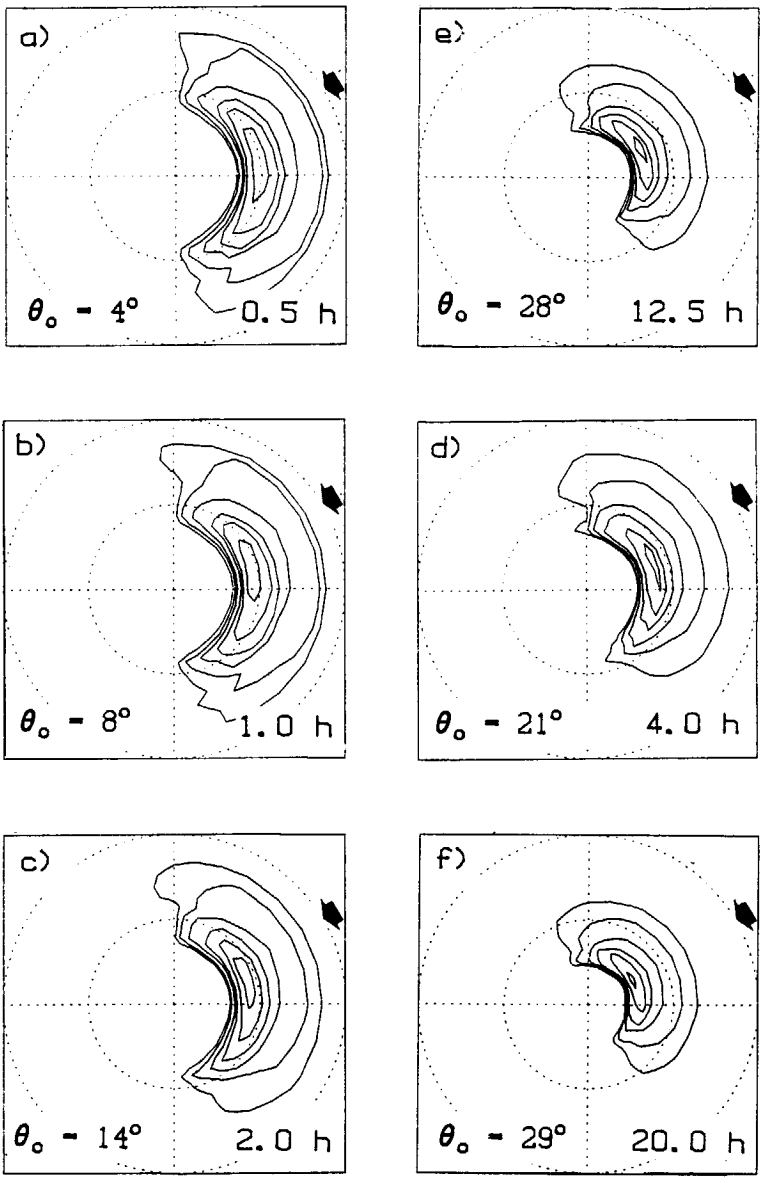

Fig. 3.21 Polar plots of normalized two-dimensional energy density spectrum after a sudden shift of 30° of the wind direction as a function of frequency and direction, computed by the WAM model at a wind speed of 20 m/s. Explanation as for Fig. 3.12.

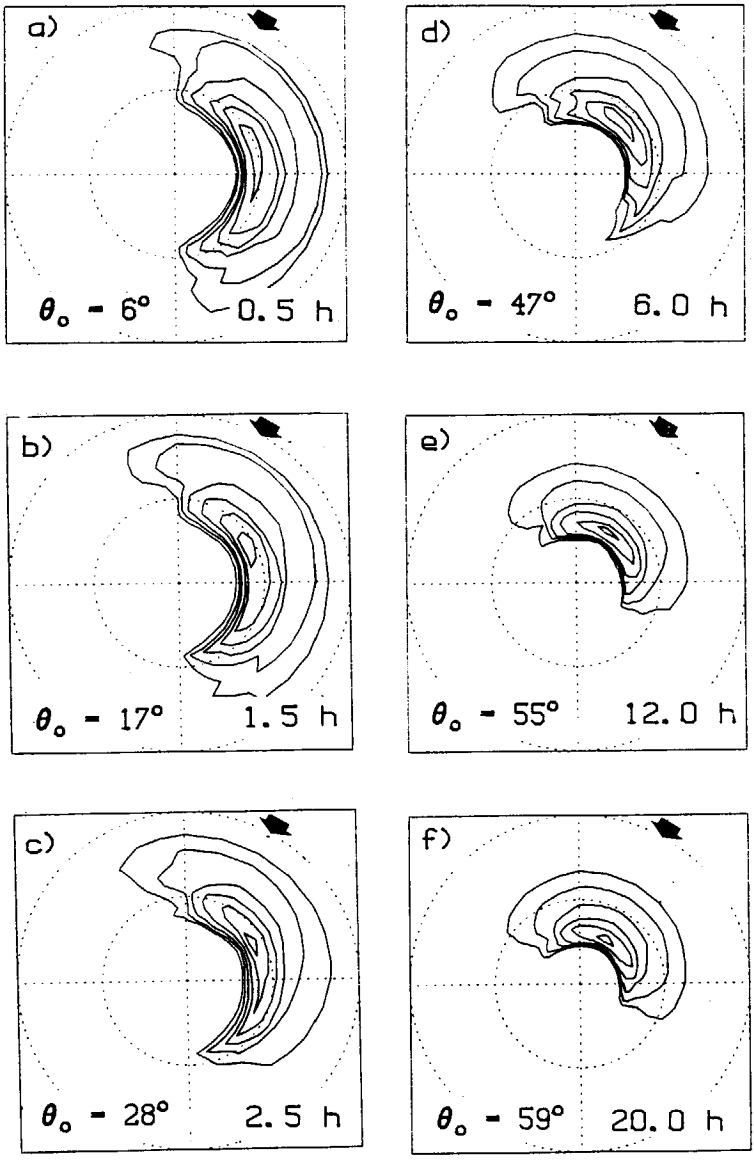

Fig. 3.22 Polar plots of normalized two-dimensional energy density spectrum after a sudden shift of 60° of the wind direction as a function of frequency and direction, computed by the WAM model at a wind speed of 20 m/s. Explanation as for Fig. 3.12.

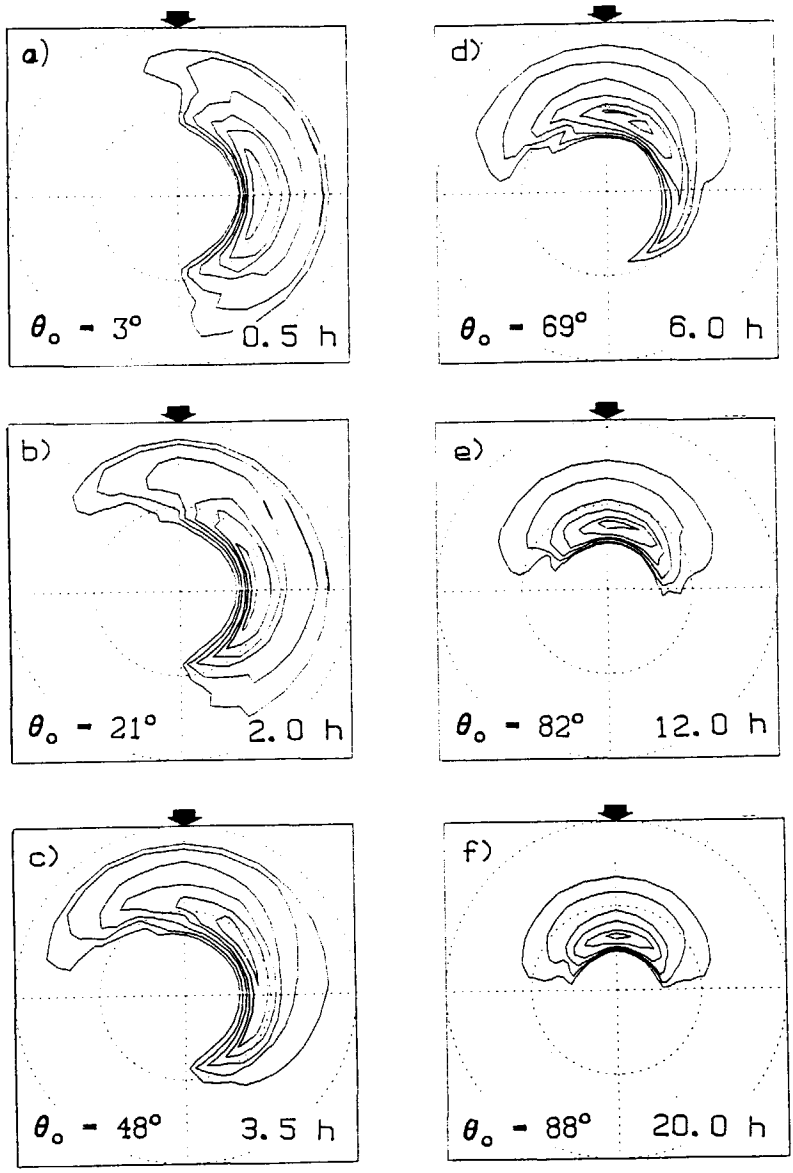

Fig. 3.23 Polar plots of normalized two-dimensional energy density spectrum after a sudden shift of 90° of the wind direction as a function of frequency and direction, computed by the WAM model at a wind speed of 20 m/s. Explanation as for Fig. 3.12.

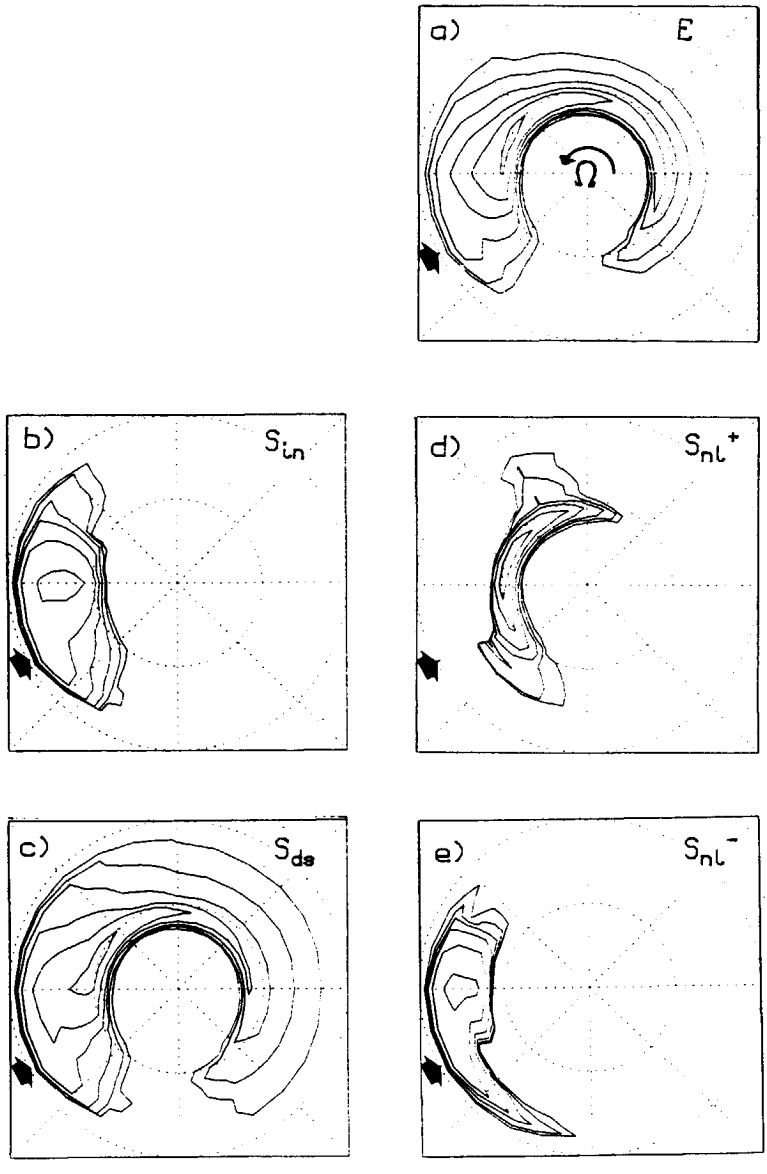

Fig. 3.24 Polar plots of normalized two-dimensional energy density spectrum and corresponding normalized source functions of the equilibrium situation (θ_w = 207° and θ_0 = 147°) for the constantly turning wind case with Ω = 10°/h and U_{10} = 10 m/s. Computed with the EXACT-NL model. Explanation as for Fig. 3.15.

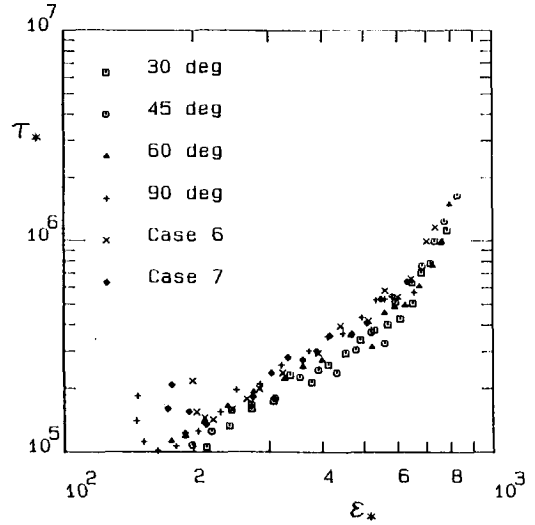

Fig. 3.25 Dimensionless time scale τ_* as a function of dimensionless wave energy ε_*, computed with the EXACT-NL model at a wind speed of 20 m/s, for the cases 1-4 and 6-7 of Table 3.1.

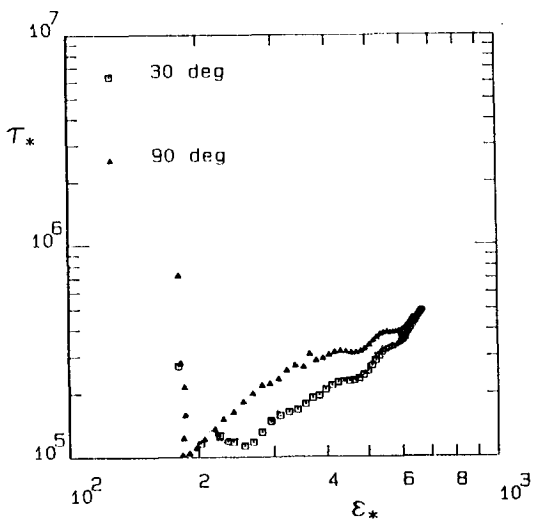

Fig. 3.26 Dimensionless time scale τ_* as a function of dimensionless wave energy ε_*, computed with the WAM model, for the cases of a sudden wind shift of 30°, 60° and 90° at a wind speed of 20 m/s.

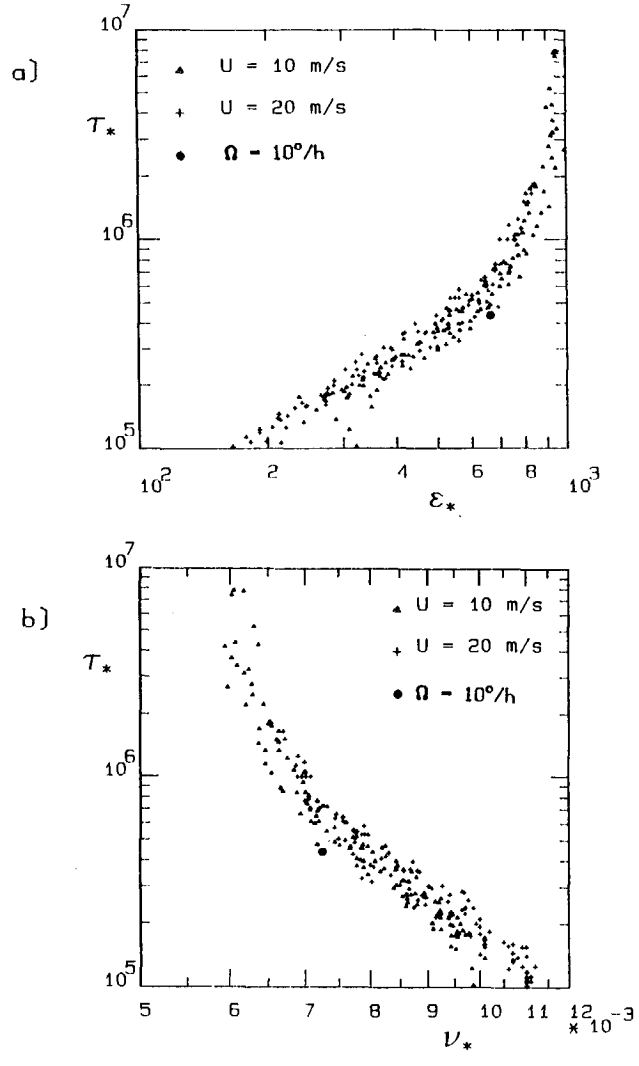

Fig. 3.27 Dimensionless time scale τ_* as a function of dimensionless wave energy ε_* (panel a), and as a function of dimensionless peak frequency ν_* (panel b). Computed with the EXACT-NL model, for all cases of Table 3.1, and for both wind speeds.

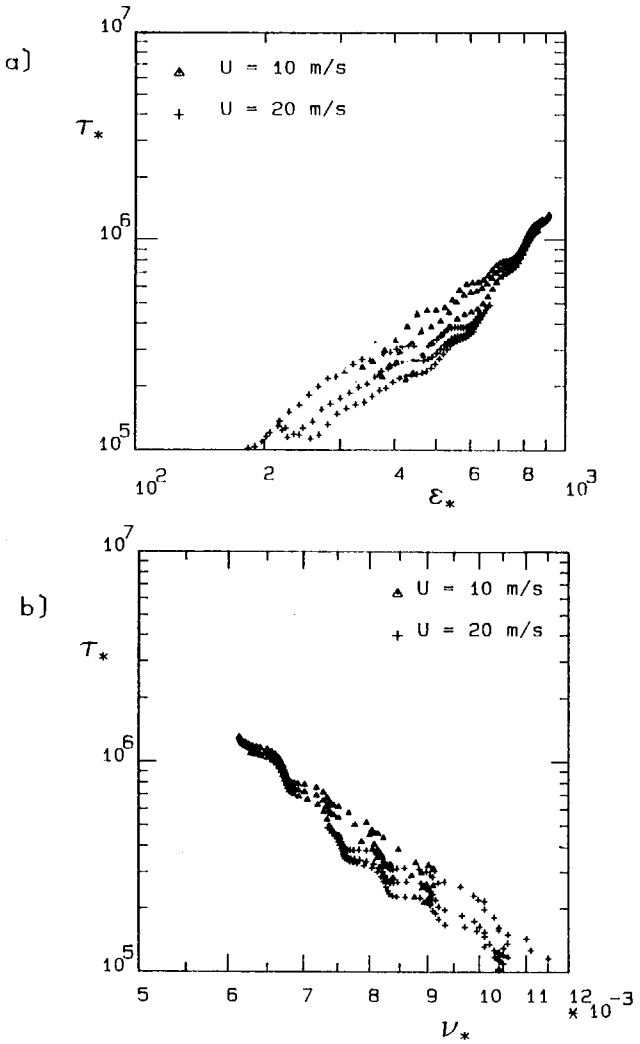

Fig. 3.28 Dimensionless time scale τ_* as a function of dimensionless wave energy ε_* (panel a), and as a function of dimensionless peak frequency ν_* (panel b). Computed with the WAM model, for the cases 1-4 and 6-7 of Table 3.1, and for both wind speeds.

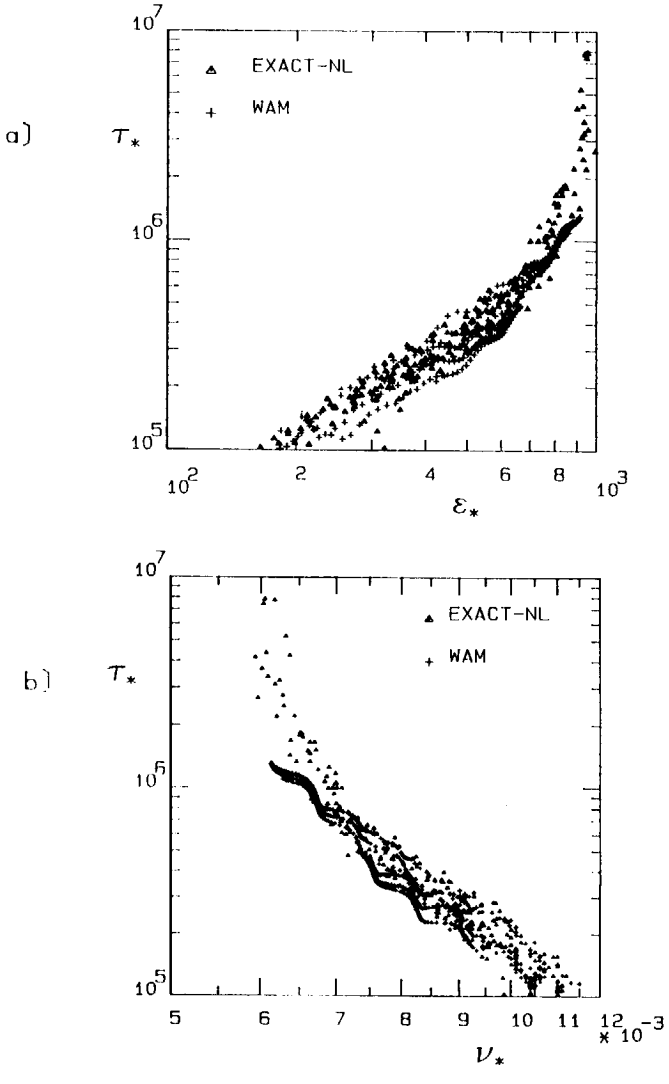

Fig. 3.29 Dimensionless time scale τ_* as a function of dimensionless wave energy ε_* (panel a), and as a function of dimensionless peak frequency ν_* (panel b). Computed with the EXACT-NL and WAM models, for the cases 1-4 and 6-7 of Table 3.1, and for both wind speeds.

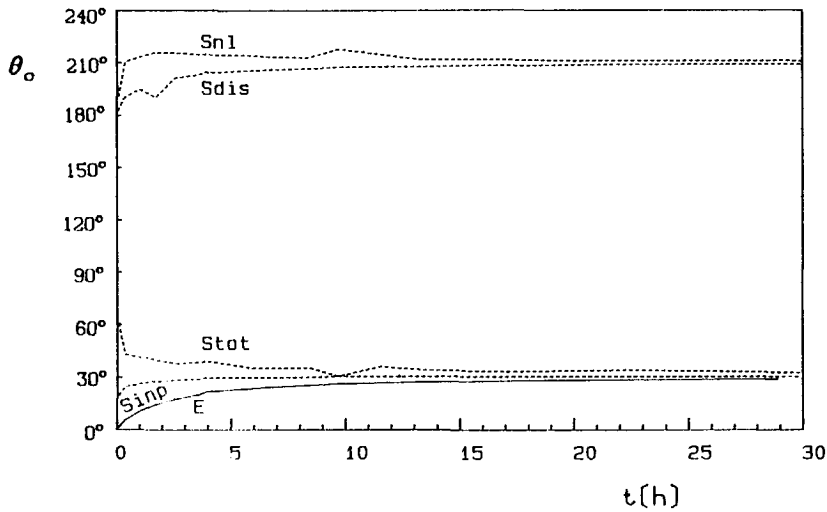

Fig. 3.30 Integral mean wave direction of spectrum and each separate source terms after a sudden wind shift of 30°, computed with the EXACT-NL model at a wind speed of 20 m/s

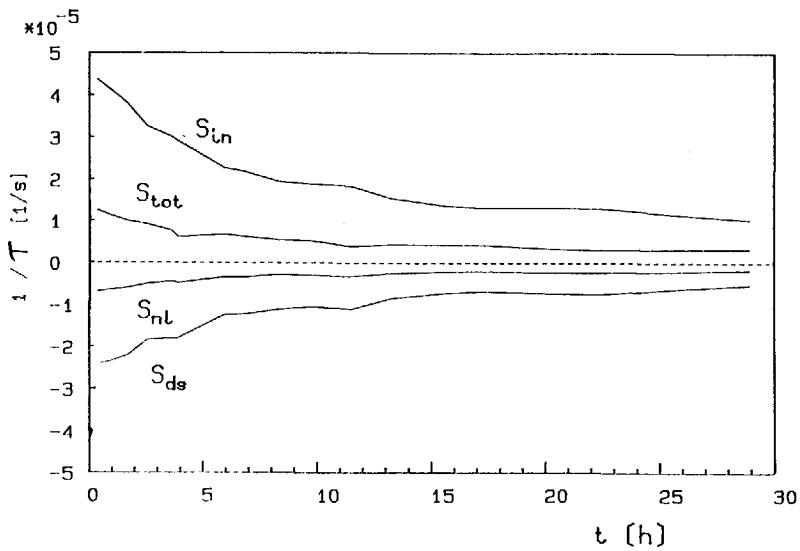

Fig. 3.31 Reciprocal values of the parameter values of τ, τ_{in}, τ_{ds} and τ_{nl}. Computed with the EXACT-NL model for the case of a sudden wind shift of 30° degrees at a wind speed of 20 m/s.

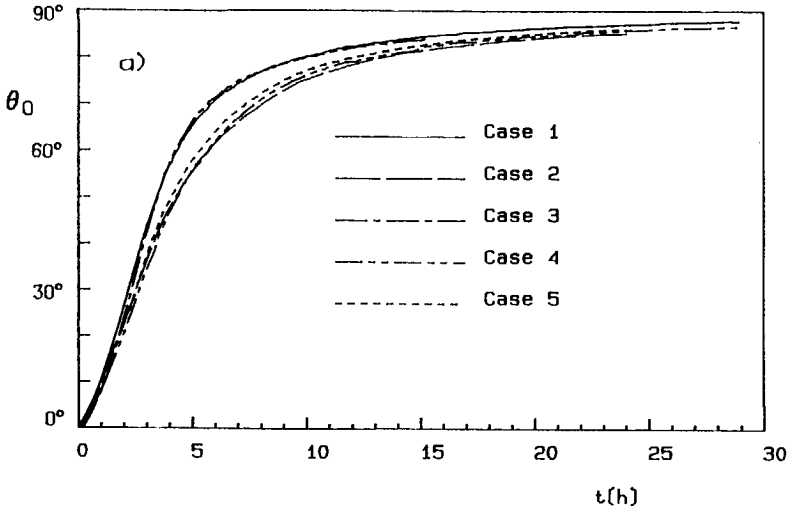
a)
θ_0
90°
60°
30°
0°
0
5
10
15
20
25
30
t(h)
Case 1
Case 2
Case 3
Case 4
Case 5

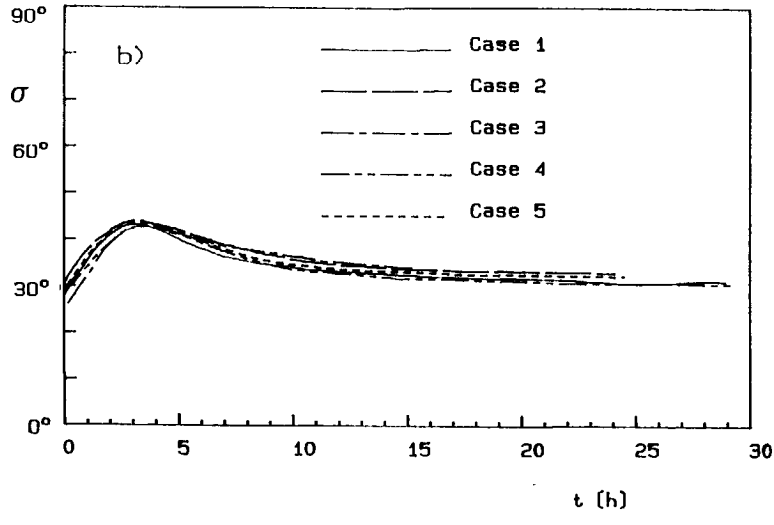
b)
σ
90°
60°
30°
0°
0
5
10
15
20
25
30
t (h)
Case 1
Case 2
Case 3
Case 4
Case 5

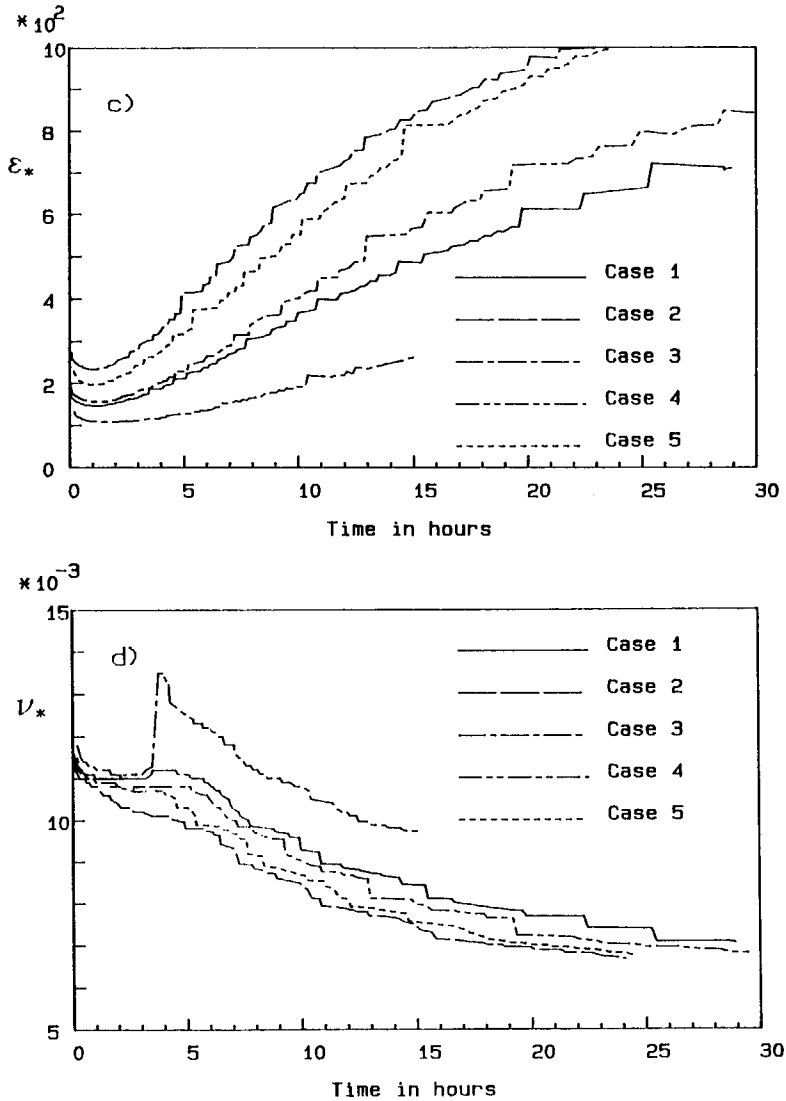

Fig. 3.32 Time series of mean wave direction (panel a), directional width (panel b), dimensionless wave energy (panel c) and dimensionless peak frequency (panel d) for the cases 1 through 5 of table 3.3. Computations with the EXACT-NL model at a wind speed of 20 m/s.

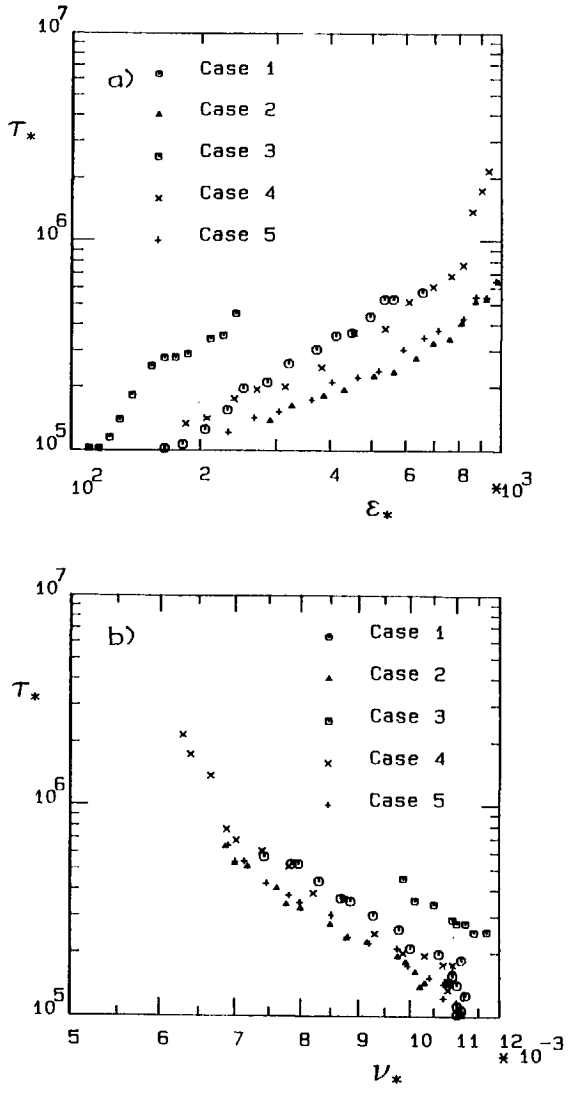

Fig 3.33 Dimensionless time scale τ_* as a function of dimensionless wave energy ε_* (panel a) and as a function of dimensionless peak frequency ν_* (panel b) for the cases 1 through 5 of the sensitivity analysis. EXACT-NL model, wind speed U = 20 m/s.

3.6 Discussion

3.6.1 Introduction

The discussion of the results of the computations of the directional response of wind waves concerns qualitative and quantitative aspects. The qualitative part addresses the response of the integral parameters for the mean wave direction, directional width, total wave energy and peak frequency. It also addresses the shape of the two-dimensional energy spectrum and corresponding source functions. The quantitative part pertains to the time scale of the response of the mean wave direction and the sensitivity analysis. For both aspects a comparison is made between the results of the EXACT-NL model and the WAM model, and for both parts results are compared with results obtained from the literature.

3.6.2 Qualitative discussion

3.6.2.1 The response of the mean wave direction, directional width, total energy and peak frequency

The curves shown in Figs. 3.8 through 3.11 are ragged, since they are based on non-filtered EXACT-NL results. Despite this behaviour they give sufficient information to discuss their characteristics.

Mean wave direction

Inspection of the response curves for relatively small wind shifts, i.e. for 30°, 45° and 60° (Fig. 3.8), shows a monotonic decrease of $\partial\theta_0/\partial t$ at a monotonically decreasing rate, just as the theoretical response curve (Fig. 3.4), whereas for a wind shift of 90° the re-

sponse curve has an S-shape, in which $\partial\theta_o/\partial t$ does not vary monotonically. This implies that the response of the mean wave direction for relatively large wind shifts cannot be considered as a relaxation process with a constant time scale. Whether or not the response of the mean wave direction for relatively small wind shift can be described as a relaxation process with a constant time scale cannot be concluded from these figures. That question is addressed in the discussion of the quantitative results.

Directional width

As can be seen in Fig. 3.9 the directional width for a wind shift of 30° is almost constant, whereas for the larger wind shifts of 45° and 60° a slight temporary increase occurs. However, for a wind shift of 90° a significant increase of the directional width occurs, before it decreases again. The fact that for relatively small wind shifts of 30° and 45° the directional width remains nearly constant, indicates that the spectral shape also remains nearly constant during the response. For the relatively large wind shift of 90° the sharp increase of the directional width possibly indicates the existence of a second spectral peak. This is confirmed by the results shown in Fig. 3.14, panels (c) and (d), in which it can be seen that during the first 10 hours of the response two wave fields exist with separate peaks, viz. one wave field which is associated with the old wave direction and one wave field which is associated with the new wind direction. However, after about 10 hours only one peak remains.

Total wave energy

Fig. 3.10 shows that for wind shifts up to 60° the total energy is increasing with time after the shift of the wind direction. However, for a wind shift of 90° a pronounced decrease of the total wave energy occurs initially. Clearly, in the first few hours after the wind

shift, the old wave system decays more rapidly than the new wave system can grow. In the present modelling of the wind input source term, the new wind sea can only develop if there is already some energy present. Shortly after the response a new wave field starts to grow in the new wind direction. However, here some time is needed for the waves to develop before the new wave field affects the mean wave direction significantly. This time lag can also be seen in the response of the mean wave direction after a wind shift of 90° (Fig. 3.8).

As time increases all growth curves for total wave energy reach the same level. However, the larger the magnitude of the wind shift the greater the time lag with respect to the growth curve of the 30° wind shift case.

Peak frequency

As can be seen in Fig. 3.11 the curves for the peak frequency after wind shifts of 30°, 45° and 60° have the same trend of a constantly decreasing peak frequency until they finally reach the same value. The exception is for the curve corresponding to the 90° wind shift, which initially shows a small decrease soon followed by an increase. This increase is due to the existence of a second spectral peak with a higher peak frequency and with a higher energy density than the 'old' wave system (see also Fig. 3.14, panel c and d). After about five hours the peak frequency starts decreasing at about the same rate as for the other cases.

3.6.2.2 The shape of the two-dimensional spectrum and the physical processes

This section discusses the shape of the two-dimensional spectra and the physical processes occurring after a sudden wind shift of 30°, 60° and 90°, for which reference is made to the Figs. 3.12, 3.13 and 3.14.

From the Figs. 3.12 through 3.14 it can be seen that for the relatively small wind shift of 30° the directional distribution of the spectrum remains nearly symmetric around the mean wave direction for all frequencies. This is also indicated by the corresponding values of the directional width during the response (see Fig. 3.9). For the larger wind shifts of 60° and 90°, the spectral shape becomes strongly skewed towards the new wind direction, and a second peak exists for a relatively long period of time. These findings have also been found by Young et al. (1987), see also section 3.6.2.4.

In all situations wave energy is generated at the higher frequencies and in the direction of the wind. In all cases studied a second spectral peak develops in the direction of the new wind direction and in the high frequency region. However, for the relatively small wind shift this second peak is quickly absorbed in the spectrum by the nonlinear interactions, whereas for the large wind shifts of 60° or more this second peak remains for a longer period.

For the extreme wind shifts of 30° and 90° a detailed picture of the response is obtained by considering the shape of the spectrum and corresponding source functions at three times during the response; shortly after the wind shift, approximately halfway the transient response (in terms of θ_0) and when the mean wave direction is almost equal to the new wind direction.

The 30° wind shift

Shortly after the wind shift (see Fig. 3.15) the spectrum is bi-modal, and almost symmetric around the old wind direction. The wind input source function is located around the new wind direction. The dissipation source function resembles the shape of the spectrum. Like the dissipation source function the nonlinear interaction source function is almost symmetric around the old wind direction. Therefore, these two source functions have no effect on the change of the mean wave direction.

Approximately halfway the response (Fig. 3.16, $\theta_0 = 10^{\circ}$) the situation is slightly changed. The spectrum is uni-modal and skewed towards the new wind direction. The dissipation source function resembles the shape of the energy spectrum except for the high frequency part of the spectrum in the direction of the wind. In this part of the spectrum considerable dissipation takes place. This is an effect of the chosen modelling of the dissipation source function. The effect is that the dissipation source function counteracts the build up of the second spectral peak more strongly than that it dissipates the old spectral peak, so that effectively the dissipation counteracts the turning of the integral mean wave direction to the new wind direction. The nonlinear interactions transfer energy towards an area with a direction close to the old wind direction at frequencies below the peak frequency. They also transfer energy from the newly generated high frequency wave energy and the peak of the spectrum towards both lower and higher frequencies. This counteracts the turning of the mean wave direction, and causes a shift of the peak frequency towards lower frequencies. Other parts of the energy flow are directed to areas with high frequencies and directions making angles of about 30° to 60° with the new wind direction. The net effect of the nonlinear interactions is that they counteract the effect of the wind somewhat (see Fig. 3.31).

Near the end of the response (Fig. 3.17) the spectrum and the source function are all centered around the new wind direction. The spectrum is uni-modal and almost fully developed. The sum of the source function is almost equal to zero for all frequencies and direction (not shown here).

The 90° wind shift

Shortly after the wind shift the spectrum is bi-modal (Fig. 3.18, $\theta_0 = 8°$) and skewed towards the new wind direction, especially for the higher frequencies. This skewed shape can be attributed to the role of the wind input. As can be seen in Fig. 3.18, panel (b), the wind input source function has its maximum at a frequency well above the peak frequency and at about 60°. The shape of the dissipation function is almost similar to that of the energy spectrum but with a second peak at the position where the wind input source function has its maximum. The nonlinear interactions (Fig. 3.18, panels d and e) transfer energy from the area of maximum wind input and from an area near the peak of the spectrum with frequencies just above the peak frequency towards an area located in the direction of the old wind direction with frequencies below the peak frequency. The other area to which wave energy is directed is located at an angle of about 60° and with frequencies well above the peak frequency but lower than the frequency of the area with maximum wind input.

The spectrum halfway (Fig. 3.19, panel a, $\theta_0 = 42°$) has one peak again. The peak which existed only one hour before the present situation (Fig. 3.14, panel d) has been absorbed in the spectrum. The wind input term (Fig. 3.19, panel b) has its maximum close to the new wind direction. The shape of the dissipation source function (Fig. 3.19, panel c) largely resembles the shape of the energy spectrum except for the high frequency part of the spectrum in the direction of the wind. Inspection of the contour plots for the nonlinear source function (Fig. 3.19, panels d and e) shows that the mean direction of the

negative part of the nonlinear transfer is closer to the new wind direction than the mean direction of the positive part of the nonlinear transfer. This means that the newly generated wave energy in the high frequency part of the spectrum is transferred towards the old wind direction, resulting in a uni-modal spectrum attaining a standard spectral shape (i.e. a spectral shape which would be obtained in an ideal wave generation situation). Thus the nonlinear interactions counteract the turning of the mean wave direction. Fig. 3.19 (panels d and e) also showsthat the nonlinear interactions transfer wave energy from the higher frequencies towards the frequencies near the peak of the spectrum.

Near the end of the response (Fig. 3.20, $\theta_0 = 88^\circ$) the spectrum is uni-modal and symmetric around the wind direction and with a peak frequency close to the Pierson-Moskowitz frequency. The corresponding source functions are also symmetric.

The behaviour of the source functions indicate that the dissipation and nonlinear interactions counteract the turning of the mean wave direction due to the wind input. This behaviour is confirmed by the quantitative analysis, discussed in section 3.6.3.

The constantly turning wind case

Values of three spectral parameters in the equilibrium situation are given in section 3.5.2 for the EXACT-NL model result. These values are different from corresponding Pierson-Moskowitz values. The peak frequencies f_p are higher than the Pierson-Moskowitz value of 0.13 Hz. Further, the total wave energies are lower than the Pierson-Moskowitz value of 0.37 m^2 and the directional widths are significantly larger than the equilibrium value of about 30° for a constant wind direction (see Fig. 3.9). The spectrum cannot grow to its standard shape corresponding to an ideal wave growth situation. This is prevented by the constant turning of the wind. Computations (not shown here) with the

EXACT-NL model indicate that the faster the wind is turning, the less developed the wave spectrum, i.e, the higher the peak frequency, the lower the total wave energy, but they also indicate a larger directional width.

The equilibrium situation is further analysed by inspection of the spectrum and corresponding source functions obtained with the EXACT-NL model (Fig. 3.24). In panel (a) it can be seen that the spectrum is strongly skewed towards the direction of the wind, the higher frequencies being more aligned with the wind direction than the lower frequencies. Numerical results (not shown here) indicate that the peak direction is almost equal to the mean wave direction. This means that for this case the response of the peak of the spectrum is representative for the response of the mean wave direction. The direction of the maximum wind input is closer to the direction of the spectral peak (with a lead of about 20°) than to the direction of the wind (panel b). Most wave energy is generated at frequencies that are somewhat higher than the peak frequency. The shape of the dissipation source function (panel c) resembles the shape of the energy spectrum with a strong lobe towards the area in f-θ space where the wind input is concentrated.

The flow of energy due to the nonlinear interactions is shown in the panels (d) and (e). From these figures it follows that energy flows from the area of the maximum wind input towards an area near the peak of the spectrum, the maximum of the positive flow being located between the mean wave direction and the direction of the wind. The effect of the nonlinear interactions is to turn the mean wave direction towards the peak of the spectrum, thus counteracting the turning of the waves.

General characteristics

The effect of each source term on the response of the spectrum can be described as follows. The wind input source function generates energy in the high frequency part of the spectrum and mainly in the direction of the wind. The net effect of this source function is to turn the mean wave direction towards the new wind direction. The net effect of the dissipation is to turn the mean wave direction away from the new wind direction, thus counteracting the turning of the mean wave direction. The effect of the nonlinear interactions is primarily to force the spectrum into a uni-modal shape, meanwhile transferring energy from the newly generated wave energy to the main peak of the wave spectrum in the old wind direction. Like the dissipation source function, the nonlinear interactions counteract the turning of the mean wave direction somewhat.

The above described behaviour of the nonlinear interactions suggests that at the end of the response (i.e. when the mean wave direction is almost equal to the new wind direction) they will contribute to the turning of the mean wave direction, although this contribution will be rather weak since the spectrum is almost fully developed (see the discussion of Fig. 2.1). Such a behaviour, however, is not found in the present model results (see section 3.6.3.2).

For moderate angles of the wind shift, say up to 60°, the interactions force the spectrum into a uni-modal shape rather quickly. However, for a wind shift of 90°, the nonlinear interactions cannot prevent the growth of a second high frequency spectral peak in the new wind direction. For such angles the coupling between the two spectral peaks is too weak, so that multi-modal spectra can exist for a relatively long period of time.

3.6.2.3 Comparison between EXACT-NL and WAM-model results

For the comparison of both models reference is made to the Figs. 3.12, through 3.14 for the EXACT-NL model results and to the Figs. 3.21 through 3.23 for the WAM model results.

Although both models use the same source functions for wind input and dissipation they differ in the computation of the nonlinear interactions. Therefore, differences in the results of these models can be attributed to differences in the modelling of the nonlinear transfer.

An important difference is that that the spectra and the source functions in the WAM model results are broader than those in the EXACT-NL model results. It is suggested that in the WAM model the coupling between the spectral components is less than in the EXACT-NL model, resulting in a larger spectral width. This may be attributed to the more limited treatment of the nonlinear interactions in the discrete interaction approximation, since in this approximation only two wavenumber configurations are used, whereas in the EXACT-NL model a much larger number of wavenumber configurations is used.

3.6.2.4 Comparison with previous results

The computations presented above are similar to those of Young et al. (1987). The present findings are in general agreement with their results, except for a number of differences which are discussed below. In their analysis of energy flows within the spectrum, Young et al. (1987) noted that the nonlinear interactions counteract the growth of the second peak; however, they did not note that this also counteracts the turning of the integral mean wave direction. Concerning the role of the dissipation source function, Young et al. (1987) only note that the 'old' wave system is dissipated. A new finding of the present study is that the dissipation source function counteracts the build up of the second spectral peak more strongly than that it dissipates the

old spectral peak, so that effectively the dissipation counteracts the turning of the integral mean wave direction to the new wind direction.

In addition to the results of Young et al. (1987) the present results show that even for relatively small wind shifts a second spectral peak is observed, although this peak is quickly absorbed. These peaks may have escaped detection by Young et al. (1987) since did not inspect as many two-dimensional spectra as in the present study.

Young et al. (1987) also used the WAM model to simulate the directional response of the energy density spectrum. As in the present study they find that the energy density spectra of the WAM model results are generally broader than the EXACT-NL model results. 3.6.3

3.6.3 Quantitative analysis

3.6.3.1 Time scale of the rate of change of the mean wave direction

Sudden wind shift cases

The results obtained with the EXACT-NL model, shown in Fig. 3.27, show that the time scale τ_* depends on the growth stage of the waves. The time scale τ_* increases with increasing growth stage, i.e. with increasing dimensionless energy ε_* (panel a) and with decreasing dimensionless peak frequency ν_* (panel b). For higher values of ε_* (or low values of ν_*), when the waves reach the fully developed state, the time scale τ_* increases considerably, which is in qualitative agreement with the model of Holthuijsen et al. (1987), see section 2.3.4.

Comparison of the computed time scales for both wind speeds (Fig. 3.27) shows good agreement. This indicates that the computed relationship trend between τ_* and ε_* or between τ_* and ν_* is independent of wind speed.

The quantitative results for the time scale obtained with the WAM model runs (Figs. 3.26 and 3.28) are in general agreement with the EXACT-NL results (see Fig. 3.29). Like the EXACT-NL results, the time scale τ_* increases with the growth stage.

In contrast to the EXACT-NL results, the WAM model results disagree for the separate wind speeds with respect to the intervals of ε_* or ν_* in which the time scale estimates appear. For the computations with U_{10} = 10 m/s the maximum dimensionless energies (corresponding to fully developed waves) are much lower than those for the computations with a wind speed of 20 m/s. This rather strange result is in general agreement with growth characteristics of the WAM model. The WAM model has been calibrated so as to produce a growth curve in agreement with the EXACT-NL model results for wind speeds of about 15 m/s (P.A.E.M.

Janssen, 1989, KNMI, personal communication). For an ideal growth situation and for relatively low wind speeds (say U_{10} = 10 m/s) the WAM model tends to underpredict the total wave energy compared with the EXACT-NL model results. For the same situation but with relatively large wind speeds (say U_{10} = 20 m/s) the WAM model overpredicts the total wave energy.

For practical purposes a parameterization of the present results is desirable. To that end a power-law model $\tau_* = a\ \nu_*^b$ is fitted to the EXACT-NL time scale estimates shown in Fig. 3.25 (panel b), using a least squares linear regression of $\log(\tau_*)$ on $\log(a) + b\ \log(\nu_*)$. Since the time scales go to infinity for the fully developed state, the fit is only applied to estimates for which $\nu_* > 0.007$. Based on 173 samples the fit procedure gives $\tau_* = 0.002\ \nu_*^{-4}$.

The constantly turning wind case

Fig. 3.25 (EXACT-NL model result) shows that for the equilibrium situation the τ_*-ν_* and τ_*-ε_* combination agrees reasonably well with the results of the time scale analysis of the sudden wind shift cases.

3.6.3.2 Time scale per source term

The results of the time scale analysis per source term (Fig. 3.31) indicate that most of the turning of the mean wave direction is due to the wind input. Of the other source terms the dissipation source term has time scales that are about twice as large as for the wind input, whereas the nonlinear interactions have time scales that are about 5 to 7 times as large as those of the wind input. The results of the similar time scale analysis of the constantly turning wind case (see section 3.5.4.2) agree with this in the sense that most of the turning of the mean wave direction is due to the wind input. They disagree in the relative magnitude of the time scale of the dissipation source

term, which in constantly turning winds is about a factor 6 higher than the one for the wind input source term.

3.6.3.3 Comparison with previous results

Fig. 3.34 shows a comparison of model results obtained with the EXACT-NL model using U_{10} = 20 m/s and previously presented model results, viz. the model results of Young et al. (1987), using b = 1.0×10^{-4} (Table 2.2) and the theoretical result of Holthuijsen et al. (1987). (The EXACT-NL results using U_{10} = 10 m/s are not used here to avoid cluttering of the figures. Moreover, the differences with the EXACT-NL results for U_{10} = 20 m/s are negligible.) The following characteristics are discernible:

1) For nearly developed conditions the model results predict a rapid increase in τ_* with increasing growth stage; the model of Holthuijsen et al. (1987) predicts the same trend, though for a lower value of ν_*. This is due to another normalization of the peak frequency at the "fully developed" state.

2) The transformed (see section 2.3.4) computational results of Young et al. (1987) are representative for ν_*-values in the range (0.011-0.017), i.e. for young seas. For ν_*-values of about 0.011 they approach the EXACT-NL model results, but with a much weaker trend.

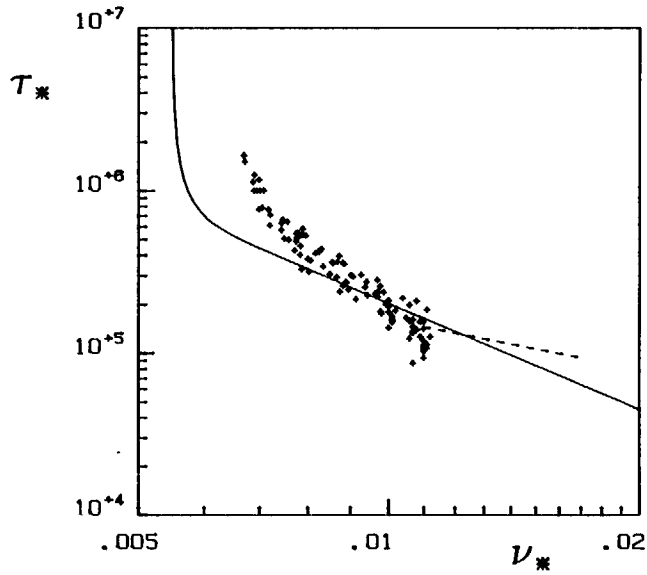

Fig. 3.34 Dimensionless time scale τ_* as a function of dimensionless peak frequency ν_*. Results of computations are indicated with the symbol 'x'. Theoretical model by Holthuijsen et al. (1987) (———) and computational results of Young et al. (1987) (- - -).

The present computational results are also compared with the model of Holthuijsen et al. (1987) in which the time scale τ_* is estimated from the computed growth characteristics. To that end their model is re-written by using the friction velocity for the nondimensionalization:

$$\tau_{*,H} = \left(\frac{1}{\varepsilon_*} \frac{\partial \varepsilon_*}{\partial t_*} \right)^{-1} \qquad (3.44)$$

in which t_* is dimensionless time. The subscript H refers to Holt-

huijsen et al. (1987). The time scales $\tau_{*,H}$ are computed from the smoothed time series of the total wave energy E_{tot} and its smoothed time derivative $\partial E_{tot}/\partial t$. Results for the case of a wind shift of 30°, 45°, 60° and 90°, with U_{10} = 20 m/s are given in Fig. 3.35, together with the estimates of the time scale τ_*, computed with Eq. (3.30), and the theoretical results of Holthuijsen et al. (1987).

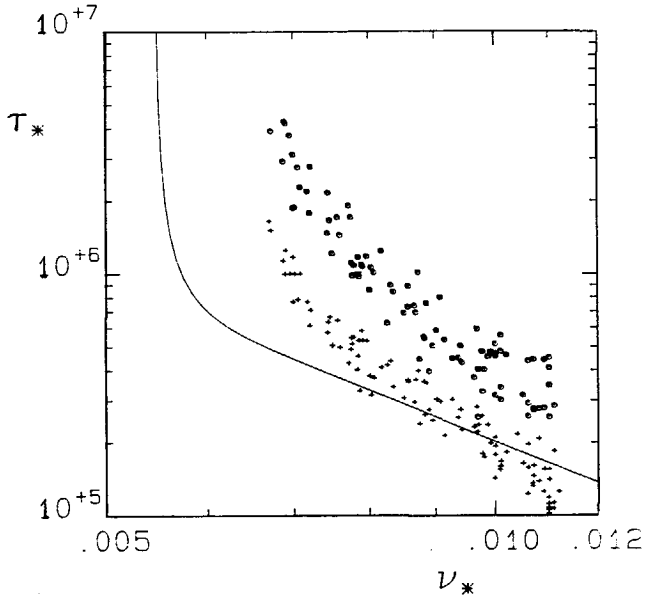

Fig. 3.35 Time scales τ_* and $\tau_{*,H}$ as a function of dimensionless peak frequency ν_* for the cases 1-4 and 6-7 of table 3.1 computed with the EXACT-NL model at a wind speed of 20 m/s. Estimates of τ_* (+), estimates of $\tau_{*,H}$ (o). Theoretical model of Holthuijsen et al. (1987) (———).

The results in Fig. 3.35 indicate that in general the time scales $\tau_{*,H}$ are larger than the time scales τ_*. However, both models results have the same trend, in the sense that the time scale depends on the growth stage of the waves, with τ_* and $\tau_{*,H}$ increasing with decreasing ν_*.

Moreover both series of results show that the time scale goes to infinity when the waves approach the fully developed state, for constant wind direction.

A possible reason for the differences between τ_* and $\tau_{*,H}$ refers to the second assumption used in the derivation of Eq. (3.44) by Holthuijsen et al. (1987) (see also section 2.3.3). In that derivation Holthuijsen et al. (1987) assume that the direction of the total source term is equal to the direction of the wind, $\theta_s = \theta_w$. However, the results shown in Fig. 3.30 indicate that this is not true for the first part of the response. Only after about 5 hours both directions are almost equal. During the first part of the response the difference $|\theta_s - \theta_0|$ is larger than the difference $|\theta_w - \theta_0|$. The effect of this difference is discussed below.

Rewriting Eq. (2.60) gives:

$$\frac{\partial \theta_0}{\partial t} = \frac{1}{\tau_H} \sin(\theta_s - \theta_0) \tag{3.45}$$

in which τ_H is the time scale according to Holthuijsen et al. (1987), and θ_s is the mean direction of the total source function (see also section 2.3.3). In this study another time scale is used:

$$\frac{\partial \theta_0}{\partial t} = \frac{1}{\tau} \sin(\theta_w - \theta_0). \tag{3.46}$$

In the present intercomparison both models (3.45) and (3.46) use the same (observed) values of $\partial\theta_0/\partial t$, so that the computed time scales τ and τ_H are related by:

$$\frac{\tau}{\tau_H} = \frac{\sin(\theta_w - \theta_0)}{\sin(\theta_s - \theta_0)} . \tag{3.47}$$

Since $|\theta_s - \theta_0| \geq |\theta_w - \theta_0|$ and thus $\sin(\theta_s - \theta_0) \geq \sin(\theta_w - \theta_0)$ it follows that in general $\tau_H \geq \tau$ and thus $\tau_{*,H} \geq \tau_*$.

The fact that the time scale estimates $\tau_{*,H}$ are higher than the theoretical model results of Holthuijsen et al. (1987), as indicate by the solid line in Fig. 3.35, may be due to the difference in growth rate between the theoretical model of Holthuijsen et al. (1987) and the growth rate as computed from the time series of the total wave energy. In the theoretical model of Holthuijsen et al. (1987) an average growth curve was used, that is based on wave growth in ideal situations. The present study deals with a turning wind situation, yielding lower growth rates. Since the time scale $\tau_{*,H}$ is inversely proportional to the growth rate, lower growth rates yield higher time scales.

3.6.4 Sensitivity analysis

Introduction

This section addresses the sensitivity of the response of the integral wave parameters θ_0, σ, ε_* and ν_*, and model values of τ to variations in the parameterization of the dissipation source function. Results obtained with the simulation run of case 1 (Table 3.3, page 3.20) are used as a reference. For that case the coefficients of the dissipation source function are equal to the values found by Komen et al. (1984). (i.e. $C = 3.33 \times 10^{-5}$, $m = 2$, $n = 2$). In the following both qualitative and quantitative aspects are discussed.

Qualitative aspects

Fig. 3.32 shows the response of four spectral parameters for different values of the coefficients of the dissipation source; the mean wave direction θ_0 (panel a), directional width σ (panel b), dimensionless wave energy ε_* (panel c) and dimensionless peak frequency ν_* (panel d). Since for all cases the effect on the directional width is negligible, only the effect of the variations on the other parameters is given below.

For the mean wave direction θ_0 the response for case 3 is practically the same as for the reference case, whereas for the other cases the response of θ_0 is faster. Concerning the total wave energy it should be noted that for case 3 the total wave energy grows much slower than for the reference case. It does not even reach the fully developed state within the present computation time. The response for case 4 is slightly faster than for case 1, whereas for the case 5 and 2 the response of the total wave energy is much faster. Comparison of the responses of the peak frequencies shows that for case 3 a significant shift in the peak frequency occurs which is due to the development of

a second spectral peak at a much higher frequency than the old one. For the other cases the response peak frequencies have no temporary increase as for case 1. For case 2 the decrease is faster than for the cases 4 and 5.

Characteristics of the dissipation source function per case

For case 2 the level of dissipation is linear with the relative wave steepness (i.e. $S_{ds} \therefore (\hat{\alpha}/\hat{\alpha}_{PM})$). Since the waves are relatively steep ($\hat{\alpha} > \hat{\alpha}_{PM}$), the overall level of dissipation in case 2 is lower than in case 1 where the dissipation varies in proportion to $(\hat{\alpha}/\hat{\alpha}_{PM})^2$, resulting in a faster growth of wave energy in the new wind direction and a faster decrease of the peak frequency.

For case 3 the level of dissipation is proportional to the third power of the relative wave steepness (i.e. $S_{ds} \therefore (\hat{\alpha}/\hat{\alpha}_{PM})^3$). This results in a higher overall level of dissipation which strongly reduces the growth of the spectrum as can be seen in Fig. 3.32c.

For case 4 the level of dissipation is proportional to the third power of the relative frequency (i.e. $S_{ds} \therefore (\omega/\omega_m)^3$) instead of the second power as in the reference case. The result is a higher level of dissipation for frequencies above the mean frequency. This causes a slower growth of high frequency wave energy in the new wind direction, and reduces the rate of change of the mean wave direction in the first four hours after the wind shift (Fig. 3.32a).

For case 5 the overall level of dissipation is decreased with a factor two. The results is a lower level of dissipation, causing a faster growth of wave energy in the new wind direction. The net effect is a faster response.

Quantitative aspects

Based on the computational results of the time scale analysis as shown in Figs. 3.33 the sensitivity of the time scale to variations in the coefficients of the dissipation source function is determined in two steps. In the first step the coefficient a in the relation $\tau_* = a\ \nu_*^{-4}$ is estimated with the procedure described in section 3.6.3.1. In the second step the sensitivity is determined as the ratio between the relative changes in the coefficient a and the parameter ξ respectively $(\Delta a/a)/(\Delta\xi/\xi)$. The results are given in Table 3.4.

case	code	parameter value (ξ)	sensitivity $(\Delta a/a)/(\Delta\xi/\xi)$
2	m^-	m = 1	0.6
3	m^+	m = 3	1.6
4	n^+	n = 3	-0.2
5	C^-	$C = 1.67 \times 10^{-5}$	0.4

Table 3.4: Sensitivity of the time scale τ_* to variations in the coefficients of the dissipation source function (Eq. 2.40).

The different sensitivities for the cases 2 and 3 indicate that the variations in the parameter m were too large to assume a linear dependence between variations in the parameter m and those in the time scale τ. The results in Table 3.4 also indicate that changes in the parameter n have a smaller effect on the time scale than changes in the parameter m. A reduction in the level of dissipation reduces the time scale, which is in agreement with the notion that dissipation counteracts the turning of the waves.

3.7 Conclusions

The following conclusions can be drawn from the computations performed with the EXACT-NL model and the WAM model.

1. Calculations with the EXACT-NL model show that the turning of the wave field in a turning wind is primarily due to the effect of the wind, but that it is counteracted to some degree by the effects of dissipation and nonlinear wave-wave interactions.

2. After a sudden shift of the wind direction a second spectral peak always develops initially. However, for relatively small wind shifts this second peak is rapidly absorbed in the spectrum by the nonlinear interactions.

3. The response of the mean wave direction for sudden wind shifts up to 60° can be regarded as a relaxation process. For these cases the response curve of the mean wave direction has monotonically decreasing values of $\partial\theta_0/\partial t$, the total wave energy grows monotonically and the peak frequency decreases monotonically. For the wind shift of 90° this is only true after some time just after the shift.

4. Since the time scale for the integral mean wave direction response must be allowed to vary with growth stage, the method used to estimate it must be capable of detecting these variations. The method developed by Young et al. (1987) for an analysis per frequency is not suited for this purpose, since they assume a constant time scale τ per frequency.

5. The computations show that the time scale of the response of the mean wave direction strongly depends on the growth stage of the waves, with increasing time scale as the waves become more developed. For the sudden wind shift cases the time scale rapidly increases as the waves approach the fully developed state, as predicted by the theoretical model of Holthuijsen et al. (1987).

6. The relation between dimensionless time scale and growth stage of the waves is independent of the wind speed used in the EXACT-NL computations. However, this invariance cannot be detected in the WAM model results.

7. The results of the sensitivity analysis show that lower time scales are obtained by increasing the level of dissipation with relative frequency, by decreasing it with relative average wave steepness, or by decreasing the overall level of dissipation.

8. For the sudden wind shift cases simulated in this study the WAM model reproduces most of the features of the directional response as found by the EXACT-NL model. However, the two-dimensional energy density spectra as computed by the WAM model are generally broader than those obtained with the EXACT-NL model.

CHAPTER 4

OBSERVATIONS OF THE RESPONSE OF THE MEAN WAVE DIRECTION TO VEERING WINDS

4.1 Introduction

This chapter describes a method of analysis to infer from directional wave measurements the time scale τ of the directional response of the frequency integrated mean wave direction θ_0 in response to variations in the wind direction θ_w, its application to North Sea data, and the results obtained. The analysis centers on the relaxation model:

$$\frac{\partial \theta_0}{\partial t} = \frac{1}{\tau} \sin(\theta_w - \theta_0). \qquad (4.1)$$

Directional wave measurements have been carried out with pitch-and-roll buoys located in the central North Sea. The analysis of each wave record obtained with these buoys comprises the computation of the mean wave direction and total wave energy. Thus time series are generated of the mean wave direction, which in turn are used to estimate its rate of change. At the same time wind speed and wind direction observations have been carried out in the area of the wave observations.

At a fixed location the observed rate of change of the mean wave direction depends on local processes (generation of wave energy by the local wind, dissipation and nonlinear wave-wave interactions) and on radiation from elsewhere.

For the present study only local effects are of interest. Therefore the effects of transport are quantified which allows an estimate of the locally induced rate of change of the mean wave direction from the directional wave observations.

Estimation of the effect of transport of wave energy requires directional wave information in a number of locations around the location of measurement. This information is obtained from a numerical hindcast model. The hindcast model used for this estimation is the deep water wave prediction model WINCH, in use at the Norwegian Meteorological Institute, Oslo.

The method described above does not allow all wave and wind measurements to be used for estimating the rate of change of the mean wave direction. Selection criteria are still necessary to select those measurements for which the effect of the local wind on the mean wave direction can be estimated with sufficient accuracy and reliability. For that purpose an error analysis is performed for the time scale estimates. Only time scale estimates with a relatively small error will be selected for further analysis or interpretation.

The contents of this chapter are as follows. The methods for measuring the waves and the wind velocity and wind direction are described in section 4.2. A description of the measuring devices and of the preprocessing of the obtained data is included. Section 4.3 treats the method of isolating the local effect in the directional wave measurements by quantifying and removing the effects of transport. In addition the error analysis of the time scale estimates is described. The hindcast model that is used to assess the effects of energy transport on the wave direction is described in section 4.4. The geophysical conditions during the measurement periods are given in section 4.5. Section 4.6 deals with the criteria for the selection of the wave and wind data to be used in the final analysis. The results of the analysis are presented in section 4.7 and discussed in section 4.8. Finally, conclusions are drawn in section 4.9.

4.2 Methods of observation

4.2.1 Introduction

The methods that are used in this study to observe waves, wind speed and wind direction are treated in the following. A distinction is made between the measurement devices and the data processing.

4.2.2 Wave measurements

4.2.2.1 Introduction

For the present study two WAVEC pitch-and-roll buoys, deployed by the Ministry of Transport and Public Works in the Netherlands, are used. They were located near the offshore platforms AUK-α and K13-α. The locations of these platforms are 56°23'29''N, 02°03'56''E and 53°13'01''N, 03°13'12''E for AUK-α and K13-α respectively (see Fig. 4.1).

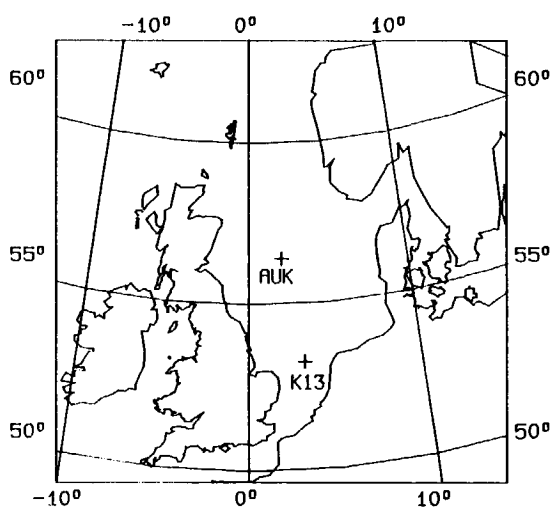

Fig. 4.1 Geographic location of the observations points.

These locations are away from any coastline. The water depth is approximately 70 m near the AUK-α platform and about 30 m near the K13-α platform. For most wave conditions these depths can be considered as relatively deep (see section 4.5). Wind measurements were made simultaneously at the nearby offshore platforms.

4.2.2.2 Pitch-and-roll buoys

A pitch-and-roll buoy is a free floating buoy that follows the elevation and slope of the water surface. It records the vertical elevation and two orthogonal slopes of the ocean surface as a function of time. The vertical elevation and the two orthogonal slopes are referred to as heave, pitch and roll respectively. The resulting time signals of these parameters are used to obtain estimates of the frequency spectrum and the directional characteristics of the two-dimensional energy spectrum for a number of frequencies. It was shown by Longuet-Higgins et al. (1963) that the first four Fourier coefficients of the directional distribution function $D(\theta)$ as a function of frequency can be derived from the auto-, co- and quad- spectra of these signals (see Appendix A).

Numerous techniques exist for the processing of the heave and the slope signals of the buoy. In general these techniques can be divided in two classes. The methods of the first class try to reconstruct the directional distribution, whereas the methods of the second class compute a number of characteristic parameters of the directional distribution. For the present study a method of the latter category has been used to which the present author contributed (Kuik et al., 1988). It yields estimates for mean wave direction, directional width, skewness and kurtosis per frequency.

The WAVEC (WAve VECtor) buoy has been developed in 1980 jointly by the

Datawell B.V. (Haarlem, the Netherlands) and the Ministry of Transport and Public Works in the Netherlands (Van der Vlugt et al., 1981 and Van der Vlugt, 1984). It has been in operation since 1984. The WAVEC buoy hull has the shape of a discus, with a diameter of 2.5 m and a height of 1.7 m (excluding antenna). An illustration of the WAVEC buoy is given in Fig. 4.2. The buoy mass is about 700 kg. Its natural frequencies are about 1.1 Hz for heave motion and about 1.3 Hz for pitch and roll. The buoy is moored to the sea bed by a flexible rubber line.

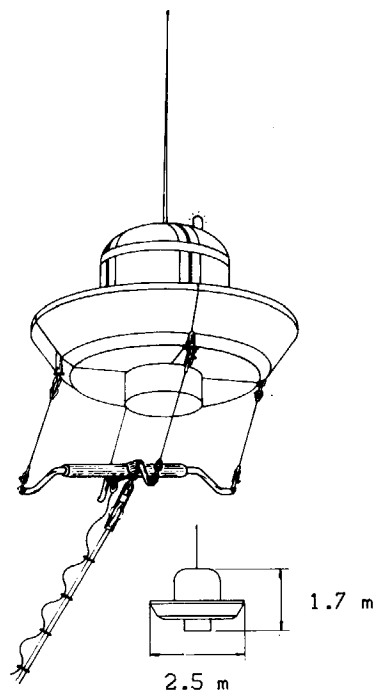

Fig. 4.2 The WAVEC buoy.

The essential instruments of the WAVEC buoy are the Datawell Hippy-120A sensor and a fluxgate compass which are placed in the hull of the buoy. The Hippy-120A sensor measures the heave and two slopes for pitch and roll in a reference frame fixed to the buoy. The fluxgate

compass determines the orientation of the buoy in the Earth magnetic field using the three orthogonal components of the field in the local coordinate system of the buoy.

The above mentioned six signals are digitized in the buoy with a sampling rate of 1.28 Hz to obtain discrete time series of 20 minute duration. These time series are transmitted via a radio link from the buoy to a receiving station (CIC) in Hook of Holland in the Netherlands. From the latter location the buoy data are transmitted to the Ministry of Transport and Public Works, Division of Hydro Instrumentation (Rijswijk, The Netherlands).

Processing of the WAVEC buoy data

The method for processing the buoy data has been developed by the Institute for Applied Physics (TNO), Delft, the Netherlands. A detailed description thereof is given in Markus and Kapsenberg (1985) and Kuik et al. (1988). Only a summary of the most important aspects of the data processing is given here.

Every 30 minutes results of the data processing are available, based on 20 minute duration time series of the six basic buoy signals. These results consist of auto-, co- and quad-spectra with a resolution of 5 mHz for the frequency range 30 mHz to 150 mHz and 10 mHz for the frequency range 150 mHz to 500 mHz. The equivalent degrees of freedom of these estimates are 12 and 24 respectively. From these spectra the first four Fourier coefficients of the directional distribution function per frequency are computed (see appendix A).

For the present study only the frequency integrated mean wave direction θ_0, the total wave energy E_{tot} and the peak frequency f_p are needed. The first two of these parameters are defined by the Eqs. (2.25) and (2.42) respectively. The peak frequency is the frequency at which the frequency spectrum E(f) has its maximum.

4.2.3 Wind measurements

The measurements of wind speed and wind direction which have been used in this study are routinely collected by the Ministry of Transport and Public Works, Directorate for the North Sea. The measuring devices are located on top of the offshore platforms AUK-α (owned jointly by the oil companies Shell and BP) and K13-α (owned by the oil company PENNZOIL). On the AUK-α platform NBA (Nick-Ben-Anscombe, made by Controls, Ltd., England) wind sensors are used, located at the top of the highest part of the platform at a height of 102 m above mean sea level. For the K13-α platform KNMI (Royal Netherlands Meteorological Institute, de Bilt) wind sensors have been installed (made by the KNMI), located at a height of 72.9 m above mean sea level. Both sensors have a sampling frequency of 4 Hz.

For the present study, 30 minute averages of observed wind speed and wind direction have been obtained at intervals of 30 minutes. The average wind speed is computed as a scalar mean, whereas the mean wind direction is computed as a vectorial mean weighted with the wind speed (i.e. by using a definition similar to that used for the mean wave direction, Eq. 2.25).

Wind speeds were converted to the 10 m level by assuming a logarithmic velocity profile (Eq. 2.50) with the drag coefficient C_d given by Eq. (2.53). For the K13-α platform the wind measurements are also corrected for the effect of flow distortions caused by the platform. An estimate of this effect is based on results of wind tunnel experiments (Vermeulen et al., 1985). These experiments indicate that for the K13-α platform the influence of the platform itself is less than 2%, which is considered negligible. However, the wind speed is influenced by an antenna that is placed on the top of the tower. This effect on the wind speed varies from -6% to +8% depending on the wind direction. For the AUK-α platform no correction for the effect of flow distortions was deemed necessary (H.C. Peters, Ministry of Transport and

Public Works, Directorate for the North Sea, 1987, personal communication).

For both locations the wind direction was corrected to account for the Ekman effect in the lowest part of the atmospheric boundary layer. In the conversion to the 10 m level a directional correction of 5° anticlockwise is used for both locations (with respect to the direction to which the wind is blowing, see chapter 2, section 2.2.7.4).

4.3 Computation of time scale estimates

4.3.1 Introduction

This section treats two aspects of the method for estimating the time scale of the locally induced directional response. The first aspect describes the estimation of local effects on the mean wave direction. The second aspect pertains to the method for estimating the corresponding time scales and the corresponding errors.

4.3.2 Estimation of local effects

The method for the estimation of local effects on the wave direction is described in two steps. First, the general principle of the method is described in terms of continuous functions of two-dimensional spectra and source functions, meanwhile assuming that the buoy measures the true two-dimensional spectrum. In the second step the limitations of the buoy and hindcast results are accounted for. These limitations are of two kinds. First, wave data and hindcast model results are available at discrete times. Secondly, a pitch-and-roll buoy is not able to measure the complete two-dimensional spectrum, but only the first four Fourier coefficients of the directional distribution per frequency. Therefore the method is reformulated in terms of these Fourier coefficients.

Based on the energy balance equation (Eq. 2.34) the local effects of wave generation, dissipation and nonlinear wave-wave interactions are expressed in terms of the source function $S(f,\theta;\underline{x},t)$:

$$S(f,\theta;\underline{x},t) = \frac{\partial E(f,\theta;\underline{x},t)}{\partial t} + T(f,\theta;\underline{x},t) \qquad (4.2)$$

in which $T(f,\theta;\underline{x},t)$ is the transport term:

$$T(f,\theta;\underline{x},t) = \underline{c}_g(f,\theta)\cdot\nabla E(f,\theta;\underline{x},t)$$

$$= c_g(f)\left\{\cos(\theta)\frac{\partial E(f,\theta;\underline{x},t)}{\partial x} + \sin(\theta)\frac{\partial E(f,\theta;\underline{x},t)}{\partial y}\right\}. \qquad (4.3)$$

An estimate of the source term S, which represents the local wind effects, is obtained by estimation of the two terms on the right-hand side of Eq. (4.2). Of these terms, the local rate of change of the spectral density is estimated from the buoy measurements, whereas the transport term T is estimated by means of a numerical hindcast model. Once the source term S is computed, the effect of local wave and wind conditions on the energy spectrum in a certain time interval with a duration $2\Delta t$ can be computed as:

$$E_L(f,\theta;\underline{x},t+2\Delta t) = E(f,\theta;\underline{x},t) + \int_t^{t+2\Delta t} S(f,\theta;\underline{x},t')dt' \qquad (4.4)$$

in which the subscript L refers to locally induced wave growth (i.e. without effects of transport).

From the measured energy density spectrum $E(f,\theta)$ at time t and the locally induced energy spectrum $E_L(f,\theta)$ at time $t + 2\Delta t$ two mean wave directions are computed by using Eq. (2.25). From these two directions the locally induced change of mean wave direction in the time interval $(t, t + 2\Delta t)$ is computed and subsequently the time scale τ of the directional response (see section 4.3.5.1).

Discretization

In the following it is assumed that the wave and wind observations are available at discrete points of time at constant intervals Δt.

A numerical approximation of the integral in Eq. (4.4) is obtained by using a representative value of the source term S in the time interval $(t, t + 2\Delta t)$. This is the source function at a time halfway the interval, resulting in:

$$E_L(f,\theta;\underline{x},t+2\Delta t) \approx E(f,\theta;\underline{x},t) + (2\Delta t)\, S(f,\theta;\underline{x},t+\Delta t). \qquad (4.5)$$

An estimate of the source function $S(f,\theta;\underline{x},t + \Delta t)$ is obtained through the estimation of the remaining terms in Eq. (4.2). The first term in this equation is estimated from the wave measurements with a central difference scheme in time:

$$\frac{\partial E(f,\theta;\underline{x},t+\Delta t)}{\partial t} \approx \frac{E(f,\theta;\underline{x},t+2\Delta t) - E(f,\theta;\underline{x},t)}{2\Delta t}. \qquad (4.6)$$

An estimate of the transport term $T(f,\theta;\underline{x},t+\Delta t)$ is computed from results obtained with a hindcast model. The procedure for this is described in the next paragraph 4.3.3.

Combining Eqs. (4.2), (4.5) and (4.6) gives an expression for the locally induced two-dimensional spectrum density at time $t + 2\Delta t$, without effects of transport:

$$E_L(f,\theta;t+2\Delta t) \approx E(f,\theta;t+2\Delta t) + (2\Delta t)\, T(f,\theta;t+\Delta t). \qquad (4.7)$$

In this way a time interval $(t, t+2\Delta t)$ is generated in which the wave field can be considered as homogeneous.

4.3.3 Estimation of transport term

According to Eq. (4.7) the transport term T must be estimated at discrete points of time, but also at the location in space of the buoy (denoted by the location vector $\underline{x}_b$). This estimate is derived from output of the two-dimensional spectrum obtained from a numerical wave hindcast model. The output model spectra are denoted as $E_M(f,\theta)$.

Generally the results of the hindcast model will not be available at the times $t + \Delta t$, $t + 2\Delta t, \ldots$, but at times associated with the hindcast model. To get this information at the proper times, linear interpolation in time is used.

In general the buoy location does not coincide with one of the model grid points. Bilinear interpolation in space is used to obtain results in the point of measurement $\underline{x}_b$ from the nearest four hindcast grid points surrounding $\underline{x}_b$. These grid points form a rectangle with sides Δx and Δy. The relative position of the point of measurement in this rectangle is specified by the parameters λ_x and λ_y (Fig. 4.3).

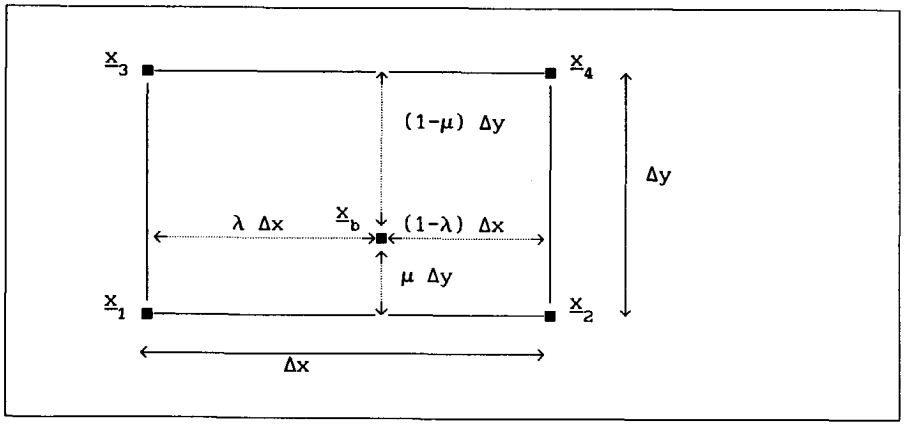

Fig. 4.3 Bilinear interpolation in space for transport term.

The computation of the transport term $T(f,\theta;\underline{x}_b,t+\Delta t)$ is performed in three steps. Firstly, at the model times $t = t_m$ the spatial derivatives $\partial E_M/\partial x$ and $\partial E_M/\partial y$ are estimated in the point of measurement using bilinear interpolation in space from the four surrounding model spectra:

$$\frac{\partial E_M(f,\theta;\underline{x}_b,t_m)}{\partial x} = (1-\lambda_y)\ \frac{E_M(f,\theta;\underline{x}_2,t_m) - E_M(f,\theta;\underline{x}_1,t_m)}{\Delta x}$$

$$+\ \lambda_y\ \frac{E_M(f,\theta;\underline{x}_4,t_m) - E_M(f,\theta;\underline{x}_3,t_m)}{\Delta x} \qquad (4.8)$$

and similarly for the y-derivative.

In Eq. (4.8) $\underline{x}_1$, $\underline{x}_2$, $\underline{x}_3$ and $\underline{x}_4$ are the position vectors of the four surrounding grid points (see Fig. 4.3). Secondly, the transport term $T(f,\theta;\underline{x}_b,t_m)$ is determined by substitution of the estimates of $\partial E_M/\partial x$ and $\partial E_M/\partial y$ in Eq. (4.3). In the third and last step, linear interpolation in time is used to compute the transport term per spectral component at time $t + \Delta t$.

4.3.4 Computation of locally induced mean wave direction

To compute the locally induced mean wave direction at time $t = t + 2\Delta t$ all equations leading to Eq. (4.7) are reformulated in terms of the first two Fourier coefficients, leading to two equations:

$$a_L(t+2\Delta t) = a_E(t+2\Delta t) + (2\Delta t)\ a_T(t+\Delta t) \qquad (4.9)$$

$$b_L(t+2\Delta t) = b_E(t+2\Delta t) + (2\Delta t)\ b_T(t+\Delta t) \qquad (4.10)$$

in which a_E and b_E are the weighted Fourier coefficients of the energy

density spectrum, defined in section 2.2.3.1, Eqs. (2.28) and (2.29), and in which a_T and b_T are the weighted Fourier coefficients of the transport term $T(f,\theta)$. The latter two coefficients are defined by (dropping the time dependence from the notation):

$$a_T = \int_0^{2\pi} \int_0^{\infty} \cos(\theta)\ T(f,\theta)\ df\ d\theta \tag{4.11}$$

and

$$b_T = \int_0^{2\pi} \int_0^{\infty} \sin(\theta)\ T(f,\theta)\ df\ d\theta. \tag{4.12}$$

In the Eqs. (4.9) through (4.12) and in the following the subscript T refers to transport.

The locally induced mean wave direction $\theta_{0,L}$ is computed as:

$$\theta_{0,L} = \arctan\left[\frac{b_L}{a_L}\right]. \tag{4.13}$$

4.3.5 Time scale analysis

4.3.5.1 Estimation of time scale

To estimate the time scale τ from the relaxation model (4.1) the locally induced rate of change of the mean wave direction is estimated with a central difference scheme as:

$$\frac{\partial\theta_0(t+\Delta t)}{\partial t} \approx \frac{\theta_{0,L}(t+2\Delta t) - \theta_0(t)}{2\Delta t} \tag{4.14}$$

whereas the sine term in Eq. (4.1) is estimated at the central time $t + \Delta t$. In this way the time scale τ is estimated at times $t + \Delta t$ as:

$$\tau(t+\Delta t) \approx \frac{\sin\left(\theta_w(t+\Delta t) - \theta_0(t+\Delta t)\right)}{\theta_{0,L}(t+2\Delta t) - \theta_0(t)} (2\Delta t). \qquad (4.15)$$

Estimates of the time scale τ are normalized with the friction velocity u_* and the gravitational acceleration g to $\tau_* = \tau g/u_*$. They are given as a function of growth stage, which can be expressed in terms of the dimensionless peak frequency ν_* or the dimensionless energy ε_*:

$$\nu_* = f_p \, u_*/g \qquad (4.16)$$

and

$$\varepsilon_* = E_{tot} \, g^2/u_*^4. \qquad (4.17)$$

4.3.5.2 Statistical variability of time scale estimates

Introduction

The purpose of this section is to describe the method with which the error in each time scale estimate can be objectively quantified. Knowledge of this error is needed to select only those time scale estimates with a relative error lower than a certain threshold value. For that purpose a conventional method is used to quantify these errors. This method uses first order error propagation theory and it is based on the assumption that the error in the variables determining the time scale τ are mutually uncorrelated. The validity of this assumption is addressed below.

To illustrate the procedure for the estimation of the error in the

estimates of the time scale τ Eq. (4.15) is written in the general form:

$$\tau = \Phi(\xi_1, \xi_2, \ldots, \xi_N) \tag{4.18}$$

in which $\xi_1, \xi_2, \ldots, \xi_N$ represent the independent variables determining the time scale τ. In case the errors in the independent variables are uncorrelated it follows by application of first order error propagation theory (cf. Mood et al., 1974, their page 181) that the mean square error σ^2_τ in the time scale estimates can be is approximated by:

$$\sigma^2_\tau \approx \sum_{i=1}^{N} \left(\frac{\partial \Phi}{\partial \xi_i} \right)^2 \sigma^2_{\xi_i} \tag{4.19}$$

in which σ^2_τ and $\sigma^2_{\xi_i}$ are the mean square errors of the estimates of the time scale τ and the independent variable ξ_i respectively.

Dependency analysis

To determine the dependence of τ on the variables determining it, Eq. (4.15) is written explicitly:

$$\tau(t + \Delta t) = \frac{\sin\left(\theta_w(t+\Delta t) - \theta_0(t+\Delta t) \right)}{\arctan\left[\dfrac{a_E + (2\Delta t)\, a_T}{b_E + (2\Delta t)\, b_T} \right] - \theta_0(t)} (2\Delta t). \tag{4.20}$$

The Fourier coefficients a_E and b_E are given at time $(t+2\Delta t)$, and the Fourier coefficients a_T and b_T at time $(t+\Delta t)$. The Fourier coefficients a_E and b_E are written as:

$$a_E = \cos(\theta_0)\, E_{tot} \tag{4.21}$$

and

$$b_E = \sin(\theta_0)\, E_{tot}. \tag{4.22}$$

To determine the dependence of the Fourier coefficients a_T and b_T it is assumed that the model spectrum in the point of measurement is narrow with a model peak frequency $f_{p,M}$ and a model mean wave direction θ_M. The representative model group velocity is taken equal to the one for the peak frequency:

$$c_g = \frac{g}{4\pi f_{p,M}}. \tag{4.23}$$

The Fourier coefficients a_T and b_T are approximated as:

$$a_T = \cos(\theta_M)\, \frac{g}{4\pi f_{p,M}} \left[\cos(\theta_M)\, \frac{\partial E_{tot,M}}{\partial x} + \sin(\theta_M)\, \frac{\partial E_{tot,M}}{\partial y} \right] \tag{4.24}$$

and

$$b_T = \sin(\theta_M)\, \frac{g}{4\pi f_{p,M}} \left[\cos(\theta_M)\, \frac{\partial E_{tot,M}}{\partial x} + \sin(\theta_M)\, \frac{\partial E_{tot,M}}{\partial y} \right]. \tag{4.25}$$

in which $E_{tot,M}$ is the model total wave energy in the point of measurement. Based on the above analysis it follows that in the time interval $(t, t+2\Delta t)$ the independent variables determining the time scale $\tau(t+\Delta t)$ are the wind direction $\theta_w(t+\Delta t)$, the measured mean wave directions $\theta_0(t)$, $\theta_0(t+\Delta t)$ and $\theta_0(t+2\Delta t)$, the measured total wave energy $E_{tot}(t+2\Delta t)$, the model mean wave direction $\theta_M(t+\Delta t)$, the model peak frequency $f_{p,M}(t+\Delta t)$ and the spatial derivatives $\partial E_{tot,M}(t+\Delta t)/\partial x$ and $\partial E_{tot,M}(t+\Delta t)/\partial y$.

For the present analysis these variables are considered as stochastic

variables with mean square errors: $\sigma^2_{\theta_w}$, $\sigma^2_{\theta_0}$, σ^2_E, $\sigma^2_{\theta_M}$, $\sigma^2_{f_{p,M}}$, $\sigma^2_{\partial E_{tot,M}/\partial x}$ and $\sigma^2_{\partial E_{tot,M}/\partial y}$ respectively. In the above it is assumed that the mean square error in the estimates of the three observed mean wave directions are all equal to $\sigma^2_{\theta_0}$.

Correlations between errors

The stochastic variables mentioned above can be divided in three groups; the first group consists of the measured wind direction, the second group contains observed wave parameters and the third one contains hindcast model results. Since the parameters in a group are estimated independently from parameters in another group, it is assumed that the errors of the variables are groupwise independent.

Within the second group the three mean wave directions have some correlation, however their associated errors are assumed uncorrelated since they are based on different time series of surface elevation which are sufficiently separated in time to assume independence between them. The correlation between errors in the estimates of the mean wave direction and total wave energy can be assumed to be negligible.

In the third group the error in the spatial derivatives is neglected, as is argued at the end of this section. The correlation between the errors in the estimates of the model peak frequency $f_{p,M}$ and the model mean wave direction θ_M is assumed to be zero.

Mean square time scale errors

Assuming that the errors in the independent variables are uncorrelated or zero, as indicated above, the mean square error σ^2_τ of the time scale estimate τ can be written as:

$$\sigma_\tau^2 \approx \left(\frac{\partial \Phi}{\partial \theta_w(t+\Delta t)} \right)^2 \sigma_{\theta_w}^2 + \left(\frac{\partial \Phi}{\partial E_{tot}} \right)^2 \sigma_E^2 +$$

$$\left\{ \left(\frac{\partial \Phi}{\partial \theta_0(t)} \right)^2 + \left(\frac{\partial \Phi}{\partial \theta_0(t+\Delta t)} \right)^2 + \left(\frac{\partial \Phi}{\partial \theta_0(t+2\Delta t)} \right)^2 \right\} \sigma_{\theta_0}^2 +$$

$$\left(\frac{\partial \Phi}{\partial f_{p,M}(t+\Delta t)} \right)^2 \sigma_{f_{p,M}}^2 + \left(\frac{\partial \Phi}{\partial \theta_M(t+\Delta t)} \right)^2 \sigma_{\theta_M}^2 . \qquad (4.26)$$

To elaborate Eq. (4.26) the function Φ is replaced by Eq. (4.15) in which the term $\theta_{0,L}$ is given by Eq. (4.13). Upon introducing the constant $\alpha = (2\Delta t)g/(4\pi)$ the Fourier coefficients a_L and b_L in Eq. (4.13) can be written as:

$$a_L = E_{tot} \cos(\theta_0) + \alpha f_{p,M}^{-1} \cos(\theta_M) \left(\cos(\theta_M) \frac{\partial E_{tot,M}}{\partial x} + \sin(\theta_M) \frac{\partial E_{tot,M}}{\partial y} \right) \qquad (4.27)$$

and

$$b_L = E_{tot} \sin(\theta_0) + \alpha f_{p,M}^{-1} \sin(\theta_M) \left(\cos(\theta_M) \frac{\partial E_{tot,M}}{\partial x} + \sin(\theta_M) \frac{\partial E_{tot,M}}{\partial y} \right). \qquad (4.28)$$

Elaboration of all partial derivatives in Eq. (4.26) yields:

$$\sigma_\tau^2 \approx \left[\frac{\cos\left(\theta_w(t) - \theta_0(t+\Delta t)\right)}{\theta_{0,L}(t+2\Delta t) - \theta_0(t)} (2\Delta t) \right]^2 \left(\sigma_{\theta_w}^2 + \sigma_{\theta_0}^2 \right) +$$

$$\left[\frac{\sin\left(\theta_w(t) - \theta_0(t+\Delta t)\right)}{\left(\theta_{0,L}(t+2\Delta t) - \theta_0(t) \right)^2} (2\Delta t) \right]^2 .$$

$$\left\{ \sigma_{\theta_0}^2 + \left(\frac{\partial \theta_{0,L}}{\partial \theta_0(t+2\Delta t)} \right)^2 \sigma_{\theta_0}^2 + \left(\frac{\partial \theta_{0,L}}{\partial E_{tot}(t+\Delta t)} \right)^2 \sigma_{E_{tot}}^2 + \right.$$

$$\left. \left(\frac{\partial \theta_{0,L}}{\partial f_{p,M}(t+\Delta t)} \right)^2 \sigma_{f_{p,M}}^2 + \left(\frac{\partial \theta_{0,L}}{\partial \theta_M(t+\Delta t)} \right)^2 \sigma_{\theta_M}^2 \right\} . \qquad (4.29)$$

It is noted here that due to the occurrence of $\left(\theta_{0,L} - \theta_0 \right)$ terms in two denominators in Eq. (4.29), small changes of the locally induced mean wave direction increase the corresponding mean square error considerably. In this way relatively high time scales, corresponding to a small change of mean wave direction, are discarded by the error analysis. This may bias the results somewhat to lower time scales.

In Eq. (4.29) a number of partial derivatives of $\theta_{0,L}$ appear. Elaboration of its partial derivative with respect to $\theta_0(t+2\Delta t)$ yields:

$$\frac{\partial \theta_{0,L}}{\partial \theta_0(t+2\Delta t)} = \frac{\frac{\partial b_L}{\partial \theta_0(t+2\Delta t)} a_L - \frac{\partial a_L}{\partial \theta_0(t+2\Delta t)} b_L}{a_L^2 + b_L^2} \qquad (4.30)$$

and similarly for the partial derivatives of $\theta_{0,L}$ with respect to E_{tot}, $f_{p,M}$ and θ_M. In the resulting expressions partial derivatives of

a_L and b_L with respect to θ_0, E_{tot}, $f_{p,M}$ and θ_M appear. They are given below:

$$\frac{\partial a_L}{\partial \theta_0} = -\sin(\theta_0)\, E_{tot} \tag{4.31}$$

$$\frac{\partial a_L}{\partial E_{tot}} = \cos(\theta_0) \tag{4.32}$$

$$\frac{\partial a_L}{\partial f_{p,M}} = -\alpha\, f_{p,M}^{-2} \left[\cos^2\left(\theta_M\right) \frac{\partial E_{tot,M}}{\partial x} + \frac{1}{2}\sin\left(2\theta_M\right) \frac{\partial E_{tot,M}}{\partial y} \right] \tag{4.33}$$

$$\frac{\partial a_L}{\partial \theta_M} = \alpha\, f_{p,M}^{-1} \left[-\sin\left(2\theta_M\right) \frac{\partial E_{tot,M}}{\partial x} + \cos\left(2\theta_M\right) \frac{\partial E_{tot,M}}{\partial y} \right] \tag{4.34}$$

$$\frac{\partial b_L}{\partial \theta_0} = \cos(\theta_0)\, E_{tot} \tag{4.35}$$

$$\frac{\partial b_L}{\partial E_{tot}} = \sin(\theta_0) \tag{4.36}$$

$$\frac{\partial b_L}{\partial f_{p,M}} = \alpha\, f_{p,M}^{-2} \left[\frac{1}{2}\sin\left(2\theta_M\right) \frac{\partial E_{tot,M}}{\partial x} + \sin^2\left(\theta_M\right) \frac{\partial E_{tot,M}}{\partial y} \right] \tag{4.37}$$

$$\frac{\partial b_L}{\partial \theta_M} = \alpha\, f_{p,M}^{-1} \left[\cos\left(2\theta_M\right) \frac{\partial E_{tot,M}}{\partial x} + \sin\left(2\theta_M\right) \frac{\partial E_{tot,M}}{\partial y} \right]. \tag{4.38}$$

These parameters are computed for each accepted time interval. To compute the error in each time scale estimate, values of the various mean square errors ($\sigma^2_{\theta_0}$, ect.) are also needed. These are given below.

Quantification of mean square errors

For the measured mean wave direction θ_0 the routine analysis of the WAVEC data yields estimates of θ_0 with a theoretically estimated mean square error of 3° (Kuik et al., 1988). In view of additional effects, such as instrument noise, the overall rms error is taken to be 4°. For the mean square sampling error of the total wave energy E_{tot}, Long (1980) gives an estimate of 6.2%. Since this estimate is based on a certain spectrum, and to account for instrumental errors, the somewhat more conservative value of 10% is used in this study. Holthuijsen et al. (1987) indicate a mean square error in the estimates of the wind direction of between 5° to 10°. For this study a value of 8° is used.

The errors for the model mean wave direction θ_M and the model peak frequency $f_{p,M}$ are computed relatively simply. They are defined as the mean of the squared differences of the measured and computed mean wave direction and peak frequency respectively, where the averaging is performed over the time intervals that are used for the time scale analysis. Results are given in section 4.7.

The spatial derivatives $\partial E_{tot,M}/\partial x$ and $\partial E_{tot,M}/\partial y$ in the Eqs. (4.24) and (4.25) are linear functions of the four energy densities in each of the four model grid points surrounding the point of measurement. These estimates are strongly correlated. This may be explained by noting that errors in the wave model results are predominantly due to errors in the wind field driving the model. The spatial scale of errors in the wind field is much larger than the grid spacing ($\Delta x, \Delta y$) in the wave model for which reason errors in the model wave energy (or wave height) prediction are assumed to be strongly correlated. For the present study the correlation between the absolute errors is assumed to be 100 %, in which case the random errors in the estimates of $\partial E_{tot,M}/\partial x$ and $\partial E_{tot,M}/\partial y$ are equal to zero.

4.4 The hindcast model

4.4.1 Introduction

As explained in the introduction of this chapter a hindcast model is used for the quantification of the effect of transport on the observed rate of change of the mean wave direction. This section contains a description of the WINCH model chosen for this study. In addition a description is given of the wind fields that are used as input for the hindcast model.

At the initiation of this study three hindcast models could be used for obtaining the necessary spatial directional wave information, viz. the GONO model (**GO**lven **NO**ordzee) of the KNMI, de Bilt, the Netherlands, the wave model of the British Meteorological Office (BMO), Bracknell, England, and the WINCH model implemented at the Norwegian Meteorological Institute (DNMI), Oslo. Although in principle each of these models could be used, the WINCH model was selected since it was best accessible for the locations in the North Sea under investigation. A description of the WINCH model is given below.

4.4.2 Description of the hindcast model WINCH

Introduction

The following brief description is based on Greenwood et al. (1985), Eide et al. (1986) and Reistad (1986, personal communication). The WINCH (Waves Incident on Norwegian Coast, Hindcast) model is a discrete hybrid wave prediction model that has been developed by Oceanweather Inc., Cos Cob, USA.

The WINCH model is a version of the SAIL model which was used in the SWAMP (1985) study, modified for use on the Norwegian continental

shelf. It is used routinely by the Norwegian Meteorological Institute (DNMI), Oslo.

Spectral resolution

The WINCH model divides the spectrum in 24 directional bands (15 degree resolution) and 15 frequency bands. The central frequencies of the frequency bands are given on a logarithmic scale with $\Delta f/f = 0.136356$ in which Δf is the spacing between adjacent frequencies. The lowest and highest frequency in the model are 0.04 Hz and 0.23 Hz respectively. In the highest frequency band the energy of the entire tail of the spectrum from 0.23 Hz to infinity is lumped, assuming an f^{-5}-tail.

The space grid

The WINCH model has been implemented on a grid covering the North Sea, the Norwegian Sea and a large part of the North Atlantic Ocean, as illustrated in Fig. 4.4. The grid consists of two parts which have different mesh sizes. In the eastern part the mesh size is approximately 75 km, while the western part of the grid has a courser spatial resolution of about 150 km.

The position of the northern boundary of the model is not fixed but depends on the position of the ice boundary in the Norwegian Sea. Information on this boundary is obtained via satellite observations. The ice boundary information is updated every month for use in the wave model.

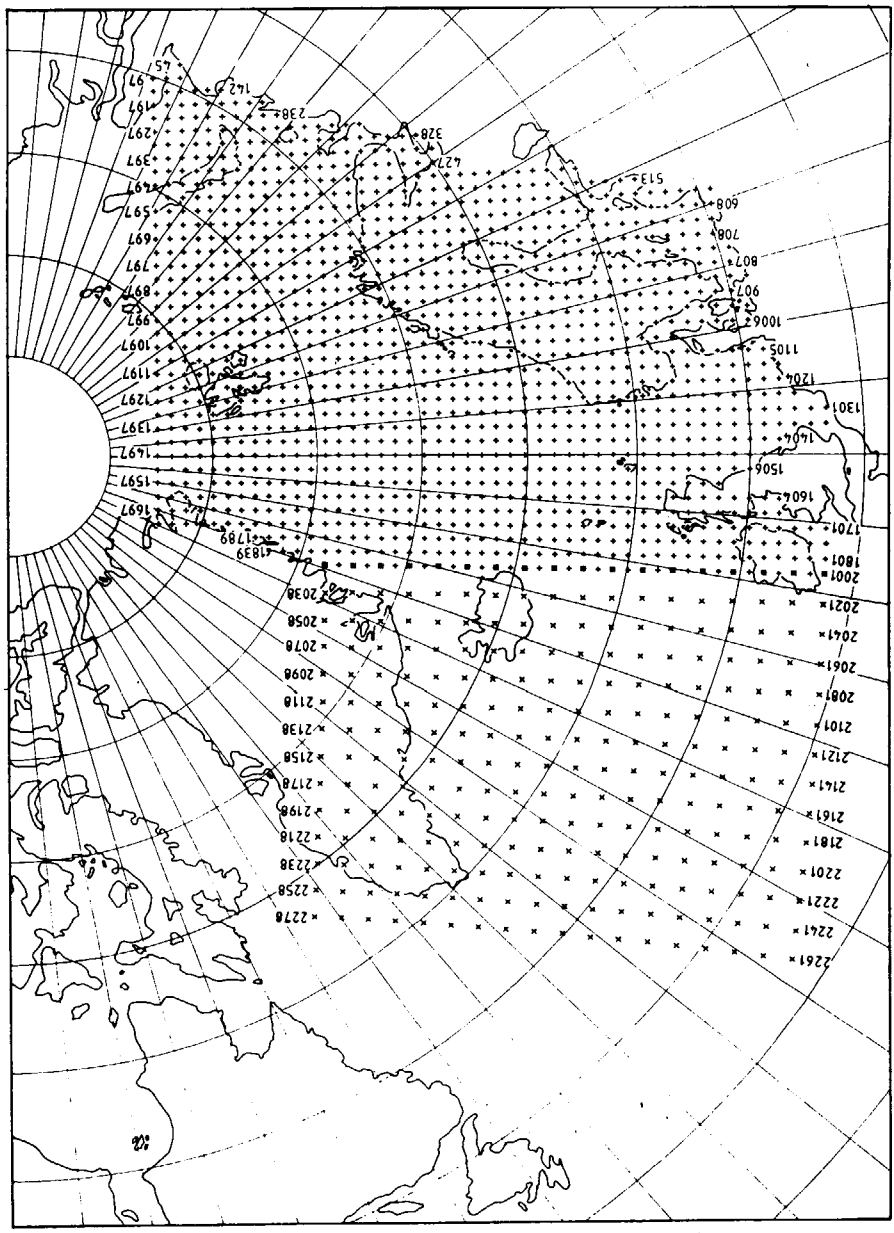

Fig. 4.4 Computational grid of the WINCH model.

Wind scaling

The wind scaling is performed in terms of the friction velocity u_*. The friction velocity u_* is derived from the wind speed at 10 m height assuming a logarithmic velocity profile (Eq. 2.50). However, in contrast to the method described in section 2.2.7, in WINCH the Von Karman constant κ is taken as 0.35, and the roughness length z_0 is given by $z_0 = \max(3.15 \times 10^{-4}\ \text{m},\ 0.035\ u_*^2/g)$, which is a modification of the relation proposed by Garratt (1977) in accordance with the measurements of Large and Pond (1981).

Spectral bands

For the treatment of spectral growth in WINCH the spectrum is divided into a number of regions in the frequency domain, such as the forward face of the spectrum and the equilibrium range. The forward face has frequencies lower than the local peak frequency. The equilibrium range is the range of frequencies that are higher than both the Pierson-Moskowitz frequency and the local peak frequency.

Directional relaxation

The WINCH model uses a combination of parametric wave growth and exponential growth per discrete spectral component. Directional relaxation per spectral frequency band is treated in the following way. Spectral bands in the equilibrium range of the spectrum are assumed to be in instantaneous equilibrium with the wind direction; spectral bands on the forward face undergo relaxation towards the wind direction by means of a gradual redistribution of wave energy over all directions. Bands with frequencies lower than the Pierson-Moskowitz frequency are considered as swell and left unaltered.

Numerical solution

The energy balance equation is integrated with alternate steps for wave growth and propagation with a basic model time step Δt_m of 2 hours. In the growth step the spatial grid points are uncoupled, but the frequency and direction bins at each grid point are coupled because of parametric relations used to model the growth of the spectrum. During a propagation step the frequency bands are uncoupled, whereas the directional bands are weakly coupled because of the convergence of the meridians on the spherical Earth (i.e. a geometrical coupling), and energy is exchanged between adjacent directional bands. For the propagation of wave energy a downstream interpolation technique is used which conserves energy and which simulates the natural dispersion of the spectral bands (Greenwood and Cardone, 1977).

In order to approximate the simultaneous effects of wave growth and advection, each model time step Δt_m is divided in two steps and executed in three stages: (1) growth for $\frac{1}{2}\Delta t_m$; (2) propagation for Δt_m; (3) growth for $\frac{1}{2}\Delta t_m$. Spectral output is generated every 2 hours.

4.4.3 Wind fields

In daily practice the WINCH model is driven by numerical wind input generated at the Norwegian Meteorological Institute every six hours. For the present study this time step was considered too large. To accommodate a smaller time step the WINCH model was modified. A time step of two hours was feasible, which is equal to the model time step of the wave model. This modification required some minor changes in the computer code of the WINCH model.

Two-hourly numerical wind fields could be supplied by BMO, England. These wind fields are generated by the "UK Meteorological Office fine mesh model" which comprises 15 air layers. For this study the wind

fields from the bottom level of this model were used. These winds are considered as near surface winds at 20 m elevation. A conversion to 10 m is performed within the WINCH model.

The BMO wind fields are given on a regular longitude-latitude grid; this differs from the grid normally used by the DNMI, which is a regular grid in a polar stereographic projection (Fig. 4.5). The conversion of the BMO wind field data to the Norwegian grid is performed by bilinear interpolation in space.

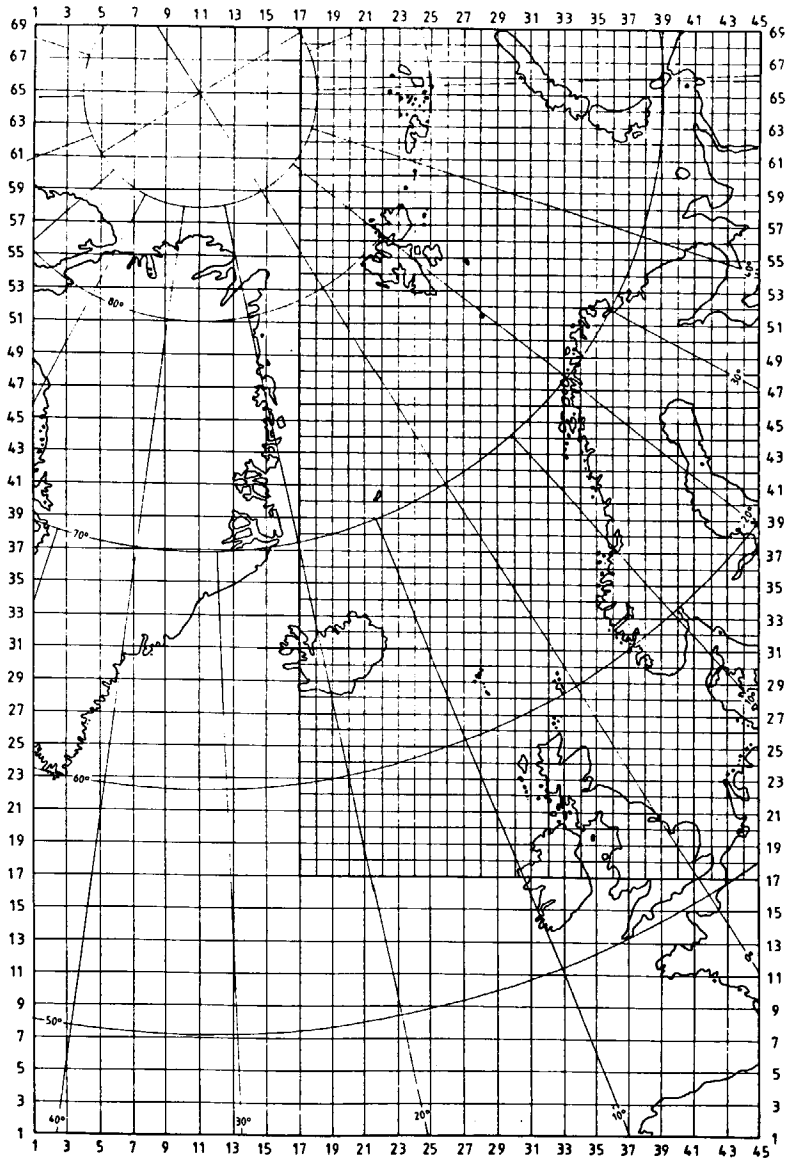

Fig. 4.5 Regular polar stereographic grid of DNMI wind fields.

4.5 Geophysical conditions

4.5.1 Introduction

This section gives information on the geophysical conditions at the locations of the buoys for the period that both wave and wind data were collected. This period is from December 25, 1985 till January 31, 1986. General information about the weather and wave conditions is taken from two monthly bulletins issued by the KNMI (1985 and 1986). Detailed information on the observed wind and wave conditions is also provided. This section ends with information on the results obtained with the WINCH hindcast model.

4.5.2 General information

In the period of observation a relatively large number of depressions passed over the North Sea. Many of these generated high seas and wind directions turning from Southerly via Westerly to Northerly directions. Reports of wind and wave conditions are routinely collected by the KNMI (1985 and 1986). For the areas near the offshore platforms AUK-α and K13-α a brief summary of this information is given below.

For the areas near the AUK-α platform strong winds with gale force were reported on December 22 and 30, 1985. Especially in January 1986 strong winds were reported on many days, e.g. the 10th, 14th, 24th, 30th and on the 31th of January. On the 10th, 24th and 31th significant wave heights of more than 7 m were reported.

For the areas near the K13-α platform strong winds were also reported at many days. Especially on January 10 a strong gale was reported. On January 24th storm force was reported from a southerly direction.

One of the depressions causing high wind driven seas and turning winds passed the North Sea on January 10th, 1986. The associated weather map

is shown in Fig. 4.6.

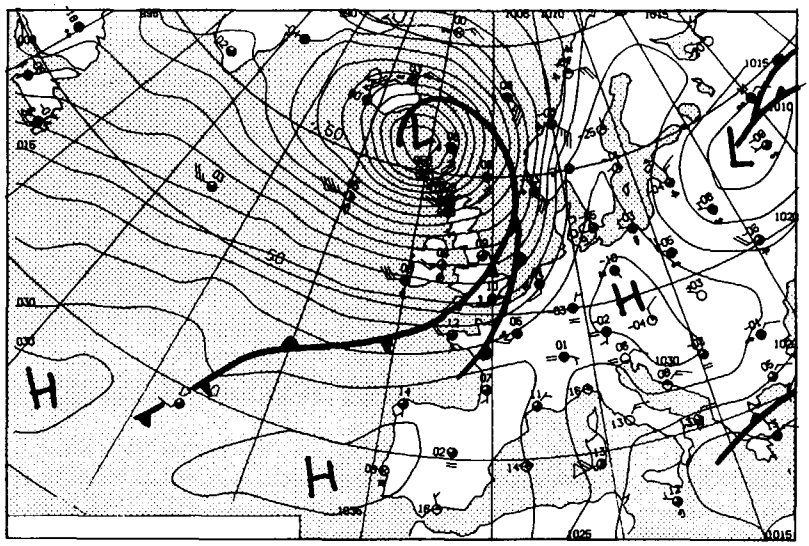

Fig. 4.6 Weather map for North Atlantic Ocean region on January 10th, 1986

The wave field generated by this storm at January 10th, 1986, 12.00 UTC as computed by the GONO model of the KNMI is shown in Fig. 4.7, together with information on the wind speed and wind direction. Shortly after this time, the wind direction turned towards a North-Westerly direction.

In general, January 1986 was extremely stormy. This is illustrated by comparison of the monthly statistics for wind speed and wave heights with average values of wind and wave conditions collected by ship observations in the period 1961-1980 (see Figs. 4.8 and 4.9). These figures show that the location of most of the wave height- exceedance isolines for January, 1986 is more Southerly than the 20-year average isolines.

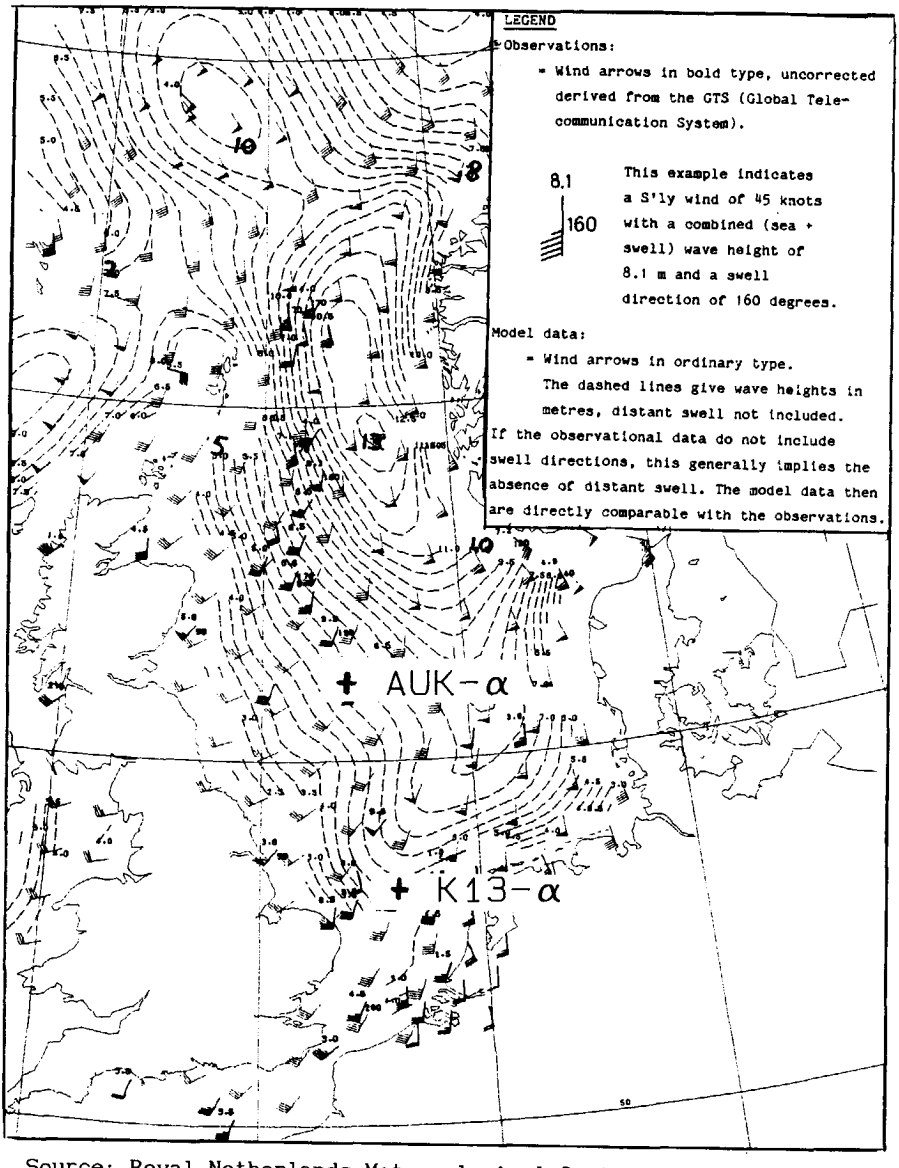

Source: Royal Netherlands Meteorological Institute

Fig. 4.7 Isolines of computed wave heights (with the GONO model) for January 10th, 12.00 UTC, 1986.

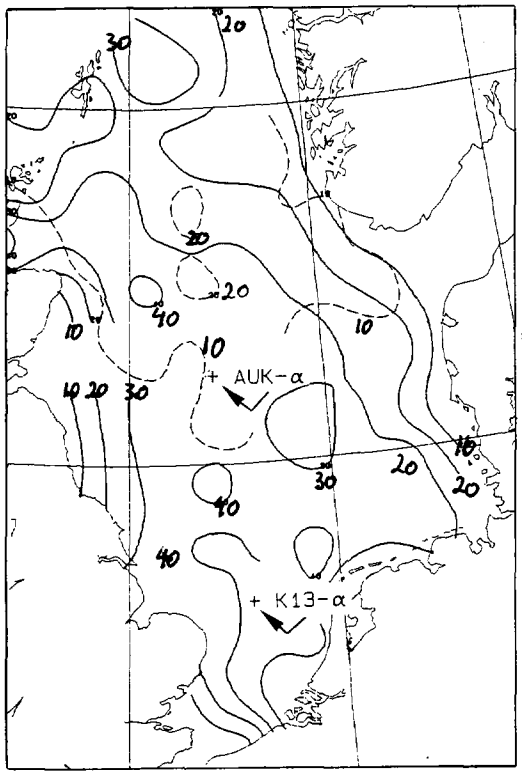

Source: Royal Netherlands Meteorological Institute

Fig. 4.8 Isolines indicating the percentage of time with wind speeds greater than 7 Beaufort; ——: January 1986; – – – –: 20-year average for January-months (1961-1980).

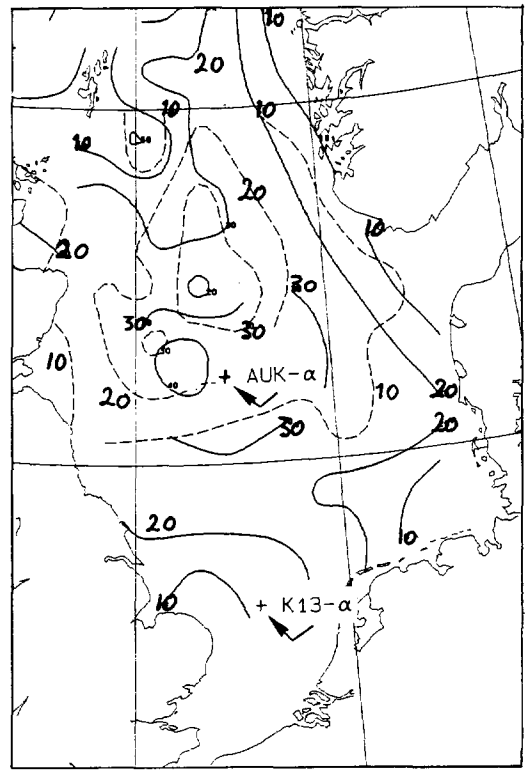

Source: Royal Netherlands Meteorological Institute

Fig. 4.9 Isolines indicating the percentage of time with wave heights greater than 4 m; ——: January 1986; – – – –: 20-year average for January-months (1961-1980).

4.5.3 Wave observations

The WAVEC buoy near the AUK-α platform became operational on December 17, 1985 and worked almost continuously till January 31, 1986. However, after January 26, the performance of this WAVEC buoy strongly deteriorated, resulting in many missing wave observations (e.g. see Fig. 4.10). The WAVEC buoy near the K13-α platform was in operation continuously during the month of December, 1985 and January 1986.

During the observation period the significant wave height varied from 1 m to 7.5 m for the AUK-α location and from 0.8 m to 6.5 m for the K13-α location (see Fig. 4.10).

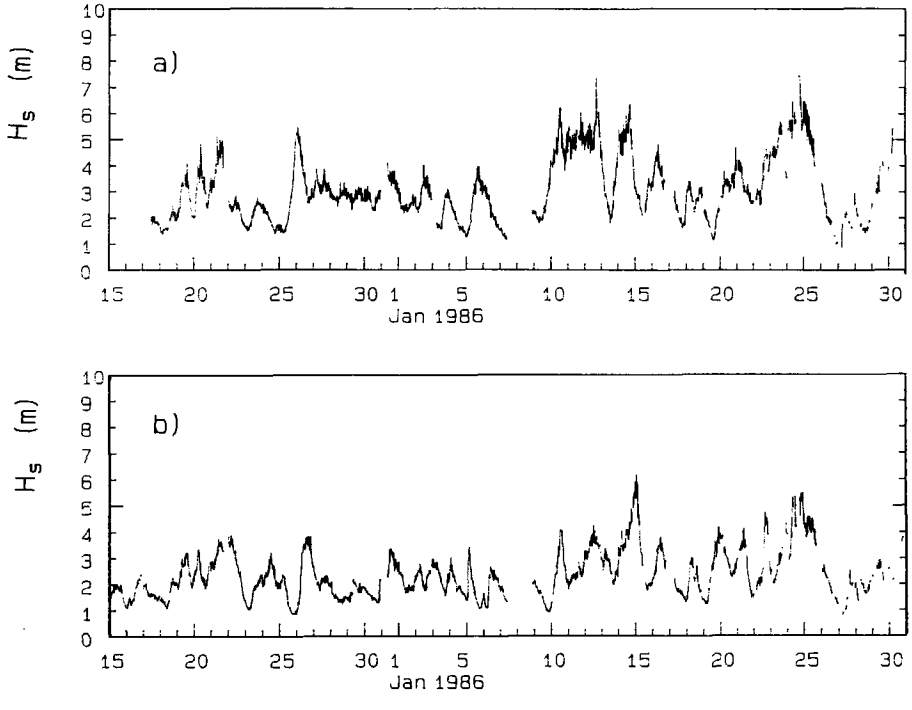

Fig. 4.10 Observed significant wave height for the AUK-α location (panel a) and for the K13-α location (panel b).

The wave heights observed at the K13-α location for this period are lower than those of the AUK-α location. This difference is probably due to the effect of bottom friction on the waves. The mean wave directions observed at each of the locations are illustrated in Fig. 4.11. Comparing the Fig. 4.10 with Fig. 4.11 shows that events of changing wave directions are usually associated with an increase in the wind speed and an increase in the significant wave height. The peak frequency of the waves varied from 0.08 Hz to 0.28 Hz for the AUK-α location and from 0.06 Hz to 0.26 Hz for the K13-α location (see Fig. 4.12).

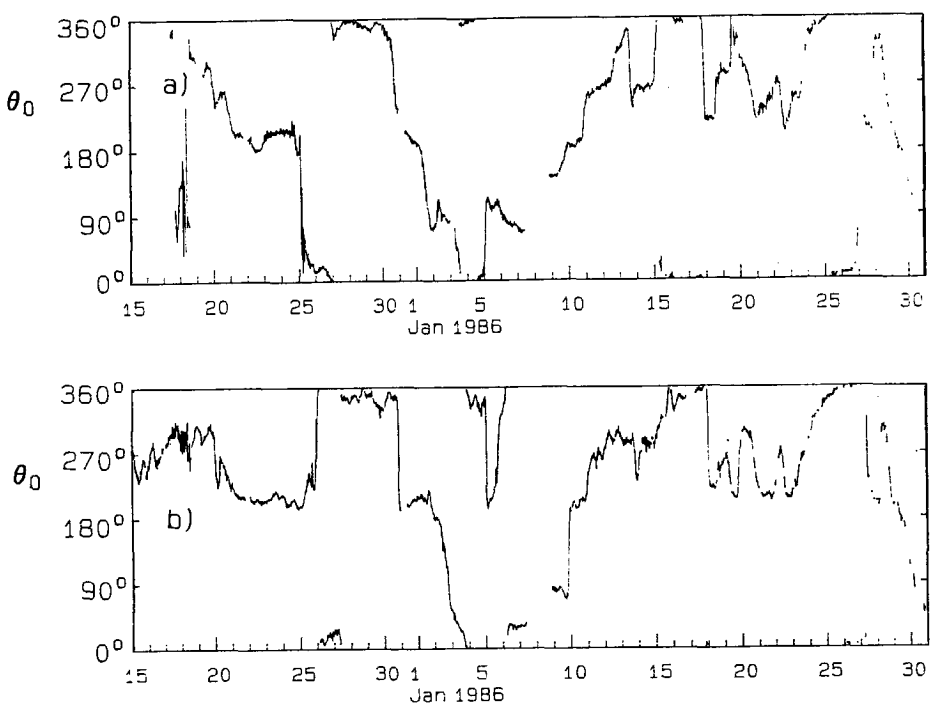

Fig. 4.11 Observed mean wave directions, direction from, counted clockwise from geographic North, for the AUK-α location (panel a), K13-α location (panel b).

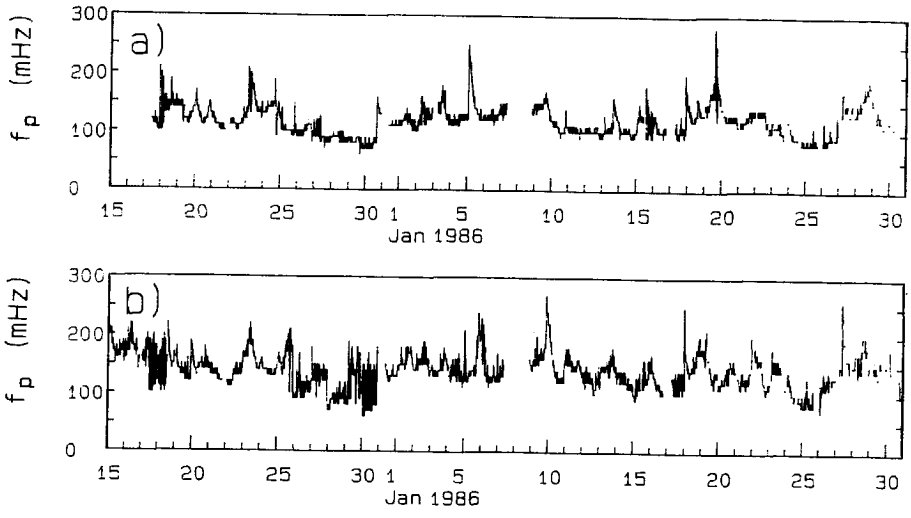

Fig. 4.12 Observed peak frequencies for the AUK-α location (panel a) and K13-α location (panel b).

4.5.4 Wind observations

For the AUK-α location wind data are available from December 24, 1985 till January 24, 1986. For the K13-α wind observations are only available for a shorter period, i.e. from December 24, 1985 until January 8, 1986 when the wind anemometer broke down. The measured wind speed and wind direction for both locations are shown in the Figs. 4.13 and 4.14 respectively.

The wind speed at the top of the offshore platforms varied from 1 m/s to 27 m/s for the AUK-α location and from 0.8 m/s to 19 m/s for the K13-α location. This significant difference between the respective maximum wind speeds is due to the fact that the maximum wind speed at AUK-α occurred in a point for which at K13-α no wind observations were made. For the periods that both anemometers were in operation the respective magnitudes of the wind speeds at the two stations are almost the same.

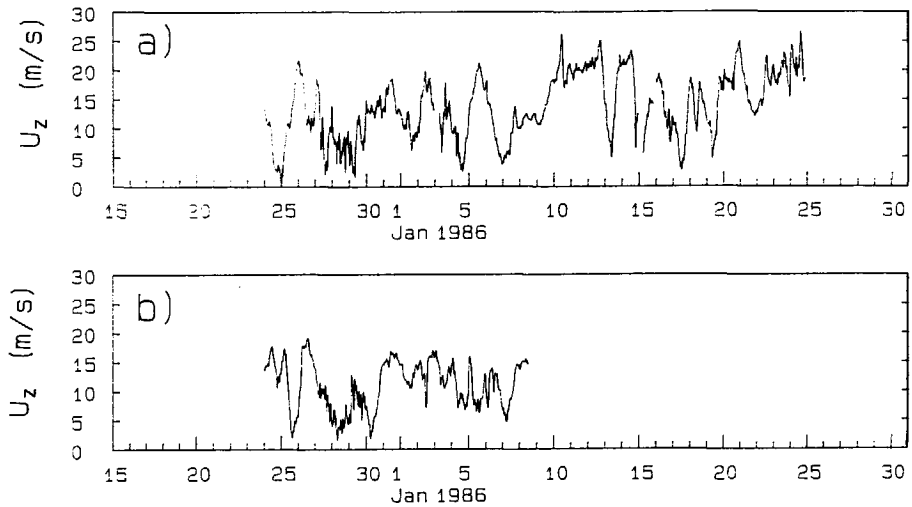

Fig. 4.13 Observed wind speed for the AUK-α location (panel a) and K13-α location (panel b).

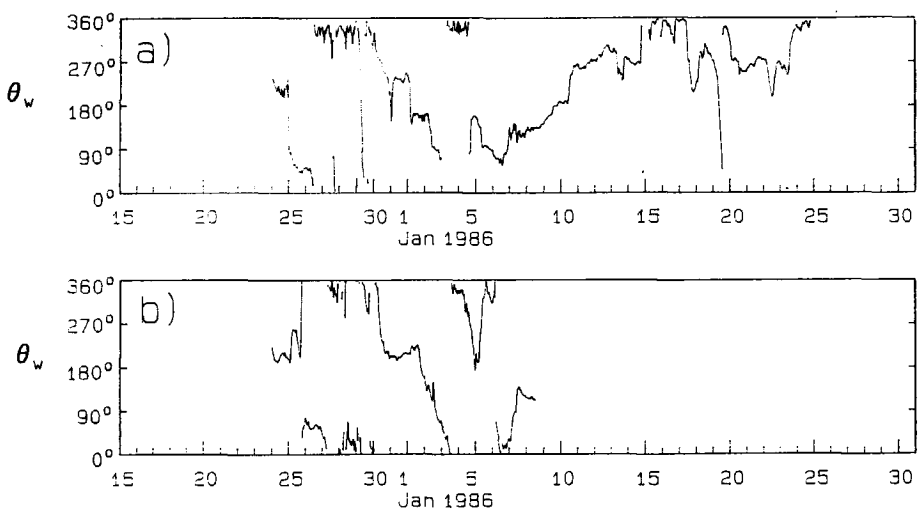

Fig. 4.14 Observed wind direction for the AUK-α location (panel a) and K13-α location (panel b), direction from, counted clockwise from magnetic North.

4.5.5 Hindcast studies

A number of hindcasts have been performed with the WINCH model for the period in which measurements of waves and wind are available, viz. from December 25, 1985 till January 31, 1986. However, for operational reasons a continuous hindcast was not feasible. Therefore, the total period was divided in the following intervals which were chosen so as to include as much of the observations intervals as possible.

1) December 21, 1985, 0.00 GMT - December 26, 1985, 6.00 GMT
2) January 1, 1986, 0.00 GMT - January 14, 1986, 6.00 GMT
3) January 16, 1986, 0.00 GMT - January 26, 1986, 6.00 GMT

Overall results of these hindcast studies are shown and compared with observations in the Figs. 4.15 and 4.16. The results are in terms of significant wave height and mean wave direction for the locations AUK-α and K13-α.

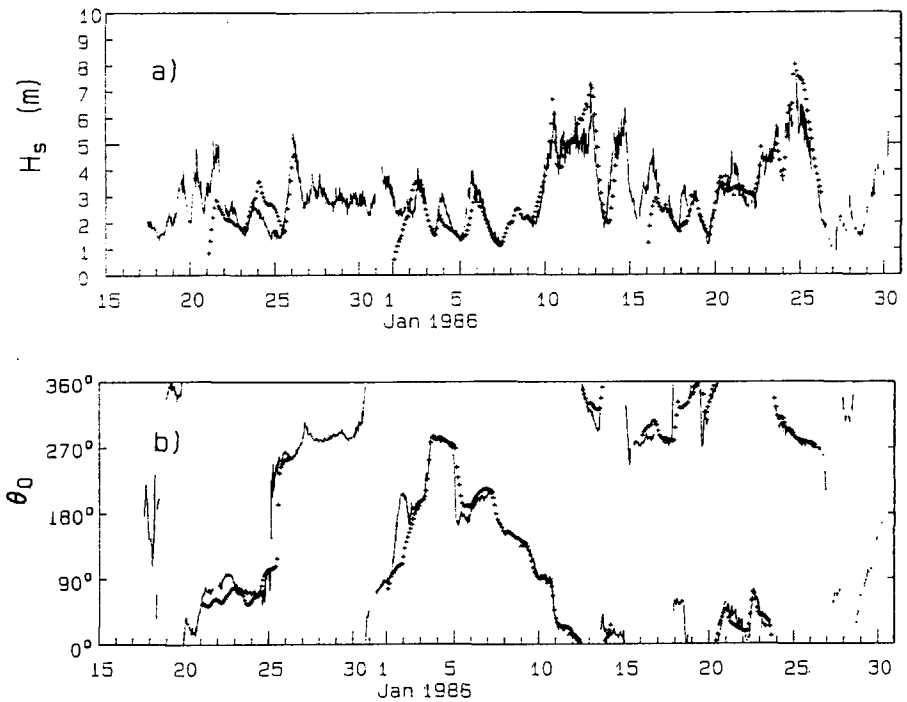

Fig. 4.15 Observed (——) and hindcasted (+) significant wave height for the AUK-α location (panel a). Observed (——) and hindcasted (+) mean wave direction for the AUK-α location, direction to, counted clockwise from geographical North (panel b).

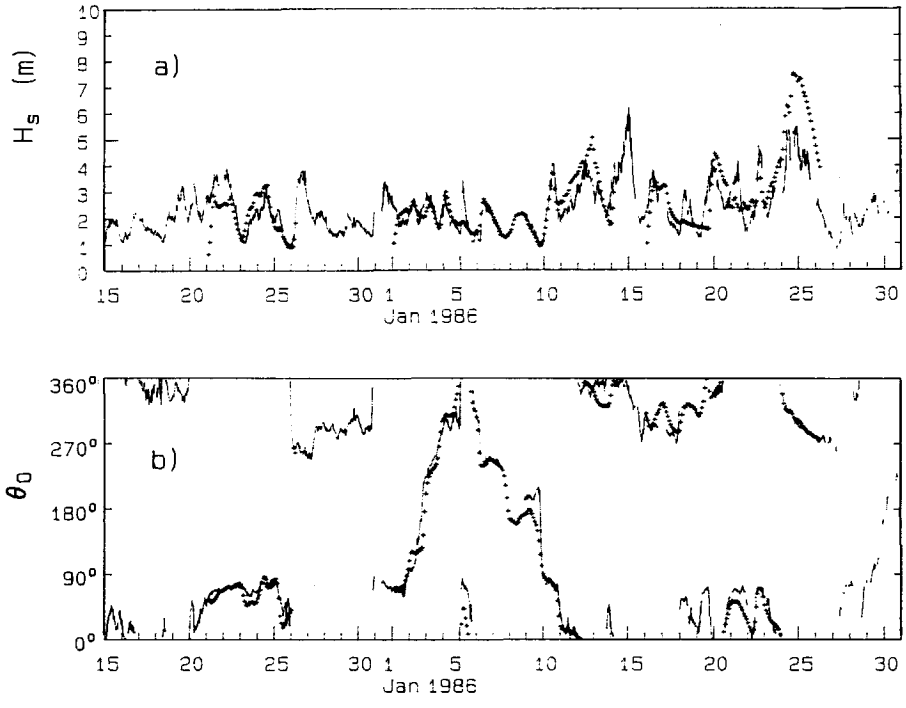

Fig. 4.17 Observed (——) and hindcasted (+) significant wave height for the K13-α location (panel a). Observed (——) and hindcasted (+) mean wave direction for the K13-α location, direction to, counted clockwise from geographical North.

4.6 Criteria for the selection of data

4.6.1 Introduction

The purpose of this study is to investigate the response of the deep water mean wave direction to changes in the wind direction. This implies that the following geophysical conditions should be fulfilled:
- actively wind-driven waves in deep water, so swell is excluded, and
- the mean wave direction turns towards the local wind.

Based on these requirements a number of selection criteria have been formulated. Application of these selection criteria leads to a set of time intervals that are available for estimating the time scales and associated errors. From this set only those time scale estimates are presented with a relative error lower than some threshold value.

Each time interval used for the estimation of the time scale τ has a duration of 60 minutes ($2\Delta t$). In each time interval a number of variables are used select for the selection. They are: the observed wind directions $\theta_w(t)$, $\theta_w(t+\Delta t)$ and $\theta_w(t+2\Delta t)$, the measured mean wave directions $\theta_0(t)$, $\theta_0(t+\Delta t)$ and $\theta_0(t+2\Delta t)$, and the computed locally induced mean wave direction at the end of the time interval, denoted by $\theta_{0,L}(t+2\Delta t)$. Also used are the observed peak frequencies $f_p(t)$, $f_p(t+\Delta t)$ and $f_p(t+2\Delta t)$. In the same time interval an estimate of the transport term T is available at time $(t+\Delta t)$, together with the model mean wave direction θ_M and model peak frequency $f_{p,M}$. These estimates are computed by linear interpolation in time from the hindcast model results, which are given at intervals of 2 hours (see section 4.3.3).

4.6.2 Selection criteria

1) For each time interval of 1 hour duration a check is made for missing data. Within each such time interval, three wave and wind observations at 30 min. intervals should be present. In addition an estimate of the effect of transport through the wave model results should be available from the WINCH model.

2) For the waves to be considered as relatively deep water waves, the wave length L_p associated with the observed peak frequency f_p of each of the three wave observations should satisfy:

$$L_p < 3\ d \tag{4.39}$$

in which d is the local water depth and in which

$$L_p = g/(2\pi f_p^{\ 2}). \tag{4.40}$$

Regarding the local water depths this implies that $f_p > 0.086$ Hz for the AUK-α location, and $f_p > 0.132$ Hz for the K13-α location.

3) Since by definition swell is not affected by the local wind, the time scale estimates obtained for situations with swell are not useful for this study. It is therefore necessary to include only windsea measurements. To determine whether or not swell is present in the wave observations the dimensionless wave energy and dimensionless peak frequency are compared with each other. For wind sea situations these parameters should be related via universal relationships (see Eq. 2.65). Following Holthuijsen et al. (1987) the following criteria are used to select wave measurements without swell:
   a) the peak frequency f_p of the spectrum is higher than the direction-corrected Pierson-Moskowitz frequency (Pierson and Moskowitz, 1964),

$$f_p > f_{PM}/\cos(\theta_w - \theta_0) \qquad (4.42)$$

in which $f_{PM} = 0.13\ g/U_{10}$.

b) The observed dimensionless wave energy ε should be within a factor 2 from the dimensionless wave energy obtained with the universal relationship (2.65) suggested by Hasselmann et al. (1976).

4) Since the response of the mean wave direction is treated as a relaxation process, the observed mean wave direction θ_0 should turn towards the observed wind direction θ_w.

5) Estimates of the time scale τ are valid only if the angle between the wind and wave direction is less than 90°. This is explained as follows. In the relaxation model (Eq. 4.1) the rate of change of the mean wave direction is proportional to the sine of the angular difference ($\Delta\phi$) between the wind and wave direction. For angular differences $\Delta\phi_1$ and $\Delta\phi_2 = \pi - \Delta\phi_1$ the values of the sines are equal, although the situations are fundamentally different in both instances. Therefore it is required that:

$$|\theta_w(t+\Delta t) - \theta_0(t+\Delta t)| < 90^\circ. \qquad (4.42)$$

6) The time scale estimates have a relative error σ_τ/τ smaller than some threshold value (see section 4.7).

Summary of selection criteria

A qualitative summary of the selection criteria is given below:

1) no missing data
2) peak frequency subject to certain minimum to obtain only deep water observations
3) relation between dimensionless peak frequency and dimensionless total wave energy close to universal relationship to discard observations with swell
4) mean wave direction turns towards wind direction
5) difference between wind and wave direction subject to maximum
6) sufficiently reliable time scale estimates

4.7 Results

The basic data set used for the time scale analysis consists of 1261 time intervals of 1 hour duration, each comprising three wave, three wind observations and one wave model result. The size of this data set was reduced by application of the selection criteria mentioned in section 4.6.2, resulting in 133 time intervals for which estimates of the time scale could be made. The effect of each of these selection criteria is summarized in Table 4.1, showing percentage of time intervals which are not accepted for further analysis if applied separately, and the percentage if all criteria are applied together.

Rejection criterion	Percentage rejected
• Peak frequency too low	40 %
• $(\theta_w - \theta_0) > 90^\circ$	7 %
• Waves do not turn towards wind direction	65 %
• ν and ε do not satisfy universal relationship	40 %
• all	89 %

Table 4.1 Percentage of time intervals rejected for the time scale analysis by different selection criteria if applied separately, and if applied together.

For each of the 133 remaining time scale estimates the corresponding relative error σ_τ/τ was determined with the procedure described in section 4.3.5.2.

For the selected time intervals the root mean square error of the model mean wave direction θ_M and model peak frequency $f_{p,M}$ have been

determined as 21° and 0.022 Hz respectively. These values have been used to quantify the error in the time scale estimates.

The number of accepted estimates is shown in Table 4.2 for four different threshold values of the maximum allowable relative error (σ_τ/τ):

threshold value	number of estimates
∞	133
1	34
0.75	19
0.5	7

Table 4.2 Threshold values and resulting number of accepted time scale estimates.

The observed dimensionless time scales τ_* are shown in Fig. 4.17 as a function of the observed dimensionless wave energy ε_* and as a function of the observed dimensionless peak frequency ν_*. The results in Fig. 4.17 show that without any selection (Fig. 4.17a) the time scale estimates are widely distributed in ε_*-τ_* space as well as in ν_*-τ_* space with no significant correlation. By imposing stricter restrictions on the maximum allowable relative error (Fig. 4.17, panels b to d) the number of time scales estimates decreases together with a trend becoming visible, the trend being an increase in time scale with increasing growth stage.

The data shown in Fig. 4.17 are considered to be the main result of the analysis of the observations.

For the set of time scale estimates with relative error $\sigma_\tau/\tau \leq 1$, the power-law relation $\tau_* = a\ \nu_*^{\ b}$ has been fitted to the time scale estimates. The fit procedure consists of a least squares linear regression

of $\log(\tau_*)$ on $\log(a) + b \log(\nu_*)$. The results of the fit procedure yield:

$$\tau_* = 37\ \tau_*^{-1.7}. \qquad (0.006 < \nu_* < 0.012) \qquad (4.43)$$

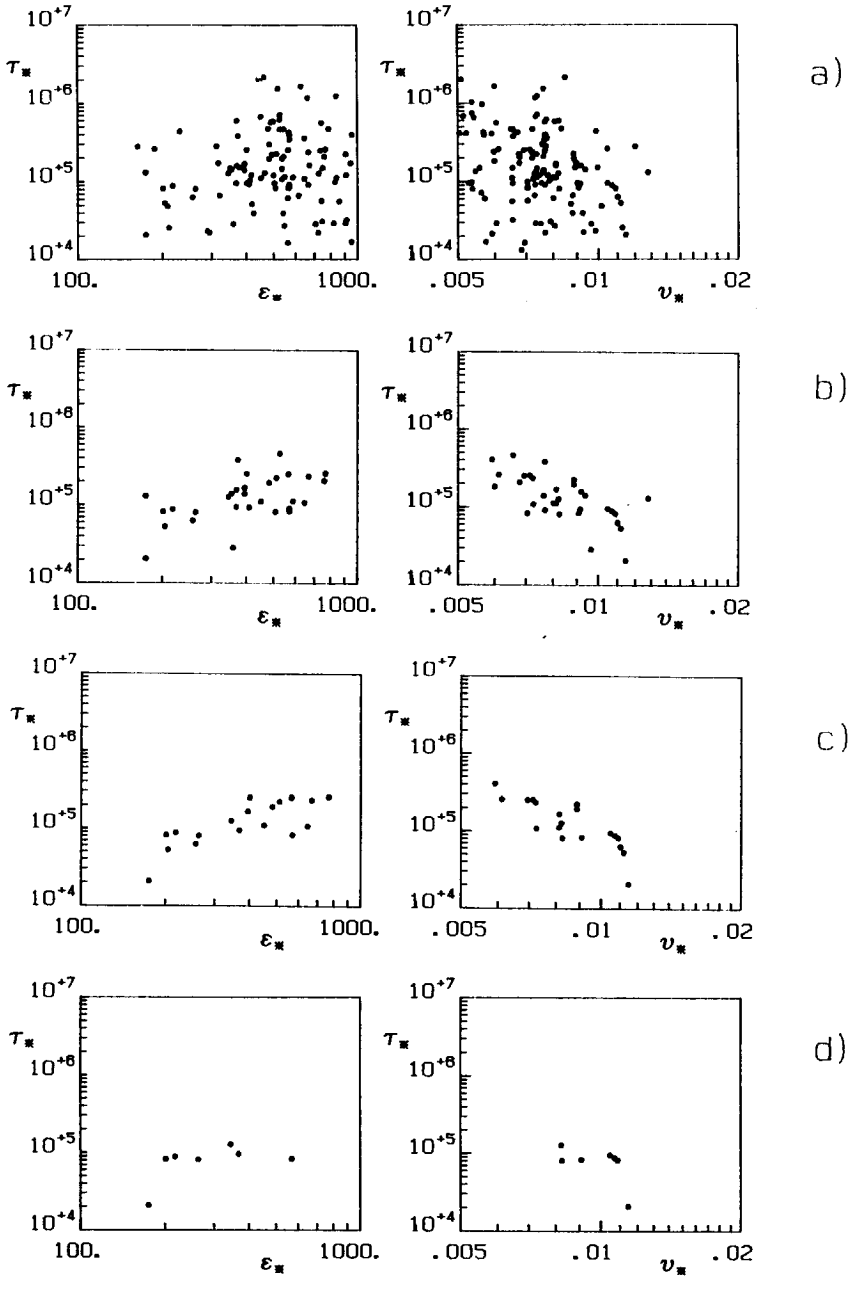

Fig. 4.17 Observed dimensionless time scale τ_* as a function of dimensionless wave energy ε_* and dimensionless peak frequency ν_* for four different threshold values: ∞ (panel a), 1 (panel b), 0.75 (panel c) and 0.5 (panel d).

4.8 Discussion

The present method of analysing directional wave measurements with respect to the directional response of the frequency integrated mean wave direction to turning winds contains two new elements compared to previous methods.

First, the problem of inhomogeneities in the wave and wind field has been solved by using the results of a numerical hindcast model to quantify the effect of transport on the rate of change of the mean wave direction, and the subsequent treatment of the observations to determine the locally induced change of the mean wave direction. In this way the use of more or less subjective criteria to select homogeneous wave and wind conditions becomes superfluous.

Second, the present method performs an error analysis on each time scale estimate to estimate its error. Based on this information the data have been selected with respect to their relative error to obtain reliable time scale estimates. In this method the effect of measurement errors in the error of each time scale estimate is taken into account automatically.

The results show that without any selection the scatter in the results is too large to draw any conclusions about a possible relation between τ_* and ν_*. Decreasing the threshold value of allowable relative error reduces the scatter, resulting in a trend of increasing time scales with increasing growth stage. However, for the small threshold value of 0.5, the number of time scale estimates becomes too small to draw firm conclusions. Only for the sets of time scale estimates corresponding to threshold values of 1 and 0.75 a trend is clearly visible. Of these two sets the one with a threshold value of 1 is used in the following for comparison purposes.

The empirical results of the present study (data and power law fit) are compared in Fig. 4.18 with empirical results obtained by Holt-

huijsen et al. (1987), the parameterized results of Günther et al. (1981) and with the parameterized, re-analysed data of Hasselmann et al. (1980) and Allender et al. (1983), as given previously in Fig. 2.2b.

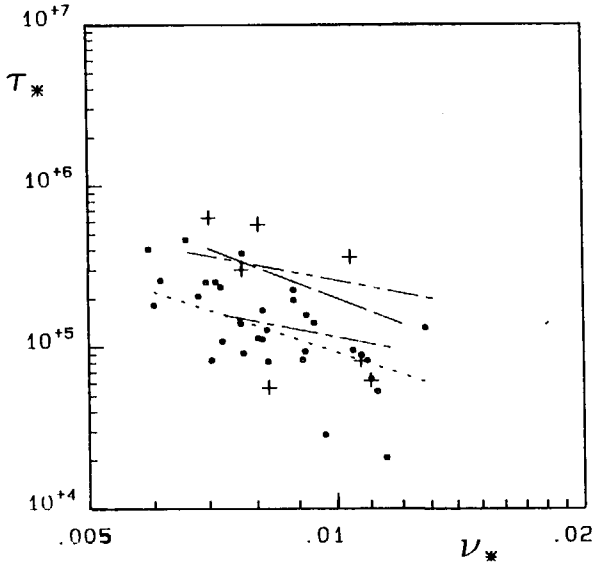

Fig. 4.18 Comparison of observed time scale τ_*; present observational results (o) (using a threshold $\sigma_\tau/\tau = 1.0$), best fit line of present observations (– – – –), empirical results from Holthuijsen et al., 1987 (+), parameterized data of Hasselmann et al., 1980 (—— – – ——), parameterized data of Allender et al., 1983 (—— – ——) and parameterized data of Günther et al., 1981 (—— ——).

The time scale estimates of the present data set cover about the same range as those of Holthuijsen et al. (1987), but they are less scattered. In contrast to the results of Holthuijsen et al. (1987) the present time scale estimates show a trend of increasing time scales with increasing growth stage.

The trend in the present results is in good agreement with the trend in the parameterized results of Günther et al. (1981), but the present values are significantly lower.

The present observations compare reasonably well with the results of the re-analysed data of Allender et al. (1983). They are about a factor two to three lower than the results of the re-analysed data of Hasselmann et al. (1980). It is noted that the results presented by Hasselmann et al. (1980) are based on 37% of their data and that the parameterized results of Günther et al. (1981) are based on only four observations.

A comparison of the present empirical results with theoretical time scale models and the results of numerical calculations is given in Chapter 5.

4.9 Conclusions

Based on a careful analysis of directional wave measurements in actively wind driven seas, comprising the quantification of the error of each time scale estimate, it was made possible to select these estimates with respect to their relative error. Without any selection, the scatter in the results is too large to draw conclusions about a possible relation between time scale and growth stage. The scatter in the results can be decreased by decreasing the maximum allowable relative error in the time scale estimates.

Decreasing the threshold value reveals a trend of increasing time scale with growth stage, i.e. with increasing dimensionless wave energy or with decreasing dimensionless peak frequency.

The present time scale estimates cover about the same range as the estimates obtained by Holthuijsen et al. (1987), although the scatter in the latter is much larger. The present results are also in agreement with the re-analysed data of Allender et al. (1983).

The observed trend of τ_* with ν_* is in good agreement with the trend in the parameterized results of Günther et al. (1981), and the model of Holthuijsen et al. (1987), although the observed time scales are lower than those predicted Günther et al. (1981).

Finally, it is noted that despite the care with which the observations have been analysed, a considerable scatter in the results to a factor 10 remains. This indicates that the present knowledge of the directional response of wind waves to turning winds is still rather poor.

CHAPTER 5

COMPARISON OF RESULTS

5.1 Introduction

In this chapter a comparison is made between the present computational and observational results, followed by an intercomparison of all available results. Finally, the results of these comparisons are discussed.

For the comparison reference is made to Fig. 5.1 in which the time scale τ_* is given as a function of dimensionless peak frequency ν_*. This figure contains the computational and empirical results of this study, together with results from Günther et al. (1981), Holthuijsen et al. (1987) and Young et al. (1987), and the re-analysed results of Hasselmann et al. (1980) and Allender et al. (1983).

5.2 Comparison of model results with observational results of this study

The model results shown in Fig. 5.1 refer to the EXACT-NL model computations for all cases of Table 3.1 (page 79) for U_{10} = 20 m/s. The results from the observations consist of time scale estimates for which the relative error σ_τ/τ is equal to or lower than one.

The results shown in Fig. 5.1 indicate that the measured time scales are generally lower than the computed ones. There is a tendency towards an overlap in the results for increasing ν_*, i.e. for younger sea states. The results diverge as the waves are more developed. For nearly fully developed waves the model predicts a rapid increase of

time scales; however, this behaviour is not supported by the measurements.

For both sets of time scale estimates the fitted power law relations are compared with each other; $\tau_* = 0.002\ \nu_*^{-4}$ for the EXACT-NL model results (see section 3.6.3.1) and $\tau_* = 37\ \nu_*^{-1.7}$ for the observational results (see section 4.7). These results indicate that the trend of τ_* with ν_* is stronger for the model results than for the observational results.

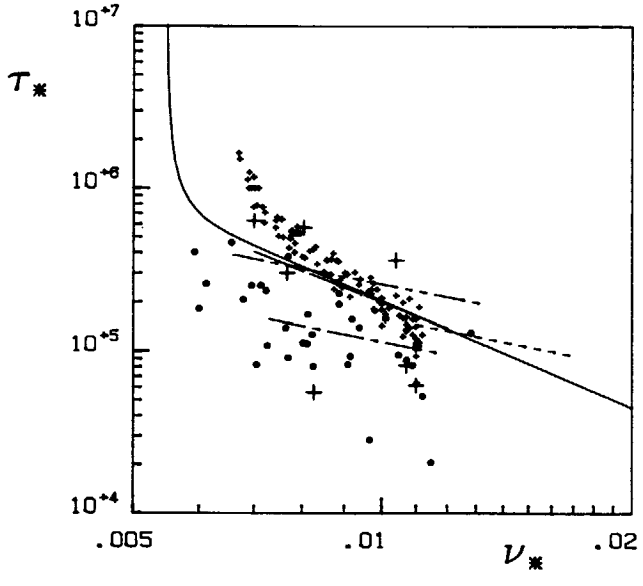

Fig. 5.1 Dimensionless time scale τ_* as a function of dimensionless peak frequency ν_*; EXACT-NL model results (+), observational results of this study (•), observational results of Holthuijsen et al., 1987 (+), re-analyzed data of Hasselmann et al., 1980 (—— – – ——), re-analyzed data of Allender et al., 1983 (—— – ——), parameterized data of Günther et al., 1981 (—— ——), model of Holthuijsen et al., 1987 (————) and computational results of Young et al., 1987 (– – – –).

5.3 Intercomparison of all available results

The re-analysis of previously published results, as presented in chapter 2, has to a large extent removed the discrepancies between these results, resulting in the vanishing of two distinct families of time scales. Ironically enough, the addition of the present carefully selected, extensive data set re-introduces two families, although at a significantly lower level of time scale values than previously (see Fig. 5.1). The new observational results, together with the re-analysed results of Allender et al., (1983) form the first family. The second family consists of the present model results, the model results of Holthuijsen et al. (1981) and Young et al. (1987), the parameterized results of Günther et al. (1981) and the re-analysed data of Hasselmann et al. (1980). The observational results of Holthuijsen et al. (1987) are too scattered to classify them in one these families.

It is noted that all available model results belong to the first family, whereas the majority of the observational results belongs to the second family.

From the comparison it follows that the second family has lower time scales than the first family. From the comparison it also follows that for younger sea states there is a tendency for convergence of all model results and the observational results of this study.

5.4 Discussion

The results in Fig. 5.1 show that the present model results differ from the observational results, in the sense that they yield higher time scales. Possible reasons for this difference are discussed below.

A reason for this difference may be an improper representation of the physics in the EXACT-NL model. This may be true for the wind input and dissipation source function but not for the nonlinear transfer. For the wind input a parameterization is used that is based on careful measurements by Snyder et al. (1981). Coefficients in this formulation have been tuned to directionally integrated characteristics, so there is the possibility that directional aspects have attained insufficient attention. However, it is not expected that realistic corrections in the formulation of the wind input source function will have much effect on the time scale of the directional response.

For the dissipation source function a quasi-linear formulation is used, which is still the topic of many studies. The coefficients in this formulation have been tuned by Komen et al. (1984) to yield realistic spectra in fully developed wave conditions. However, in their study, Komen et al. (1984) did not investigate the effect of variations in directional dependencies in the formulation of the dissipation source function on characteristics of the fully developed wave spectrum. So, this may be a source of uncertainty with respect to the proper dissipation rate.

The fact that integral wave parameters are used to scale the dissipation, viz. the mean frequency and the total wave energy, may lead to incorrect dissipation rates for high frequencies after a change of wind direction. In such a situation the model dissipation is determined by the integral wave parameters of the wave system in the 'old' wind direction, but also by the energy density of this wave system. For the new wind-sea system the ratio $(\omega/\bar{\omega})$, and the energy density are relatively large, which leads to a dissipation that is too

large for the higher frequencies, thus counteracting the growth of a windsea spectrum in the new wind direction (P.A.E.M. Janssen, 1989, KNMI, personal communication). Only if the dissipation rate of the new wind-sea system is decreased, lower time scales can be computed.

In this study the sensitivity of the time scale of the directional response to variations in all three coefficients of the dissipation source function was investigated (see chapter 3). From the results of that investigation it follows that lower model time scales are obtained when the dissipation rate is increased with relative frequency or decreased with relative average wave steepness, or when the overall level of dissipation is reduced. However, in order to decrease the time scales by about a factor two, these variations should be made so large that this leads to unrealistic spectra, and an inability to obtain an equilibrium state (see Komen et al., 1984). In this light it is also unlikely that modification of directional dependencies in the dissipation source function may remove the above difference.

The above discussion suggests that it is improbable that the differences in time scales are due to incorrect formulations of the source functions in the EXACT-NL model.

Another reason for the discrepancy may be attributed to errors in the measurements. However, the error analysis of the time scales was meant to estimate the contribution of measurement errors to the error in each time scale estimate. In this way measurement errors are already accounted for.

Another reason may be that the shape of the two-dimensional spectrum at the moment of time scale estimation is important. A systematic difference exists between conditions considered in the computations and those occurring at sea. In the computation runs the wind direction is kept constant after a sudden change in wind direction (except the constantly turning wind case, which is omitted from this discussion). In this way the wave field grows to a fully developed state and the

mean wave direction gradually becomes equal to the new wind direction. So, in the model results, the growth stage of the waves (as expressed by ν_* and ε_*) and the time scales are in fact correlated to the angle between wind direction and mean wave direction.

In the open ocean the situation is different. Ideal cases as used in the model computations will normally not exist. Even if a sudden shift occurs, the wind direction will normally change again before wave and wind direction are equal. Therefore in the observations growth stage and relative angle are less correlated than in the model situations.

As a consequence, for the nearly fully developed case, small changes in the model results will lead to high time scales, whereas in the open ocean relatively low time scales can be observed. Such a behaviour may be investigated with a numerical wave prediction model, in which the wind direction changes when the wave field has reached the nearly fully developed state.

The above discussion suggests that the relaxation model used in this study is inadequate to relate the rate of change of the mean wave direction to the local wind and the presently used integral wave parameters. This may have two reasons. First, the present parameterization of the directional response is incomplete. Other parameterizations should be developed that more or other wave parameters into account, or in another manner. Secondly, the selection criterion used to obtain actively wind-driven seas situations is inadequate. The criterion used in this study is based on a swell-sea splitter using the dimensionless integral wave parameters ε and ν, and the mean wave direction θ_0 (see section 4.6). This may be too primitive for the present study. Swell-sea splitters should be developed that take more or other wave parameters into account.

CHAPTER 6

SUMMARY AND CONCLUSIONS

In this study the directional response of wind generated waves to turning winds has been studied theoretically by using an advanced numerical wave prediction model, and empirically by using the results of directional wave measurements in the open ocean.

This study has been concentrated on two aspects of the directional response. The first aspect comprises the study of the shape of the two-dimensional spectra, and the physical processes active during the response of the waves. The second is the relation between the time scale of the directional response and local wind- and wave parameters. To that end a relaxation model was used that relates the locally induced rate of change of the mean wave direction to difference between the wind- and wave direction.

Both aspects have been studied with the EXACT-NL model, which is a third generation wave prediction model that has the ability to represent the physics of wind waves rather well. This model has been applied to homogeneous situations for two types of wind fields. These are a sudden shift of the wind direction over angles of 30°, 45°, 60° and 90° and a constantly turning wind of 10°/h. The computations have been performed for two wind speeds, viz. 10 m/s and 20 m/s.

Qualitative results obtained with this model show that for the relatively small wind shifts up to 45° the shapes of the two-dimensional spectrum and corresponding source function remain almost unchanged, and symmetric around the (turning) mean wave direction. For the larger wind shifts of 60° and 90° the spectrum and source function become strongly skewed. In all sudden wind shift cases a second spectral peak develops initially. However, for relatively small wind shift this second peak is rapidly absorbed.

The quantitative model results indicate that the turning of the waves is primarily due to the effect of the wind, but that it is counteracted to some degree by the effects of dissipation and nonlinear transfer. They also indicate that the time scale of the directional response of the mean wave direction increases with increasing growth stage of the waves. For nearly fully developed waves the results show a rapid increase in time scale.

The sensitivity of the time scale of the directional response to variations in the present modelling of the dissipation source function has been investigated. The results indicate that lower time scales can be obtained by increasing the dissipation rate with relative frequency or decreasing it with relative average wave steepness, or by decreasing the overall level of dissipation.

Part of the computations has also been performed with an operational third generation wave prediction model, viz. the WAM model. Quantitatively the WAM results are in general agreement with the EXACT-NL results, except that the WAM results do not scale with the wind speed. Qualitatively the WAM spectra and source functions are broader than those obtained with the EXACT-NL model. It is suggested that this difference is due to the more limited treatment of the nonlinear transfer in the WAM model than in the EXACT-NL model.

In the empirical part of this study directional wave measurements have been carried out with two WAVEC pitch-and-roll buoys located in the central North Sea. Based on these measurements time series were obtained of integral mean wave parameters, viz. the total wave energy, peak frequency, the direction width and the mean wave direction. At the same time wind speed and wind direction were observed at nearby offshore platforms.

To isolate local effects on the change of mean wave direction, the effect of inhomogeneities in the wave field on the rate of change of

the mean wave direction was estimated with the results of an operational numerical wave hindcast model, viz. the WINCH model.

A number of selection criteria has been applied to analyse only those measurements corresponding to actively wind driven seas in deep water. In addition it was required that the mean wave direction turns towards the wind direction. Application of these selection criteria resulted in 133 time scale estimates. These estimates have been further analysed with the results of an error analysis to quantify the error in each estimate. It has been shown that the initially large scatter in these time scale estimates can be reduced considerably by imposing stricter restrictions on the maximum allowable relative error. This also revealed a trend of increasing time scale with increasing growth stage of the waves.

Comparison of the present results from the computations with those from the observations shows that the trend of time scale with growth stage is stronger for the model results than the one for the observational results. In addition the model time scales are generally much level than the empirical ones, except for young sea states, where they tend to overlap.

Comparison of the present results with previously published results shows that the trend of the observed time scale with growth stage is in agreement with the results of Günther et al. (1981) and Holthuijsen et al. (1987), but at a much lower level. The model time scales agree reasonably well in order of magnitude with the results of Günther et al. (1981), Holthuijsen et al. (1987) and Young et al. (1987), although the trend in the model time scales with growth stage is much higher than those in the models of Günther et al. (1981) and Holthuijsen et al. (1987). The rapid increase of model time scales for nearly fully developed waves agrees with the theoretical model of Holthuijsen et al. (1987).

A re-analysis of time series of mean wave direction, published by

Hasselmann et al. (1980) and Allender et al. (1983), has shown that the reported difference in order of magnitude of these time scales with time scale models of Günther et al. (1981) and Holthuijsen et al. (1987) vanishes. It is suggested that the reported difference is largely due to the method of analysis.

This study has shown that in general model time scales estimates are higher than time scales obtained from measurements in the open ocean. This difference is attributed to an inadequate parameterization of the directional response, but also to an inadequate swell-sea splitter, as used in the present study to obtain time scale estimates in actively wind-driven seas.

LIST OF SYMBOLS

a_n	amplitude of sinusoidal wave component
A	normalization coefficient of directional energy distribution, linear growth term
$a_{..}$	Fourier coefficient of directional distribution function
b	relaxation coefficient
B	exponential growth term
$b_{..}$	Fourier coefficient of directional distribution function
c	phase speed
C	proportionality factor of dissipation source function, proportionality factor in discrete interaction approximation
C( )	covariance function of sea surface elevation
C_d	drag coefficient
c_g	group velocity
$\underline{c}_g$	group velocity vector
C_{xx}	auto-spectrum of pitch signal
C_{xy}	co-spectrum of pitch- and roll signals
C_{yy}	auto-spectrum of roll signal
C_{zz}	auto-spectrum of heave signal
d	water depth
D	interaction coefficient of nonlinear transfer
D( )	directional energy distribution
E( )	energy density
E_J( )	energy density spectrum of JONSWAP type
E_L( )	locally induced energy density spectrum
E_M( )	model energy density spectrum
E_{PM}	energy density spectrum of Pierson-Moskowitz type
E_{tot}	total wave energy
$E_{tot,M}$	total wave energy of wave model
f	frequency
F( )	continuous time signal
F_d	first derivative to time of smoothed discrete time series
F_s	smoothed discrete time series

f_{lim}	limiting frequency used in integration scheme of WAM model
f_{high}	highest model frequency in WAM model
f_m	harmonic mean frequency
f_p	peak frequency
f_{PM}	Pierson-Moskowitz frequency
f^+	upper frequency of interacting wavenumber in discrete interaction approximation
f^-	lower frequency of interacting wavenumber in discrete interaction approximation
g	gravitational acceleration
G	coupling coefficient of nonlinear interactions
G'	coupling coefficient of nonlinear interactions
G( )	smoothed continuous time signal
I_i	one-dimensional integral
J	Jacobian
k	wavenumber ($k = \|\underline{k}\|$ and $k = 2\pi/L$)
$\underline{k}$	wavenumber vector
k_x	x-component of wavenumber vector
k_y	y-component of wavenumber vector
k_0	peak wavenumber
$\underline{k}_0$	peak wavenumber vector
L	wave length
$\underline{L}$	local wavenumber vector
L_p	wave length associated with peak frequency
m	exponent in dissipation source function
m_E	frequency averaged centered Fourier coefficient
$m_{1,f}$	centered Fourier coefficient per frequency
n	exponent in dissipation source function
N( )	action density spectrum
P_j	shape factor of Gaussian surface
Q_j	shape factor of Gaussian surface
Q_{zx}	quad-spectrum of heave- and pitch signal
Q_{zy}	quad-spectrum of heave- and roll signal
$\underline{r}$	displacement vector
R_j	shape factor of Gaussian surface

s	exponent in directional distribution function
$S( )$	source function
S_{in}	wind input source function
S_{dis}	dissipation source function
S_{nl}	nonlinear transfer source function
t	time
t'	integration variable
T	Jacobian used in appendix A
$\underline{T}$	transport vector of wave energy
$T( )$	transport term in energy balance equation
t_m	time at which wave model output is available
U_z	wind speed at height z above mean sea level
u_*	air friction velocity at sea surface
U_j	shape factor of Gaussian surface
$\underline{v}$	current velocity vector
V_j	shape factor of Gaussian surface
w_i	weights for discrete convolution
w_i'	weights for discrete convolution of first time derivative
$W( )$	window function in convolution filter
x	x-coordinate
y	y-coordinate
$\underline{x}$	location vector
$\underline{x}_b$	location vector of buoy location
z	z-coordinate, positive upwards
z_0	roughness length

α	energy scale parameter of energy density spectrum, constant in error analysis
$\hat{\alpha}$	average wave steepness
$\hat{\alpha}_{PM}$	average wave steepness of Pierson-Moskowitz spectrum
β	energy scale parameter of Toba frequency spectrum, scale factor in wind input source term
γ	peak enhancement factor of JONSWAP frequency spectrum
$\Gamma(\ )$	gamma function
$\delta(\ )$	delta function
Δt	time interval
Δt_m	time step of wave model
Δx	grid spacing in x-direction
Δy	grid spacing in y-direction
$\Delta\theta$	directional resolution, angular difference
$\Delta\theta_0$	change of mean wave direction
$\Delta\phi$	angular difference
ε	spectral width of action density spectrum, dimensionless total wave energy, normalized with U_{10}
ε_*	dimensionless total wave energy, normalized with u_*
φ	phase of sinusoidal wave component
$\Phi(\ )$	theoretical function, used in error analysis
$\eta(\ )$	surface elevation
θ	direction
$\tilde{\theta}$	smoothed estimate of mean wave direction
$\tilde{\theta}'$	smoothed estimate of first derivative of mean wave direction
θ_{ds}	mean direction of dissipation source function
θ_{in}	mean direction of wind input source function
θ_{nl}	mean direction of nonlinear transfer source function
θ_s	mean direction of total source function
θ_w	wind direction
$\theta_{w,s}$	magnitude of wind shift
θ_0	frequency integrated mean wave direction
$\theta_{0,f}$	mean wave direction per frequency
$\theta_{0,L}$	locally induced integral mean wave direction

κ	von Karman constant
λ	x-component of local wavenumber,
	factor in discrete interaction approximation
λ_x	parameter specifying buoy location in model grid
λ_y	parameter specifying buoy location in model grid
ν	dimensionless peak frequency, normalized with U_{10}
ν_*	dimensionless peak frequency, normalized with u_*
σ	frequency averaged directional spread
σ_a	shape parameter of JONSWAP frequency spectrum
σ_b	shape parameter of JONSWAP frequency spectrum
σ_f	directional spread per frequency
$\sigma^2_{..}$	mean square error of parameter <..>
τ	surface stress
	time lag
	time scale of directional response
$\tilde{\tau}$	dimensionless time scale, normalized with U_{10}
τ_*	dimensionless time scale, normalized with u_*
$\Psi(\ )$	dimensionless shape function of two-dimensional spectrum
ψ_d	dissipation coefficient
ρ_a	density of air
ρ_w	density of water
μ	y-component of local wave number
χ	relaxation coefficient in model of Günther et al. (1981)
ω	radian frequency
$\bar{\omega}$	mean radian frequency
Ω	angular velocity
Ω_{nl}	dimensionless shape function of two-dimensional nonlinear
	transfer
ξ_i	independent variable
∂	partial differentiation operator
∇	second order partial differential operator

REFERENCES

Allender, J.H., J. Albrecht and G. Hamilton, 1983: Observations of directional relaxation of wind sea spectra. *J. Phys. Oceanogr.*, **13**, No. 8, 1519-1525.

Allender, J.H., T.P. Barnett and M. Lybanon, 1985: The DNS model: An improved spectral model for ocean wave prediction. *Ocean Wave Modeling*, The SWAMP group, Plenum Press.

Barnett, T.P., 1968: On the generation, dissipation and prediction of ocean wind waves. *J. Geophys. Res.*, **73**, No. 2, 513-529.

Battjes, J.A., T.J. Zitman and L.H. Holthuijsen, 1987: A reanalysis of the spectra observed in JONSWAP. *J. Phys. Oceanogr.*, **17**, No. 8, 1288-1295.

Borgman, L.E., 1969: Directional spectra models for design use. *Offshore Technology Conf.*, Houston, Amer. Inst. Mining, Metallurg., Petrol Eng. and others, paper 1069, 721-746.

Bouws, E. and G.J. Komen, 1983: On the balance between growth and dissipation in an extreme depth-limited wind-sea in the southern North Sea. *J. Phys. Oceanogr.*, **13**, No. 9, 1653-1658.

Brown, R.A. and W.T. Liu, 1982: An operational large-scale marine planetary boundary layer model, *J. Appl. Meteor.*, **21**, No. 3, 261-269.

Charnock, H., 1955: Wind stress on a water surface. *Quart. J. Roy. Meteor. Soc.*, **81**, 639-640.

Dobson, F.W., 1983: Review of reference height for and averaging time of surface wind measurements at sea. *WMO Marine Meteorology Rep. No. 3.*

Donelan, M.A., J. Hamilton and W.H. Hui, 1985: Directional spectra of wind-generated waves. *Phil. Trans. Roy. Soc. London*, **A 315**, 509-562.

Dungey, J.C. and W.H. Hui, 1979: Nonlinear energy transfer in a narrow gravity-wave spectrum. *Proc. Roy. Soc. London*, **A 368**, 239-265.

Eide, L.I., M. Reistad and J. Guddal, 1986: A comparison of hindcast studies with a) a coupled discrete wave model and b) a coupled hybrid wave model. *Proc. Int. Workshop on Wave Hindcasting and Forecasting*, Halifax, Nova Scotia, Sept. 23-26. Environmental Studies Revolving Funds, Report Series No. 065. Ottawa, 153-159.

Ewing, J.A., 1971: A numerical wave prediction method for the North Atlantic Ocean. *Dtsch. Hydrogr. Z.*, **24**, 241-261.

Forristall, G.Z., 1981: Measurements of a saturated range in ocean wave spectra, *J. Geophys. Res.*, **86**, No. C9, 8075-8084.

Fox, M.J.H., 1976: On the nonlinear transfer of energy in the peak of a gravity-wave spectrum. II. *Proc. Roy. Soc. London*, **A 348**, 467-483.

Garratt, J.R., 1977: Review of drag coefficients over oceans and continents, *Mon. Weather Rev.*, **105**, No. 7, 915-929.

Gelci, R., J. Cazalé and J. Vassal, 1956: Utilization des diagrammes de propagation à la prévision énergétique de la houle. *Bulletin d'information du comité Central d'océanographie et d'études des côtes*, **8**, No. 4, 169-187.

Greenwood, J.A. and V.J. Cardone, 1977: Development of a global ocean wave propagation algorithm, final report to Navy fleet numerical weather centre, Monterey, CA, Constract N-00228-76-C-3081.

Greenwood, J.A., V.J. Cardone and L.M. Lawson, 1985: Intercomparison test version of the SAIL wave model. *Ocean wave modeling*, The SWAMP group, Plenum Press.

Gumbel, E.J., J.A. Greenwood and D. Durand, 1953: The circular normal distribution: Theory and tables. *American Statistical Assoc. J.*, March, 131-152 (quoted in Borgman, 1969).

Günther, H., W. Rosenthal and M. Dunckel, 1981: The response of surface gravity waves to changing wind direction. *J. Phys. Oceanogr.*, **11**, No. 5, 718-728.

Hasselmann, D.E., M. Dunckel and J.A. Ewing, 1980: Directional wave spectra observed during JONSWAP 1973, *J. Phys. Oceanogr.*, **10**, No. 8, 1264-1280.

Hasselmann, K., 1960: Grundgleichungen der Seegangsvoraussage, *Schiffstechnik*, **7**, No. 39, 191-195.

Hasselmann, K., 1962: On the non-linear energy transfer in a gravity-wave spectrum, Part 1. General theory. *J. Fluid Mech.*, **12**, 481-500.

Hasselmann, K., 1963a: On the non-linear energy transfer in a gravity wave spectrum, Part 2. Conservation theorems; wave-particle analogy; irreversibility. *J. Fluid Mech.*, **15**, 273-281.

Hasselmann, K., 1963b: On the non-linear energy transfer in a gravity-wave spectrum, Part 3. Evaluation of energy flux and swell-sea interaction for a Neumann spectrum. *J. Fluid Mech.*, **15**, No. 385-398.

Hasselmann, K., 1974: On the spectral dissipation of ocean waves due to white capping. *Bound.-Layer Meteor.*, **6**, 107-127. Hasselmann, K., T.P. Barnett, E. Bouws, H. Carlson, D.E. Cartwright, K. Enke, J.A. Ewing, H. Gienapp, D.E. Hasselmann, P. Kruseman, A. Meerburg, P. Müller, D.J. Olbers, K. Richter, W. Sell and H. Walden, 1973: Measurements of wind-wave growth and swell decay during the Joint North Sea Wave Project (JONSWAP). *Dtsch. Hydrogr. Z.*, Ergänzungsheft Reihe Reihe A (8°), Nr. 12.

Hasselmann, K., D.B. Ross, P. Müller and W. Sell, 1976: A parametric wave prediction model. *J. Phys. Oceanogr.*, **6**, No. 2, 200-228.

Hasselmann S. and K. Hasselmann, 1981: A symmetrical method of computing the nonlinear transfer in a gravity wave spectrum. *Hamburger. Geophys. Einzelschriften, Reihe A*, Heft 52.

Hasselmann, S. and K. Hasselmann, 1985a: The wave model EXACT-NL. In *Ocean wave modeling*, the SWAMP group, Plenum Press, New York and London.

Hasselmann, S. and K. Hasselmann, 1985b: Computations and parameterizations of the nonlinear energy transfer in a gravity-wave spectrum. Part I: A new method for efficient computations of the exact nonlinear transfer integral. *J. Phys. Oceanogr.*, **15**, No. 11, 1369-1377.

Hasselmann, S., K. Hasselmann, J.H. Allender and T.P. Barnett, 1985c: Computations and parameterizations of the nonlinear energy transfer in a gravity-wave spectrum. Part II: Parameterizations of the nonlinear transfer for application in wave models. *J. Phys. Oceanogr.*, **15**, No. 11, 1378-1391.

Holthuijsen, L.H., 1983: Observations of the directional distribution of ocean-wave energy in fetch-limited conditions. *J. Phys. Oceanogr.*, **13**, No. 2, 191-207.

Holthuijsen, L.H., A.J. Kuik and E. Mosselman, 1987: The response of wave directions to changing wind directions. *J. Phys. Oceanogr.*, **17**, No. 7, 845-853.

Janssen, P.A.E.M., 1989: Wave-induced stress and the drag of air flow over sea waves. *J. Phys. Oceanogr.*, **19**, No. 6, 745-754.

Janssen, P.A.E.M., G.J. Komen and W.J.P. de Voogt, 1984: An operational coupled hybrid wave prediction model. *J. Geophys. Res.* **89**, No. C3, 3635-3654.

Janssen, P.A.E.M., G.J. Komen and W.J.P. de Voogt, 1987: Friction velocity scaling in wind wave generation, *Bound.-Layer Meteor.*, **38**, 29-35.

Jeffreys, H., 1925: On the formation of water waves by wind, II, *Proc. Roy. Soc.*, **A 107**, Vol. 110, 189-206.

Kahma, K.K., 1981: A study of the growth of the wave spectrum with fetch. *J. Phys. Oceanogr.*, **11**, No. 11, 1503-1515.

Kitaigorodskii, S.A., 1983: On the theory of the equilibrium range in the spectrum of wind-generated gravity waves. *J. Phys. Oceanogr.*, **13**, No. 5, 816-827.

KNMI, 1985: Monthly Bulletin North Sea, December 1985: F.B. Koek, C.G. Korevaar and R.A. van Moerkerken, Eds., Publ. No. KNMI-167, Royal Netherlands Meteorological Institute, de Bilt, The Netherlands.

KNMI, 1986: Monthly Bulletin North Sea, January 1986: F.B. Koek, C.G. Korevaar and R.A. van Moerkerken, Eds., Publ. No. KNMI-167, Royal Netherlands Meteorological Institute, de Bilt, The Netherlands.

Komen, G.J., S. Hasselmann and K. Hasselmann, 1984: On the existence of a fully developed wind-sea spectrum, *J. Phys. Oceanogr.*, **14**, No. 8, 1271-1285.

Kuik, A.J., G.Ph. van Vledder and L.H. Holthuijsen, 1988: A method for the routine analysis of pitch-and-roll buoy wave data, *J. Phys. Oceanogr.*, **18**, No. 7, 1020-1034.

Kuik, A.J. and L.H. Holthuijsen, 1981: Buoy observation of directional wave parameters. *Proc. Conf. on Directional Wave Spectra Applications*, R.L. Wiegel, Ed., University of California, Berkeley, 14-16 Sept., 1981, ASCE, New York, 61-70.

Large, W.G. and S. Pond, 1981: Open ocean momentum flux measurements in moderate to strong winds. *J. Phys. Oceanogr.*, **11**, 324-336.

Long, R.B., 1980: The statistical evaluation of directional spectrum estimates derived from pitch/roll buoy data. *J. Phys. Oceanogr.*, **10**, No. 6, 944-952.

Longuet-Higgins, M.S., 1976: On the nonlinear transfer of energy in the peak of a gravity-wave spectrum: A simplified model. *Proc. Roy. Soc.* **A 347**, 311-328.

Longuet-Higgins, M.S., D.E. Cartwright and N.D. Smith, 1963: Observations of the directional spectrum of sea waves using the motions of a floating buoy. *Ocean Wave Spectra*, Prentice-Hall, 111-136.

Maat, N., C. Kraan and W.A. Oost, 1989: The roughness of wind waves. Accepted for publication in *Bound.-Layer Meteor.*

Markus, J.C. and Th. Kapsenberg, 1985: Wavec Local Processing System, Technisch Physische Dienst TNO-TH, Delft, The Netherlands, Rep. No. 416.442.

Mardia, K.V., 1972: *Statistics of directional data*, Academic Press.

Masuda, A., 1980: Nonlinear energy transfer between wind waves. *J. Phys. Oceanogr.*, **10**, No. 12, 2082-2093.

Miles, J.W., 1957: On the generation of surface waves by shear flows, *J. Fluid Mech.*, **3**, No. 2, 185-204.

Miles, J.W., 1959: On the generation of surface waves by shear flows. Part 2. *J. Fluid Mech.*, **6**, No. 4, 568-582.

Mitsuyasu, H., F. Tasai, T. Suhara, S. Mizuno, M. Ohkusu, T. Honda and K. Rikiishi, 1975: Observations of the directional spectrum of ocean waves using a cloverleaf buoy. *J. Phys. Oceanogr.*, **5**, 750-760.

Mitsuyasu, H., F. Tasai, T. Suhara, S. Mizuno, M. Ohkusu, T. Honda and K. Rikiishi, 1980: Observations of the power spectrum of waves using a cloverleaf buoy. *J. Phys. Oceanogr.*, **10**, 286-296.

Mood, A.E., F.A. Graybill and D.C. Boes, 1974: *Introduction to the theory of statistics*, 3rd ed., McGraw-Hill Kogakusha. Ltd.

Phillips, O.M., 1957: On the generation of waves by turbulent wind, *J. Fluid Mech.*, **2**, No. 5, 417-445.

Phillips, O.M., 1958: The equilibrium range in the spectrum of wind-generated ocean waves. *J. Fluid Mech.*, **4**, 426-434.

Phillips, O.M., 1977: *The Dynamics of the Upper Ocean*, 2nd ed., Cambridge University Press.

Phillips, O.M., 1985: Spectral and statistical properties of the equilibrium range in wind-generated gravity waves. *J. Fluid Mech.*, **156**, 505-531.

Pierson, W.J., G. Neumann and R.W. James, 1955: Practical methods for observing and forecasting ocean waves by means of wave spectra and statistics. H.O. Pub. No. 603, *U.S. Navy Hydrographic Office*, Washington, D.C.

Pierson, W.J. and L. Moskowitz, 1964: A proposed spectral form for fully developed wind seas based on the similarity theory of S. A. Kitaigorodskii, *J. Geophys. Res.*, **69**, (24), 5181-5190.

Riissanen, J., 1975: Some features of wind variation in the friction layer at Helsinki airport. *Finnish Met. Inst. Contr.*, **80**.

Rye, H., R.C. Byrd and A. Tørum, 1974: Sharply peaked wave energy spectra in the North Sea, Proc. Offshore Technology Conference, Houston, *Offshore Technology Conf.*, Houston, Amer. Inst. Mining, Metallurg., Petrol Eng. and others, OTC 2107, 739-747.

Sell, W. and K. Hasselmann, 1972: Computations of nonlinear energy transfer for JONSWAP and empirical wind-wave spectra. *Rep. Inst. Geophys.*, Univ. Hamburg.

Sobey, R.J., 1986: Wind-wave prediction, *Ann. Rev. Fluid Mech.*, **18**, 149-172.

Snyder, R.L., F.W. Dobson, J.A. Elliott and R.B. Long, 1981: Array measurements of atmospheric pressure fluctuations above surface gravity waves. *J. Fluid Mech.*, **102**, 1-59.

Sverdrup, H.U. and W.H. Munk, 1946: Empirical and theoretical relations between wind, sea, and swell, *Trans. Am. Geoph. Union*, **27**, No. 6, 823-827.

SWAMP group, 1985: Ocean wave modelling, *Plenum Press*, New York and London.

Toba, Y., 1972: Local balance in the air-sea boundary processes. I: On the growth process of wind waves. *J. Oceanogr. Soc. Japan*, **28**, No. 3, 109-120.

Toba, Y., 1973: Local balance in the air-sea boundary processes. III. On the spectrum of wind waves. *J. Oceanogr. Soc. Japan*, **29**, 209-220.

Van der Vlugt, A.J.M., 1984: Experiences with the WAVEC-buoy. *Proc. Symp. on Description and Modelling of Directional Seas*, June 18-20, 1984, Technical University, Denmark, Danish Hydraulic Institute and Danish Maritime Institute, paper A3.

Van der Vlugt, A.J.M., A.J. Kuik and L.H. Holthuijsen, 1981: The WAVEC directional buoy under development. *Proc. Conf. on Directional Wave Spectra Applications*, Wiegel, Ed., University of California, Berkeley, 14-16 Sept., 1981, ASCE, New York, 50-59.

Van Vledder, G.Ph., 1984: Computation of the nonlinear energy transfer in a narrow gravity wave spectrum with a method derived by Dungey and Hui, *Internal Rep.* No. 13-84, Delft Univ. of Technology, Dep. Civil Eng., Fluid Mech. Group.

Van Vledder, G.Ph. and S.L. Weber, 1988: Guide for the program EXACT-NL, *Max-Planck-Institut für Meteorologie*, Hamburg, Report No. 20.

Vermeulen, P.E.J., B. Oemraw and J. Wieringa, 1985: Wind tunnel measurements of the flow distortion near the anemometer positions on PENNZOIL K-13A platform, Netherlands Organization for Applied and Scientific Research, Fluid Dynamics Department, Apeldoorn, the Netherlands, Rep. No. 85-01246.

WAMDI group, 1988: The WAM model - A third generation ocean wave prediction model. *J. Phys. Oceanogr.*, **18**, No. 12, 1775-1810.

Webb, D. J., 1978: Non-linear transfers between sea waves. *Deep-Sea Res.*, **25**, 279-298.

Weber, S.L., 1987: The energy balance of finite depth gravity waves. *J. Geophys. Res.*, **93**, No. C4, 3601-3607.

Wu, J., 1982: Wind-stress coefficients over sea surface from breeze to hurricane, *J. Geophys. Res.*, **87**, No. C12, 9704-9706.

Young, I.R., S. Hasselmann and K. Hasselmann, 1985: Calculation of the nonlinear wave-wave interactions in cross seas. *Hamburger. Geophys. Einzelschriften, Reihe A*, Heft 74.

Young, I.R., S. Hasselmann and K. Hasselmann, 1987: Computations of the response of a wave spectrum to a sudden change in wind direction. *J. Phys. Oceanogr.*, **17**, No. 9, 1317-1338.

ACKNOWLEDGEMENTS

This study was funded by the Technology Foundation (STW) in the Netherlands. It was carried out in the Fluid Mechanics Group of the Faculty of Civil Engineering of Delft University of Technology.

I am very grateful to Professor J.A. Battjes for his guidance and his critical comments. I am also indebted to dr. L.H. Holthuijsen for his cooperation. I also thank other members of the Fluid Mechanics group for their help at many occasions, in particular I wish to thank S.H. de Boer, dr. H.L. Tolman and dr. N. Booij.

I gratefully acknowledge the use of the EXACT-NL and WAM routines, which were made available by Prof. K. Hasselmann and S. Hasselmann of the Max-Planck-Institut für Meteorologie, Hamburg, West Germany. Computations with the EXACT-NL model were performed at the European Centre for Medium-Range Weather Forecasts, Reading, England, with the help of the Royal Netherlands Meteorology Institute (KNMI, de Bilt). I wish to thank dr. G.J. Komen, dr. P.A.E.M. Janssen and dr. S.L. Weber for their help in these computations.

I am also indebted to dr. I.R. Young of the Australian Defense Force Academy, Canberra, Australia, for his help in the EXACT-NL computations.

The wind and wave measurements were made available by the Ministry of Transport and Public Works in the Netherlands. The help in this of A.J.M. van der Vlugt, H.C. Peters and A.P. Roskam is greatly appreciated. In addition I want to thank A.J. Kuik for his cooperation in writing the paper about the WAVEC data analysis (Kuik et al., 1989).

The numerical hindcasts have been performed at the Norwegian Meteorological Institute (DNMI), Oslo, Norway, and were made possible by Prof. J. Guddal. In these computations invaluable help was obtained

from M. Reistad. The help from dr. V.J. Cardone and dr. J.A. Greenwood of Oceanweather Inc., Cos Cob, USA, in describing the WINCH model is very much appreciated.

The wind fields used as input for the WINCH model were supplied by the British Meteorological Office, Bracknell. The help of dr. J.J. Ephraims, dr. P. Francis and C. Bracher in this is gratefully acknowledged.

This thesis was finished while I was employed at Delft Hydraulics. The support of my colleagues and the facilities offered to me are greatly appreciated.

Many more people supported me while I was preparing this thesis. Special thanks are for Cees Boerman and Hans Out.

Finally, my greatest appreciation is for Annelies Boerman for her patience and support during the preparation of this thesis.

LIST OF APPENDICES

APPENDIX A

FOURIER ANALYSIS OF PITCH-AND-ROLL BUOY WAVE DATA

A pitch-and-roll buoy measures the vertical elevation and the two slope components of the buoy as a function of time. By applying standard cross-spectral analysis to these signals, resulting in 9 auto-, co- and quad- spectral density functions, the first four Fourier coefficients of the directional distribution function per frequency can be estimated directly (Longuet-Higgins et al., 1963):

$$a_1(f) = \int_0^{2\pi} \cos(\theta)\, D_f(\theta)\, d\theta = \frac{Q_{zx}(f)}{k(f)\, C_{zz}(f)} \qquad (A1)$$

$$b_1(f) = \int_0^{2\pi} \sin(\theta)\, D_f(\theta)\, d\theta = \frac{Q_{zy}(f)}{k(f)\, C_{zz}(f)} \qquad (A2)$$

$$a_2(f) = \int_0^{2\pi} \cos(2\theta)\, D_f(\theta)\, d\theta = \frac{C_{xx}(f) - C_{yy}(f)}{k(f)^2\, C_{zz}(f)} \qquad (A3)$$

$$b_2(f) = \int_0^{2\pi} \sin(2\theta)\, D_f(\theta)\, d\theta = \frac{2C_{xy}(f)}{k(f)^2\, C_{zz}(f)} \qquad (A4)$$

in which C represents the auto- and co-spectra and Q the quad-spectra respectively with x and y indicating the two orthogonal components of the buoy slope and z indicating the heave. The wavenumber k, defined

as 2π divided by the wave length of a harmonic wave travelling in (x,y)-space, can be determined in two ways. It can be obtained with the dispersion relation of the linear wave theory or it can also be estimated from the auto-spectra by:

$$k(f) = \left(\frac{C_{xx}(f) + C_{yy}(f)}{C_{zz}(f)} \right)^{1/2} . \qquad (A5)$$

The latter method is implemented in the routine analysis of the WAVEC pitch-and-roll buoy wave data as used in this study.

APPENDIX B

INTERACTION COEFFICIENT OF NONLINEAR TRANSFER FOR DEEP WATER

The interaction coefficient for a quadruplet of resonantly interacting surface gravity waves for arbitrary water depth is given by Hasselmann (1962). For deep water this expression is simplified by Webb (1978). However, the expression given by Webb (1978) contains some apparent misprints, which are corrected by Dungey and Hui (1979). In the notation of Webb (1978) and Dungey and Hui (1979) the interaction coefficient is a factor 3 larger than the interaction coefficient for deep water of Hasselmann (1962). However, this difference is counterbalanced by a factor 3 in Hasselmann's representation of the Boltzmann integral. In the following expression for the interaction coefficient D the corrected notation of Webb (1978) is used.

$$D(\underline{k}_1,\underline{k}_2,\underline{k}_3,\underline{k}_4) = \frac{2(\omega_1+\omega_2)^2(k_1k_2-\underline{k}_1\cdot\underline{k}_2)(k_3k_4-\underline{k}_3\cdot\underline{k}_4)}{\omega^2_{1+2} - (\omega_1+\omega_2)^2}$$

$$+ \frac{2(\omega_1-\omega_3)^2(k_1k_3+\underline{k}_1\cdot\underline{k}_3)(k_2k_4+\underline{k}_2\cdot\underline{k}_4)}{\omega^2_{1-3} - (\omega_1-\omega_3)^2}$$

$$+ \frac{2(\omega_1-\omega_4)^2(k_1k_4+\underline{k}_1\cdot\underline{k}_4)(k_2k_3+\underline{k}_2\cdot\underline{k}_3)}{\omega^2_{1-4} - (\omega_1-\omega_4)^2}$$

$$+ \tfrac{1}{2}(\underline{k}_1\cdot\underline{k}_2\underline{k}_3\cdot\underline{k}_4 + \underline{k}_1\cdot\underline{k}_3\underline{k}_2\cdot\underline{k}_4 + \underline{k}_1\cdot\underline{k}_4\underline{k}_2\cdot\underline{k}_3)$$

$$- \tfrac{1}{4} g^{-2}(\underline{k}_1\cdot\underline{k}_2 + \underline{k}_3\cdot\underline{k}_4)\ (\omega_1+\omega_2)^4$$

$$+ \tfrac{1}{4} g^{-2}\ (\underline{k}_1\cdot\underline{k}_3 + \underline{k}_2\cdot\underline{k}_4)\ (\omega_1-\omega_3)^4$$

$$+ \tfrac{1}{4} g^{-2}\ (\underline{k}_1\cdot\underline{k}_4 + \underline{k}_2\cdot\underline{k}_3)\ (\omega_1-\omega_4)^2 + \tfrac{5}{2} k_1k_2k_3k_4$$

$$+ g^{-3}(\omega_1+\omega_2)^2\ (\omega_1-\omega_3)^2\ (\omega_1-\omega_4)^2\ (k_1 + k_2 + k_3 + k_4)$$

in which $k_i = |\underline{k}_i|$, $\omega_i = (g\ k_i)^{1/2}$; $i = 1,2,3,4$

$$\omega_{1+2} = (g\ |\underline{k}_1+\underline{k}_2|)^{1/2}$$

$$\omega_{1-3} = (g\ |\underline{k}_1-\underline{k}_3|)^{1/2}$$

$$\omega_{1-4} = (g\ |\underline{k}_1-\underline{k}_4|)^{1/2}.$$

The interaction coefficient D is invariant under interchanges of $\underline{k}_1$ with $\underline{k}_2$ or of $\underline{k}_3$ with $\underline{k}_4$, or of both $\underline{k}_1$ and $\underline{k}_2$ with $\underline{k}_3$ and $\underline{k}_4$.

APPENDIX C

DERIVATION OF SOURCE FUNCTION FOR MEAN WAVE DIRECTION

The derivation of the source function for the mean wave direction is after Holthuijsen et al. (1987). For clarity in the following the following two operators are defined:

$$\langle .. \rangle_c = \int_0^{2\pi} \int_0^{\infty} \cos(\theta) .. df \, d\theta \tag{C1}$$

and

$$\langle .. \rangle_s = \int_0^{2\pi} \int_0^{\infty} \sin(\theta) .. df \, d\theta. \tag{C2}$$

The mean wave direction is defined as:

$$\theta_0 = \arctan(b_1/a_1) \tag{C3}$$

with

$$a_1 = \langle E(f,\theta) \rangle_c \tag{C4}$$

$$b_1 = \langle E(f,\theta) \rangle_s . \tag{C5}$$

The source function for the mean wave direction θ_0 is obtained by differentiation of Eq. (C3) with respect to time. Upon applying the chain rule for differentiation it follows that:

$$\frac{\partial \theta_0}{\partial t} = \frac{\frac{\partial}{\partial t} \langle E(f,\theta) \rangle_s - \tan(\theta_0) \frac{\partial}{\partial t} \langle E(f,\theta) \rangle_c}{\left(1 + \tan^2(\theta_0) \right) \langle E(f,\theta) \rangle_c} . \tag{C6}$$

For a homogeneous wave field the energy balance equation is reduced to:

$$\frac{\partial E(f,\theta)}{\partial t} = S(f,\theta) \tag{C7}$$

so that Eq. (C6) can be written as:

$$\frac{\partial \theta_0}{\partial t} = \frac{\langle S(f,\theta)\rangle_s - \tan(\theta_0)\,\langle S(f,\theta)\rangle_c}{\left(1 + \tan^2(\theta_0)\right)\,\langle E(f,\theta)\rangle_c} \,. \tag{C8}$$

If the mean direction θ_s of the source function $S(f,\theta)$ is defined similar to θ_0, i.e. by replacing $E(f,\theta)$ by $S(f,\theta)$ in (C3) then Eq. (C8) can be written as:

$$\frac{\partial \theta_0}{\partial t} = \frac{\left(\tan(\theta_s) - \tan(\theta_0)\right)\,\langle S(f,\theta)\rangle_c}{\left(1 + \tan^2(\theta_0)\right)\,\langle E(f,\theta)\rangle_c} \,. \tag{C9}$$

Since

$$\frac{\left(\tan(\theta_s) - \tan(\theta_0)\right)}{\left(1 + \tan^2(\theta_0)\right)} = \frac{\cos(\theta_0)}{\cos(\theta_s)}\,\sin(\theta_s - \theta_0) \tag{C10}$$

Eq. (C9) can be written as:

$$\frac{\partial \theta_0}{\partial t} = \frac{\cos(\theta_0)\,\langle S(f,\theta)\rangle_c}{\cos(\theta_s)\,\langle E(f,\theta)\rangle_c}\,\sin(\theta_s - \theta_0) \tag{C11}$$

or in full form:

$$\frac{\partial \theta_0}{\partial t} = \frac{\cos(\theta_0)\displaystyle\int_0^{2\pi}\int_0^{\infty} \cos(\theta) S(f,\theta)\,df\,d\theta}{\cos(\theta_s)\displaystyle\int_0^{2\pi}\int_0^{\infty} \cos(\theta) E(f,\theta)\,df\,d\theta}\,\sin(\theta_s - \theta_0). \tag{C12}$$

APPENDIX D

SCALING LAW FOR NONLINEAR TRANSFER OF SIMILAR SPECTRA

Introduction

In this appendix a scaling law is derived relating the nonlinear transfer of similar spectra. The nonlinear transfer is described by the Boltzmann integral expression of Hasselmann (1962, 1963a). The derivation of the scaling law is performed in two steps. In the first step the delta functions in the Boltzmann integral are removed and dimensionless variables are introduced. In the second step a general shape function is introduced describing the energy spectrum. The scaling law will be given in terms of the peak frequency f_p and the energy scale parameter α. Three examples are given illustrating in what ways this scaling law can be used to obtain a relation between the nonlinear transfer of two similar spectra.

Derivation of scaling law

The Boltzmann integral (Eq. 2.46) is rewritten in terms of the rate of change of the energy density in $\underline{k}$-space:

$$S_{nl}(\underline{k}_4) = \frac{\partial E(\underline{k}_4)}{\partial t} =$$

$$\iiint d\underline{k}_1 d\underline{k}_2 d\underline{k}_3 \; G' \omega_4 \; \delta(\underline{k}_1+\underline{k}_2-\underline{k}_3-\underline{k}_4) \; \delta(\omega_1+\omega_2-\omega_3-\omega_4)$$

$$\times \left[\omega_4 E_1 E_2 E_3 + \omega_3 E_1 E_2 E_4 - \omega_2 E_1 E_3 E_4 - \omega_1 E_2 E_3 E_4\right] \qquad (D1)$$

with

$$G' = \pi \left(\frac{g\, D}{2\rho_w \omega_1 \omega_2 \omega_3 \omega_4} \right)^2$$

in which $k_i = |\underline{k}_i|$, $\omega_i = (gk_i)^{1/2}$, ρ_w is the density of water and D is the interaction coefficient, which is a complicated function of the four interacting wavenumbers (see appendix B). $E_i = E(\underline{k}_i)$ is the energy density at wavenumber $\underline{k}_i$. The delta functions in Eq. (D1) reflect the resonance conditions of the nonlinear transfer.

The first delta function in Eq. (D1) is readily removed by integrating Eq. (D1) with respect to $\underline{k}_2$. In order to remove the remaining delta function in Eq. (D1) the variables $\underline{k}_i$ are transformed to the variables ω_i and θ_i by:

$$\left.\begin{aligned} \omega_i &= (g\ k_i)^{1/2} \\ \theta_i &= \arctan(k_y/k_x) \end{aligned}\right\} \qquad \text{(D2)}$$

The Jacobian J of this transformation is given by:

$$J = \frac{\partial(\underline{k}_i)}{\partial(\omega_i,\theta_i)} = 2\ \omega_i^{\ 3}/g^2. \qquad \text{(D3)}$$

The remaining delta function in Eq. (D1) is removed by integrating Eq. (D1) with respect to ω_2. The Boltzmann integral (D1) can now be written as:

$$S_{nl}(\underline{k}_4) = \iiint d\theta_1 d\omega_3 d\theta_3 \omega_1^{\ 3}\omega_3^{\ 3}\omega_4\ G\ T$$

$$\times \left[\omega_4 E_1 E_2 E_3 + \omega_3 E_1 E_2 E_4 - \omega_2 E_1 E_3 E_4 - \omega_1 E_2 E_3 E_4\right] \qquad \text{(D4)}$$

in which the term T is computed as:

$$T = \int \delta(\omega_1 + \omega_2(\omega_1;\omega_3,\omega_4))\ d\omega_2$$

$$= \left[1 + d\omega_2/d\omega_1\right]^{-1}. \qquad \text{(D5)}$$

Consider an energy spectrum $E(f,\theta)$ that can be written in the form

$$E(f,\theta) = \alpha\, f_p^{-n}\, \Psi(\xi,\theta) \qquad \text{(D6)}$$

with n arbitrary, $\xi = f/f_p$, α is an energy scale parameter of the spectrum and where f_p is the peak frequency of the spectrum. $\Psi(\xi,\theta)$ is a function determining the spectral shape that only depends on the dimensionless variables ξ and θ. In order to obtain a scaling law for the nonlinear transfer functions of the spectra that are given as a function of frequency f and direction θ, the energy densities $E_i(\underline{k})$ in Eq. (D4) are transformed to energy densities in f-θ space using the transformation $\underline{k} \longrightarrow (f,\theta)$. Using the Jacobian (D3) and the equality $\omega = 2\pi f$ it is found that:

$$E(\underline{k}_i) = E(f_i,\theta_i)\, \frac{g^2}{2\, f^3 (2\pi)^3} \,. \qquad \text{(D7)}$$

Finally, the dimensionless variables $\xi_i = f_i/f_p$ are introduced to scale Eq. (D4). All quantities on the right hand side of Eq. (D4) are written as a function of the dimensionless variables ξ_i and θ_i. Since the interaction coefficient D (Appendix B) is proportional to $g^{-4}f^8$, the coupling coefficient G in Eq. (D1) scales with $g^{-4}f_p^{\ 8}$. The basic scaling law for the nonlinear transfer of similar spectra then becomes:

$$S_{nl}(f,\theta) = \alpha^3\, g^{-4}\, f_p^{\ 11-3n}\, \Omega_{nl}(\xi,\theta) \qquad \text{(D8)}$$

in which Ω_{nl} is a shape function for the nonlinear transfer that depends only on the dimensionless variables ξ and θ via the spectral shape function $\Psi(\xi,\theta)$.

Example 1

For two spectra that have the same shape function $\Psi(\xi,\theta)$ but different scale parameters α and f_p a simple relation between the corresponding nonlinear transfers can be derived as follows. Suppose that the two spectra are given by:

$$E^{(1)}(f,\theta) = \alpha_1 f_{p1}^{-n} \Psi(\xi,\theta) \tag{D9}$$

and

$$E^{(2)}(f,\theta) = \alpha_2 f_{p2}^{-n} \Psi(\xi,\theta). \tag{D10}$$

The corresponding nonlinear transfers can then be written as:

$$S_{nl}^{(1)}(f,\theta) = \alpha_1^3 f_{p1}^{11-3n} \Omega_{nl}(\xi,\theta) \quad \xi = f/f_{p1} \tag{D11}$$

and

$$S_{nl}^{(2)}(f,\theta) = \alpha_2^3 f_{p2}^{11-3n} \Omega_{nl}(\xi,\theta) \quad \xi = f/f_{p2}. \tag{D12}$$

Elimination of Ω_{nl} then yields:

$$S_{nl}^{(2)}(f/f_{p1},\theta) = S_{nl}^{(1)}(f/f_{p2},\theta)(\alpha_2/\alpha_1)^3 (f_{p2}/f_{p1})^{11-3n}. \tag{D13}$$

Example 2

Consider a reference spectrum denoted by $E^{(1)}(f,\theta)$, with scale parameters α_1 and f_{p1}, and an arbitrary spectrum denoted by $E^{(2)}(f,\theta)$, with scale parameters α_2 and f_{p2}. To use the results of the computation of the nonlinear transfer of the reference spectrum, the arbitrary spectrum is transformed along the frequency axis, such that its peak frequency becomes equal to the peak frequency of the reference spectrum. Denoting the transformed spectrum with $E^T(f,\theta)$ it is found that:

$$E^T(f,\theta) = E^{(2)}\left(f\ (f_{p2}/f_{p1}),\theta \right). \qquad (D14)$$

The result of this transformation is that the arbitrary spectrum is projected on the region of the wavenumber space that is occupied by the reference spectrum. Since no Jacobian is used in Eq. (D14) energy is not conserved.

The transformed arbitrary spectrum is now given by:

$$E^T(f,\theta) = \alpha^T f_{p1}^{-n}\ \Psi(f/f_{p1},\theta). \qquad (D15)$$

This spectrum is considered as the reference spectrum but with an unknown energy scale parameter α^T. The value of α^T in Eq. (D15) is computed by noting that the spectral density of the transformed spectrum at frequency f_{p1} is equal to that of the original arbitrary spectrum at frequency f_{p2}. For the value of α^T it then follows:

$$\alpha^T = \alpha_2\ (f_{p2}/f_{p1})^{-n}. \qquad (D16)$$

Substitution of Eq. (D16) into the scaling relation (D13) and replacing α_1 by α^T gives:

$$S_{n1}^{(2)}(f/f_{p1},\theta) = S_{n1}^{(1)}(f/f_{p2},\theta)\ (f_{p2}/f_{p1})^{11}. \qquad (D17)$$

Example 3

In the program EXACT-NL the transformation of the arbitrary spectrum along the frequency axis is not performed in terms of energy densities $E(f,\theta)$ as in example 2, but in terms of action densities in $\underline{k}$-space. The action density spectrum in $\underline{k}$-space is related to the two-dimensional spectrum in f-θ space by:

$$N(\underline{k}) = \frac{E(\underline{k})}{\omega} = \frac{1}{2} g^2 (2\pi)^{-4} f^{-4} E(f,\theta). \tag{D18}$$

The action densities of the transformed and original action density spectra are given by respectively:

$$N^{(1)}(\underline{k}) = \alpha^T f_{p1}^{n-4} \Psi(\xi,\theta) \tag{D19}$$

$$N^{(2)}(\underline{k}) = \alpha_2 f_{p2}^{n-4} \Psi(\xi,\theta). \tag{D20}$$

The value of α^T is solved from Eqs. (D19) and (D20) by noting that the action densities of $N^{(1)}$ and $N^{(2)}$ are equal for all wavenumbers relative to the peak wavenumbers. The result for α^T is:

$$\alpha^T = \alpha_1 (f_{p2}/f_{p1})^{n+4}. \tag{D21}$$

After substitution of Eq. (D21) in the scaling law (D13) the following relation is obtained:

$$S_{n1}^{(2)}(f/f_{p1},\theta) = S_{n1}^{(1)}(f/f_{p2},\theta) (f_{p2}/f_{p1})^{23}. \tag{D22}$$

From the examples 2 and 3 it follows that the relation between the nonlinear transfer of two similar spectra is independent of the power in the spectral tail, but it only depends on the peak frequencies.

APPENDIX E

COMPUTATION OF THE NONLINEAR TRANSFER WITHIN A GRAVITY WAVE SPECTRUM WITH THE METHOD OF DUNGEY AND HUI

Introduction

This appendix gives a description of the parametric method of Dungey and Hui (1979) to compute the transfer of energy within a gravity wave spectrum due to nonlinear wave-wave interactions. This method was derived for narrow spectra for which the corresponding action density spectrum is approximated by a finite number of Gaussian shaped functions.

This appendix is divided in two parts. In the first part the principal part of the method to compute the nonlinear transfer in an action density spectrum is derived. In the second part a derivation is given of the one-dimensional integrals that are used in the first part, this part can be skipped by readers who are not interested in the details.

Part I: Derivation of method

The rate of change of the action density spectrum $N(\underline{k})$ due to the nonlinear wave-wave interactions is described by the Boltzmann integral (Hasselmann, 1963b):

$$\frac{\partial N_1(\underline{k})}{\partial t} = \int_{-\infty}^{\infty}\int_{-\infty}^{\infty}\int_{-\infty}^{\infty} G(\underline{k}_1,\underline{k}_2,\underline{k}_3,\underline{k}_4)\left[N_3N_4(N_1+N_2)-N_1N_2(N_3+N_4)\right]$$

$$\times\ \delta(\underline{k}_1+\underline{k}_2-\underline{k}_3-\underline{k}_4)\ \delta(\omega_1+\omega_2-\omega_3-\omega_4)\ d\underline{k}_1\ d\underline{k}_2\ d\underline{k}_3 \qquad \text{(E1)}$$

where $N(\underline{k})$ is the action density at wavenumber $\underline{k}$ and in which G is the

coupling coefficient given by:

$$G = \frac{\pi\, g^2 D^2}{4\rho_w^2 \omega_1 \omega_2 \omega_3 \omega_4} \,. \qquad \text{(E2)}$$

In Eq. (E2) D is the interaction coefficient (see appendix B), g is the gravitational acceleration, ρ_w is the density of water and $\underline{k}$ is the two-dimensional wavenumber. In the method of Dungey and Hui (1979) the action density spectrum $N(\underline{k})$ with peak wavenumber $\underline{k}_0$ and spectral width ε (defined in section 3.2.5) is written in terms of local coordinates λ and μ which are related to the wavenumber $\underline{k}$ by:

$$\underline{k}_i = \underline{k}_0 + \varepsilon \underline{L}_i \qquad \text{for} \quad i = 1,2,3,4 \qquad \text{(E3)}$$

in which

$$\underline{L}_i = (\lambda_i, \mu_i). \qquad \text{(E4)}$$

In the following the narrow peak assumption is used to simplify the Boltzmann integral Eq. (E1).

Substitution of Eqs. (E3) and (E4) in the expression for the interaction coefficient (see appendix B) and perturbing for small ε up to first order gives an expression for the coupling coefficient G (Dungey and Hui, 1979):

$$G = \frac{4\pi k_0^6}{\rho_w^2} \left(1 + \frac{\varepsilon}{k_0} \left(3(\lambda_1+\lambda_2) - \frac{(\lambda_2-\lambda_3)^2}{\left((\lambda_2-\lambda_3)^2 + (\mu_2-\mu_3)^2 \right)^{1/2}} - \frac{(\lambda_1-\lambda_3)^2}{\left((\lambda_1-\lambda_3)^2 + (\mu_1-\mu_3)^2 \right)^{1/2}} \right) \right). \qquad \text{(E5)}$$

Dungey and Hui (1979) showed that the truncated perturbation expansion (E5) yields good approximations to the exact coupling coefficients (Hasselmann, 1963b) in the range $\varepsilon|\underline{L}| \leq \frac{1}{2}|\underline{k}_0|$. The Boltzmann integral (E1) is rewritten by introduction of the variables α, β, γ and δ that are related to the local coordinates λ_i and μ_i by the transformation:

$$\left.\begin{aligned} \lambda_i &= \lambda_1 + u_i\,\alpha + v_i\,\beta \\ \mu_i &= \mu_1 + x_i\,\gamma + y_i\,\delta \end{aligned}\right\} \quad \text{for } i = 1,2,3,4 \qquad \text{(E6)}$$

where u_i, v_i, x_i and y_i are given by:

i	u_i	v_i	x_i	y_i
1	0	0	0	0
2	1	1	1	1
3	0	1	0	1
4	1	0	1	0

Substitution of Eq. (E6) in the expression for the coupling coefficient G and subsequent substitution in Eq. (E1) yields:

$$\frac{\partial N(\lambda_1,\mu_1)}{\partial \tau} = \frac{4k_0^{\,2}}{(gk_0)^{1/2}} \int_{-\infty}^{\infty}\int_{-\infty}^{\infty}\int_{-\infty}^{\infty} G \;X\; \delta(2\gamma\delta-\alpha\beta)\; d\alpha\; d\beta\; d\gamma\; d\delta \qquad \text{(E7)}$$

in which

$$G = \frac{4\pi k_0^{\,6}}{\rho_w^{\,2}}\left(1 + \frac{\varepsilon}{k_0}\left(6\lambda_1 + 3(\alpha+\beta) - \frac{\alpha^2}{(\alpha^2+\gamma^2)^{1/2}} - \frac{\beta^2}{(\alpha^2+\delta^2)^{1/2}} + O(\varepsilon^2)\right)\right) \qquad \text{(E8)}$$

and where

$$X = N_3 N_4 (N_1 + N_2) - N_1 N_2 (N_3 + N_4)$$

$$N_i = N(\underline{L}_i) = N(\underline{k}_i)$$

$$\tau = \varepsilon^2 t.$$

The term X in Eq. (E7) is written as:

$$X = \sum_{m=1}^{4} s_m N_i N_j N_k \qquad \text{(E9)}$$

in which the values of the indices i, j, k and the sign s depend on the index m, see the table below:

m	i	j	k	s
1	1	3	4	1
2	2	3	4	1
3	1	2	3	-1
4	1	2	4	-1

A further simplification of the Boltzmann integral is achieved by writing the local action density spectrum as the sum of n Gaussian shape functions:

$$N(\underline{L}) = \sum_{j=1}^{n} R_j \exp\left[-\tfrac{1}{2} P_j (\lambda - U_j)^2 - Q_j (\mu - V_j)^2 \right] \qquad \text{(E10)}$$

in which P_j, Q_j, R_j, U_j and V_j are the parameters defining the width, scale and location of the shape functions. The term V_j was added by Van Vledder (1984) in order to approximate also directionally skewed spectra. After some algebra (given in the second part of this appendix) the Boltzmann integral (E1) can be approximated by the sum of a number of one-dimensional integrals:

$$\frac{\partial N(\lambda_1,\mu_1)}{\partial \tau} = \frac{16\pi k_o^{15/2}}{\rho_w^{\,2}\, g^{1/2}} \sum_{m=1}^{4} \sum_{p=1}^{n} \sum_{q=1}^{n} \sum_{r=1}^{n} \left\{ I_1 + \frac{\varepsilon}{k_o}\left[6\lambda_1 I_1 + 3I_2 - I_3 - I_4\right] \right\}$$

$$+ O(\varepsilon^2) \qquad \text{(E11)}$$

in which I_1, I_2, I_3 and I_4 represent one-dimensional integrals. The values of these integrals depend on the values of the parameters λ_1, μ_1, the shape factors P_j, Q_j, R_j, U_j and V_j, and on the indices m, p, q and r.

Part II: Derivation of the one dimensional integrals

Substitution of the summation (E10) in Eq. (E9) gives:

$$X = \sum_{m=1}^{4} s_m N_i N_j N_k = \sum_{\ell=1}^{4} \sum_{p=1}^{n} \sum_{q=1}^{n} \sum_{r=1}^{n} R_p R_q R_r$$

$$\times \exp\left[-\frac{1}{2} \left\{ P_p(\lambda_i - U_p)^2 + P_q(\lambda_j - U_q)^2 + P_r(\lambda_k - U_r)^2 \right\} \right]$$

$$\times \exp\left[-\frac{1}{2} \left\{ Q_p(\mu_i - V_p)^2 + Q_q(\mu_j - V_q)^2 + Q_r(\mu_k - V_r)^2 \right\} \right]. \qquad \text{(E12)}$$

Using transformation (E6) expression (E12) is rewritten in terms of the variables α, β, γ and δ as:

$$X = \sum_{m=1}^{4} s_m N_i N_j N_k = \sum_{m=1}^{4} \sum_{p=1}^{n} \sum_{q=1}^{n} \sum_{r=1}^{n} R_p R_q R_r$$

$$\times \exp\left[-\Gamma_1 - \Gamma_2\right] \exp\left(-A_1\alpha^2 + B_1\alpha\right)$$

$$\times \exp(-A_2\beta^2 + B_2\beta) \exp(-A_3\gamma^2 + B_3\gamma)$$

$$\times \exp(-A_4\delta^2 + B_4\delta) \exp(C_1\alpha\beta + C_2\gamma\delta) \qquad \text{(E13)}$$

or alternatively as:

$$X = \sum_{m=1}^{4} s_m N_i N_j N_k = \sum_{m=1}^{4} \sum_{p=1}^{n} \sum_{q=1}^{n} \sum_{r=1}^{n} \Gamma Z \qquad \text{(E14)}$$

where

$$\Gamma = R_p R_q R_r \exp\left[-\Gamma_1 - \Gamma_2\right]$$

$$Z = \exp(-A_1\alpha^2 + B_1\alpha)\ \exp(-A_2\beta^2 + B_2\beta)\ \exp(-A_3\gamma^2 + B_3\gamma)$$

$$\times\ \exp(-A_4\delta^2 + B_4\delta)\ \exp(C_1\alpha\beta + C_2\gamma\delta)$$

and

$$\Gamma_1 = \frac{1}{2}\left[P_p(\lambda_1 - U_p)^2 + P_q(\lambda_1 - U_q)^2 + P_r(\lambda_1 - U_r)^2\right]$$

$$\Gamma_2 = Q_p(\mu_1 - V_p)^2 + Q_q(\mu_1 - V_q)^2 + Q_r(\mu_1 - V_r)^2$$

$$A_1 = \frac{1}{2}\left(u_i P_p + u_j P_q + u_k P_r\right)$$

$$A_2 = \frac{1}{2}\left(v_i P_p + v_j P_q + v_k P_r\right)$$

$$A_3 = x_i Q_p + x_j Q_q + x_k Q_r$$

$$A_4 = y_i Q_p + y_j Q_q + y_k Q_r$$

$$B_1 = -2\lambda_1 A_1 + u_i P_p U_p + u_j P_q U_q + u_k P_r U_r$$

$$B_2 = -2\lambda_1 A_2 + v_i P_p U_p + v_j P_q U_q + v_k P_r U_r$$

$$B_3 = -2\mu_1 A_3 + 2\left\{x_i Q_p V_p + x_j Q_q V_q + x_k Q_r V_r\right\} = -2\mu_1 A_3 + D_3$$

$$B_4 = -2\mu_1 A_4 + 2\left\{y_i Q_p V_p + y_j Q_q V_q + y_k Q_r V_r\right\} = -2\mu_1 A_4 + D_4$$

$$C_1 = -\left(u_i v_i P_p + u_j v_j P_q + u_k v_k P_r\right)$$

$$C_2 = -2\left(x_i y_i Q_p + x_j v_j Q_q + x_k y_k Q_r\right) .$$

Substitution of Eq. (E13) in Eq. (E7) gives an expression for the Boltzmann integral, which can be written as a linear combination of four types of four-dimensional integrals:

$$I_1 = \int_{-\infty}^{\infty}\int_{-\infty}^{\infty}\int_{-\infty}^{\infty}\int_{-\infty}^{\infty} \Gamma\, Z\, \delta(2\gamma\delta - \alpha\beta)\, d\alpha\, d\beta\, d\gamma\, d\delta$$

$$I_2 = \int_{-\infty}^{\infty}\int_{-\infty}^{\infty}\int_{-\infty}^{\infty}\int_{-\infty}^{\infty} (\alpha+\beta)\, \Gamma\, Z\, \delta(2\gamma\delta - \alpha\beta)\, d\alpha\, d\beta\, d\gamma\, d\delta$$

$$I_3 = \int_{-\infty}^{\infty}\int_{-\infty}^{\infty}\int_{-\infty}^{\infty}\int_{-\infty}^{\infty} \frac{\Gamma\alpha^2}{(\alpha^2+\gamma^2)^{1/2}}\, \Gamma\, Z\, \delta(2\gamma\delta - \alpha\beta)\, d\alpha\, d\beta\, d\gamma\, d\delta$$

$$I_4 = \int_{-\infty}^{\infty}\int_{-\infty}^{\infty}\int_{-\infty}^{\infty}\int_{-\infty}^{\infty} \frac{\Gamma\beta^2}{(\beta^2+\delta^2)^{1/2}}\, \Gamma\, Z\, \delta(2\gamma\delta - \alpha\beta)\, d\alpha\, d\beta\, d\gamma\, d\delta.$$

These four-dimensional integrals can be reduced to the following one-dimensional integrals (intermediate results of these derivations can be found in Van Vledder, 1984):

Integral I_1

$$I_1 = \int_{-\infty}^{\infty}\int_{-\infty}^{\infty}\int_{-\infty}^{\infty}\int_{-\infty}^{\infty} \Gamma\, Z\, \delta(2\gamma\delta - \alpha\beta)\, d\alpha\, d\beta\, d\gamma\, d\delta$$

$$= \frac{\pi\,\Gamma}{2(A_2A_4)^{1/2}} \int_{-\pi/2}^{\pi/2} \frac{\exp\left(\frac{1}{4}v^2/u - w\right)}{u^{1/2}}\, d\varphi$$

where

$$u = u(\varphi) = \frac{A_1}{A_4}\cos^2(\varphi) + \frac{A_3}{4A_2}\sin^2(\varphi) - \frac{(2C_1+C_2)^2}{16\,A_2\,A_4}\sin^2(\varphi)\cos^2(\varphi)$$

$$v = v(\varphi) = -\left\{ \frac{B_1}{A_4^{1/2}}\cos(\varphi) + \frac{B_3}{2A_2^{1/2}}\sin(\varphi) \right.$$

$$\left. + \frac{2C_1+C_2}{4(A_2\,A_4)^{1/2}}\sin(\varphi)\cos(\varphi)\left(\frac{B_4\cos(\varphi)}{A_4^{1/2}} + \frac{B_2\sin(\varphi)}{A_2^{1/2}} \right) \right\}$$

$$w = w(\varphi) = -\frac{1}{4}\left(\frac{B_4\cos(\varphi)}{A_4^{1/2}} + \frac{B_2\sin(\varphi)}{A_2^{1/2}} \right)^2 .$$

Integral I_2

$$I_2 = \int_{-\infty}^{\infty}\int_{-\infty}^{\infty}\int_{-\infty}^{\infty}\int_{-\infty}^{\infty} (\alpha+\beta)\;\Gamma\;Z\;\delta(2\gamma\delta - \alpha\beta)\;d\alpha\;d\beta\;d\gamma\;d\delta$$

$$= \frac{\pi\;\Gamma}{2(A_2A_4)^{1/2}} \int_{-\pi/2}^{\pi/2} \frac{\exp\left(\frac{1}{4}v^2/u-w\right)}{u^{1/2}} \left(H_2 - \frac{1}{2}\,H_1\,\frac{v}{u} \right) d\varphi$$

where

$$H = H(\varphi) = \left(1 + \frac{(2C_1+C_2)}{4A_2}\sin^2(\varphi) \right) \frac{\cos(\varphi)}{A_4^{1/2}}$$

$$H_2 = H_2(\varphi) = \left(\frac{B_2}{A_2^{1/2}}\sin(\varphi) + \frac{B_4}{A_4^{1/2}}\cos(\varphi) \right) \frac{\sin(\varphi)}{2A_2^{1/2}} .$$

Integral I_3

$$I_3 = \int_{-\infty}^{\infty}\int_{-\infty}^{\infty}\int_{-\infty}^{\infty}\int_{-\infty}^{\infty} \frac{\Gamma\ \alpha^2}{(\alpha^2+\gamma^2)^{1/2}}\ \Gamma\ Z\ \delta(2\gamma\delta - \alpha\beta)\ d\alpha\ d\beta\ d\gamma\ d\delta$$

$$= \frac{\pi\Gamma}{A_4}\int_{-\pi/2}^{\pi/2} \frac{\cos^2(\varphi)\ \exp(-w)}{\left(4A_2\cos^2(\varphi)+A_4\sin^2(\varphi)\right)^{1/2}}\ \frac{1}{u}$$

$$x\left(\frac{1}{\pi^{1/2}} + \frac{v}{2u^{1/2}}\ \mathrm{erf}\left(\frac{v}{2u^{1/2}}\right)\ \exp\left(\tfrac{1}{4}v^2/u\right)\right)\ d\varphi$$

in which erf(x) is the error function defined by:

$$\mathrm{erf}(x) = \frac{2}{\pi^{1/2}}\int_0^x \exp(-t^2)\ dt.$$

Integral I_4

The integral I_4 is identical to integral I_3 when the following interchanges are carried out in the expressions for I_3, u, v and w:

$\alpha \longleftrightarrow \beta$, $\gamma \longleftrightarrow \delta$,

$A_1 \longleftrightarrow A_2$, $A_3 \longleftrightarrow A_4$,

$B_1 \longleftrightarrow B_2$, $B_3 \longleftrightarrow B_4$.

CURRICULUM VITAE

Gerbrant van Vledder werd geboren op 28 juli 1957 te Hengelo (O). Hij kreeg zijn middelbare schoolopleiding aan het Reformatorisch College Blaucapel te Utrecht en behaalde in 1975 het einddiploma Atheneum B. In datzelfde jaar begon hij zijn studie Civiele Techniek aan de Technische Hogeschool te Delft. Van juni 1980 tot en met juni 1983 was hij werkzaam als studentassistent bij het praktikum Civiel Technische Computer Toepassingen. In 1983 behaalde hij het ingenieursdiploma cum laude bij de vakgroep vloeistofmechanica. Zijn afstudeeronderwerp was het vóórkomen van golfgroepen in zeegang en deining. Voor zijn afstudeerwerk kreeg hij in 1984 een prijs van de Nederlandse Vereniging van Technici op Scheepvaartgebied.

Vanaf juli 1983 was hij in dienst bij de Stichting voor de Technische Wetenschappen. In deze periode verrichtte hij in het kader van het project "richtingsspectra van zeegolven" het onderzoek dat de basis vormt voor dit proefschrift.

Sinds april 1988 is hij in dienst bij het Waterloopkundig Laboratorium (vestiging de Voorst) bij de sektor Havens, Kusten en Offshore Technologie. Hij is nu werkzaam op het gebied van de hydrodynamica, golfklimatologie en golfvoorspellingsmethoden.